THE UNIVERSITY OF CHICAGO

MINIMAL RECONSTITUTION OF ACTIN NETWORKS TO INVESTIGATE MECHANISMS OF ACTIN BINDING PROTEINS

A DISSERTATION SUBMITTED TO
THE FACULTY OF THE DIVISION OF THE BIOLOGICAL SCIENCES
AND THE PRITZKER SCHOOL OF MEDICINE
IN CANDIDACY FOR THE DEGREE OF
DOCTOR OF PHILOSOPHY

GRADUATE PROGRAM IN CELL AND MOLECULAR BIOLOGY

BY
CAITLIN ANN ANDERSON

CHICAGO, ILLINOIS
JUNE 2021

Table of Contents

LIST OF FIGURES vi

LIST OF TABLES viii

ACKNOWLEDGMENTS ix

PREFACE x

ABSTRACT xi

1 INTRODUCTION 1
- 1.1 Actin 1
  - 1.1.1 Actin structure and polymerization 1
  - 1.1.2 Actin Binding Proteins (ABPs) 5
  - 1.1.3 F-actin networks 9
- 1.2 Approaches to studying F-actin networks 12
  - 1.2.1 Studying the actin cytoskeleton at the tissue level 12
  - 1.2.2 Studying F-actin networks at the cellular level 13
  - 1.2.3 Bypassing cell membranes to study F-actin networks 14
  - 1.2.4 Minimal reconstitution of F-actin networks *in vitro* 15
- 1.3 *In vitro* biochemistry troubleshooting 17
  - 1.3.1 Protein purification troubleshooting 17
  - 1.3.2 Troubleshooting and developing *in vitro* assays 20
- 1.4 *In vitro* reconstitution assays for biochemical characterization of ABPs . . . 20
  - 1.4.1 'Bulk' pyrene assembly assays 20
  - 1.4.2 'Bulk' sedimentation binding assays 22
  - 1.4.3 Total Internal Reflection Fluorescence Microscopy (TIRFM) 23
- 1.5 Summary 24

2 LIM DOMAIN PROTEINS IN MECHANOBIOLOGY 26
- 2.1 Abstract 26
- 2.2 Cells sense and respond to mechanical forces 26
- 2.3 Mechanosensing in adherent cells 27
- 2.4 LIM domain proteins in mechanotransduction pathways 30
- 2.5 Force-sensitive localization of LIM proteins in adherent cells 32
- 2.6 LIM domains from diverse proteins bind stressed actin filaments 34
- 2.7 Evolutionarily conserved mechanism of LIM domain-based force sensing . . . 37
- 2.8 The actin filament is a substrate for force-sensitive binding 38

3 EVOLUTIONARILY DIVERSE LIM DOMAIN-CONTAINING PROTEINS BIND STRESSED ACTIN FILAMENTS THROUGH A CONSERVED MECHANISM . 41
3.1 Abstract . . . 41
3.2 Introduction . . . 42
3.3 Results . . . 46
3.3.1 LIM domain-containing regions (LCRs) from diverse mammalian proteins bind to SFSS . . . 46
3.3.2 LIM domains from fission yeast bind to SFSS in mammalian cells via a conserved mechanism . . . 50
3.3.3 Tandem LIM domains contribute additively to SFSS localization . . 53
3.3.4 *In vitro* reconstitution of LCR recruitment to contractile actomyosin bundles . . . 59
3.3.5 Polymerization-generated stress is sufficient for LCR localization to actin 67
3.4 Discussion . . . 69
3.5 Materials and Methods . . . 73
3.5.1 Cell culture and transfection . . . 73
3.5.2 Live-cell imaging and SFSS induction . . . 74
3.5.3 Image processing and analysis for LCR Screening Assay . . . 74
3.5.4 Data analysis . . . 75
3.5.5 Single molecule analysis . . . 75
3.5.6 Plasmid constructs for SFSS screens and protein purification . . . 76
3.5.7 LIM protein expression in fission yeast . . . 77
3.5.8 Protein purification and labeling . . . 77
3.5.9 High-speed sedimentation . . . 79
3.5.10 Seeded pyrene . . . 80
3.5.11 *In vitro* contractility assay . . . 80
3.5.12 Bead symmetry breaking assay . . . 81

4 ENGINEERING A FLUORESCENTLY-LABELED FISSION YEAST ARP2/3 COMPLEX FOR SINGLE MOLECULE MECHANISTIC INVESTIGATIONS *IN VITRO* 84
4.1 Abstract . . . 84
4.2 Introduction . . . 85
4.3 Results . . . 88
4.3.1 Engineering an optimal fluorescently-labeled Arp2/3 complex for *in vitro* experiments . . . 88
4.3.2 Halo-Arp2/3 complex fission yeast cells exhibit no significant F-actin network deficiencies . . . 93
4.3.3 Halo-Arp2/3 complex can be visualized at the single molecule level . 95
4.3.4 Halo-Arp2/3 complex is active with multiple classes of nucleation promoting factors . . . 95
4.3.5 F-actin binding of Arp2/3 complex increases in the presence of VCA 99
4.4 Discussion . . . 99
4.5 Materials and Methods . . . 101

4.5.1 Cloning Arp2/3 complex fission yeast strains and *in vitro proteins* . . 101
4.5.2 Fission yeast growth assay 103
4.5.3 *In vitro* protein purification 103
4.5.4 Spontaneous pyrene 104
4.5.5 Phallicidin 105
4.5.6 Cell imaging 105
4.5.7 Patch dynamics 106
4.5.8 Glass preparation for TIRF 106
4.5.9 TIRF microscopy 106
4.5.10 Data analysis: Arp2/3 complex time to nucleation 107
4.5.11 Data analysis: Arp2/3 complex binding dynamics. 108

5 FORMINS HAVE PROPERTIES THAT ARE BEST SUITED FOR THEIR CORRESPONDING CELLULAR ROLE 109
5.1 Preface 109
5.2 Introduction 109
5.3 Results 112
5.3.1 Construction of formin chimeras for *in vitro* assays 112
5.3.2 Formin chimeras compared with TIRFM imaging 114
5.4 Materials and Methods 114
5.4.1 Plasmid construction of *in vitro* formin chimera proteins 114
5.4.2 Protein purification 115
5.4.3 TIRFM with formin chimeras 116

6 DISCUSSION AND FUTURE DIRECTIONS 117
6.1 Minimal reconstitution of F-actin networks 117
6.2 LIM domain proteins localize to stressed F-actin networks 117
6.3 LIM domain-containing regions (LCRs) are mechanosensitive 118
6.4 Future directions for investigating LCR mechanosensitivity 119
6.4.1 Determining the force-induced conformation of F-actin 119
6.4.2 Determining the force-induced F-actin:LIM binding interface 120
6.5 Arp2/3 complex branching pathway 121
6.6 Future directions: Arp2/3 complex 122
6.6.1 Addition of labeled VCA with labeled Arp2/3 complex 122
6.6.2 Fission yeast actin and profilin 124
6.6.3 Mechanosensitivity of Arp2/3 complex 124
6.7 Concluding remarks 125

REFERENCES 126

List of Figures

1.1 Monomeric and filamentous actin. . . . 3
1.2 A selection of actin binding proteins (ABPs). . . . 6
1.3 Representative F-actin networks. . . . 10
1.4 *In vitro* biochemical actin assays. . . . 21

2.1 Mechanically stressed cells and LIM domain proteins. . . . 28
2.2 Schematic of LIM domain protein localization in cells. . . . 33
2.3 Schematic of mechanosensitive LCR localization to stressed actin filaments . . . 36
2.4 Evolution of LIM domain proteins. . . . 38

3.1 Diverse LIM domains localize to SFSS. . . . 44
3.2 Diverse LIM domains from mammals localize to SFSS. . . . 48
3.3 LCR of fission yeast Pxl1 associates to SFSS and displays similar kinetics and competes at SFSS. . . . 51
3.4 LCR from fission yeast Pxl1 and zyxin compete for SFSS and display similar kinetics. . . . 53
3.5 LCRs bind to SFSS through multiple, precisely spaced domains organized in tandem. . . . 54
3.6 Phenylalanine (F) is enriched at position 66 in SFSS-binding LIM domains. . . . 56
3.7 Additional analysis of mutant LCR localization to SFSS . . . 58
3.8 Purified LCR of yeast Pxl1 and mammalian zyxin localized to stressed F-actin networks. . . . 60
3.9 Purified LIM domains have a low affinity for the sides and barbed ends of F-actin. 62
3.10 Purified LCRs localizes to stressed F-actin networks where myosin deforms F-actin bundles. . . . 65
3.11 LCR(Pxl1) localization along reconstituted F-actin networks does not correlate with myosin localization. . . . 66
3.12 SNAP-LCR(zyx) localizes to branched F-actin networks during symmetry breaking 68
3.13 Model of LCR mechanosensing. . . . 70
3.14 *In vitro* contractility assay setup . . . 82

4.1 Determining the optimal labeled Arp2/3 complex. . . . 86
4.2 Representative pyrene curves. . . . 91
4.3 Single molecule TIRFM of fluorescently-labeled Arp2/3 complex constructs . . . 92
4.4 Endogenous HaloTag on Arp2/3 complex has no effect on endocytic actin patch dynamics. . . . 94
4.5 Labeled Halo-Arp2/3 complex at branch sites. . . . 96
4.6 Majority of branch sites have single molecule of labeled Halo-Arp2/3 complex. . 97
4.7 Dip1 robustly activates Halo-labeled Arp2/3 complex nucleation. . . . 98
4.8 Binding of Arp2/3 complex in the presence or absence of VCA. . . . 100

5.1 Biochemical analysis of formin chimeras with a cdc12 tail. . . . 113

6.1 SNAP-VCA in single molecule TIRFM. 123

List of Tables

2.1 A subset of LIM domain proteins and their corresponding mechanotransduction pathways. 31

3.1 *In vitro* protein construct extinction coefficients. 79

4.1 The fission yeast strains used in this paper. 89
4.2 The primers with genome homology used to clone the Arp2/3 complex strains in this paper. 102

5.1 *In vitro* actin assembly properties of formins used to generate formin chimeras. . 112

6.1 The fission yeast strains tested for *in vitro* labeling. 122

ACKNOWLEDGMENTS

The PhD process is long and stressful, but I had a wonderful group of people to help me along the way. First, I would like to thank David Kovar for his mentorship and for creating and encouraging a great lab atmosphere. The current and past lab members made lab an enjoyable experience. I could go to just about any one of them for experimental advice, but I could also count on them for duck pond walks, endless game nights, and numerous great conversations. I would like to thank the lab members during my time: Rachel Brown, Tom Burke, Jenna Christensen, Alyssa Harker, Katie Homa, Rachel Kadzik, Patrick McCall, Alisha Morganthaler, Meghan O'Connell, Cristian Suarez, Sarah Yde, and Dennis Zimmermann. I would like to specifically thank Katie, Alyssa, and Alisha for always having great advice, being good friends, and all of the Starbucks walks. I also need to extend my gratitude to Margaret Gardel and Jon Winkelman. Margaret served as an unofficial second mentor and offered another view point on my research. Jon was instrumental in my training and driving my first project. My thesis committee (Margaret Gardel, Mike Rust, Ed Munro) and program administrators were also instrumental in my success.

My support system extended beyond the lab. Thank you to my family especially my parents, Ron and Lori Anderson, who always supported and encouraged my endeavors. My mom would proofread any paper that I sent her way. My dad sparked my interest in mathematics and would correct my assignments at 5 a.m. My husband, Daniel Cash, was there from the beginning of this experience and was along for the ups and downs. Dan always encouraged me and allowed me to vent about the bad days. Dan's family became my second family and has helped us a lot over the past few years. I have many friends that have been there for me along the way, and I specifically want to thank Courtney Berkeland, Kelsie Ford, and Megan Jorgensen.

PREFACE

This dissertation is a compliation of two distinct manuscripts and a review paper. Chapter 2 is a recently accepted review, "LIM domain proteins in mechanobiology," which was submitted to *Cytoskeleton* in February 2021. David Kovar, Margaret Gardel, and Jonathan Winkelman also contributed to Chapter 2. Chapter 3, "Evolutionarily diverse LIM domain-containing proteins bind stressed actin filaments through a conserved mechansim," was published in *PNAS*. Additional contributors to chapter 3 are Jonathan D. Winkelman, Cristian Suarez, David R. Kovar, and Margaret L. Gardel. The manuscript that makes up Chapter 4 is currently in preparation. Additional contributors to Chapter 4, "Engineering a fluorescently-labeled fission yeast Arp2/3 complex for single molecule mechanistic investigations *in vitro*," are Meghan E. O'Connell and David Kovar. Prefaces at the beginning of each chapter indicate the specific work performed by the contributors listed above.

ABSTRACT

The actin cytoskeleton is a large, complex, dynamic network that is responsible for a myriad of cellular processes, including, polarity, endocytosis, motility, cytokinesis, and force response. Distinct filamentous actin (F-actin) networks assemble from one crowded cytoplasm. The ability to build several F-actin networks simultaneously with distinct architectures, dynamics, location, and timing is a topic that has drawn a lot of interest. Each of these F-actin networks associate with a set of actin binding proteins (ABPs). How ABPs sort and and contribute to the properties of the F-actin networks is a big question in cell biology. Our lab has done extensive research on different ABPs and the roles in corresponding F-actin networks. Our lab does use fission yeast for cell level analysis of F-actin networks. However, a large part of our research is minimal reconstitution of F-actin networks *in vitro* to directly investigate actin binding proteins. My contribution to the following projects is the minimal reconstitution biochemistry experiments. A relatively new topic in our lab is mechanosensitive ABPs, and I reconstitute actomyosin networks to study mechanosensitive ABP localization.

LIM domain proteins have been studied by previous labs. There are over 70 mammalian LIM domain proteins, and several have been shown to associate with the actin cytoskeleton. In fact, many of them are involved in mechanotransduction pathways and associate with the F-actin networks in a force-dependent manner. Here, we studied the mechanism of mechanosensitive LIM domain protein recruitment with both *in vivo* assays and *in vitro* reconstitution assays. LIM domain proteins associate with force responsive F-actin networks: focal adhesions, adhesion junctions, stress fibers, and contractile rings. The LIM domain containing region (LCR) is essential for localization, and the LCR is hypothesized to bind directly to a force induced conformation of F-actin. Our lab and the Alushin lab [247, 218] made progress in understanding the LIM domain mechanosensitive mechanism, but there is still much more to be investigated.

Another ABP discussed here is Arp2/3 complex. Arp2/3 complex is a seven component protein that binds to actin filaments and nucleates branches. Arp2/3 complex networks are important for force generation, like the leading edge of motile cells or the endocytic patches. Arp2/3 complex has been studied extensively by many labs. However, the seven component structure has made fluorescent labeling difficult. We recently labeled the fission yeast Arp2/3 complex and have successfully visualized Arps/3 complex at the branch sites. We can now study the Arp2/3 complex-mediated branch formation pathway in greater detail and better understand the mechanism involved.

CHAPTER 1

INTRODUCTION

1.1 Actin

Actin is the most abundant protein and involved in the most protein-protein interactions in most eukaryotic cells [51]. Actin originated in the earliest ancestors of all life, and the gene family is well conserved with bacteria, archaea, and all eukaryotes having actin molecules that are structurally and functionally related [82]. While several eukaryotes (e.g. budding yeast, fission yeast, green algae) are able to form complex actin networks with one actin gene, vertebrates have multiple isoforms that are differentially expressed in different tissues [89]. Humans have three isoforms of α-actin (cardiac, smooth, and skeletal muscles), one β-actin (non-muscle), and two isoforms of γ-actin (smooth muscle, nonmuscle) [177]. The actin cytoskeleton has many different roles in cells, including intracellular transport, structure, motility, muscle contraction, and cytokinesis [225, 223, 220, 75]. The diversity of the actin cytoskeleton can be contributed to the formation of distinct and dynamic networks of filamentous actin (F-actin) and actin binding proteins (ABPs). Temporal and spatial accuracy is essential of F-actin network assembly to maintain proper cell function.

1.1.1 Actin structure and polymerization

Actin is a 42kDa globular protein that polymerizes to form filaments. The actin monomer (G-actin) is formed from a polypeptide that folds into a flat structure with four subdomains (Figure 1.1A). The polypeptide weaves from the N-terminus in subdomain one to subdomains two, three, and four and back to subdomain one to end with the C-terminus [177]. The protein has also been classified as the outer, smaller domain (one and two) and the inner, larger domain (three and four). While there is structural similarity between the outer and inner domains, there is little sequence similarity. It is thought that a duplication occurred

early on within the actin gene and then the sequences diverged. The connection between the two halves is relatively minimal as the polypeptide crosses over the center twice and forms the hinge. There are also two large clefts along the hinge between the halves. The upper cleft binds the ATP nucleotide and an associated cation (Mg^{2+}). The lower cleft between subdomains one and three is considered the 'target binding cleft' as many proteins bind at this site [48]. The two clefts communicate, and nucleotide-dependent conformation changes can alter the binding affinities of ABPs.

The structural basis of an actin network relies on the filamentous state of actin. Actin filaments (F-actin) form from polymerization of actin monomers (G-actin) into two protofilaments that wrap around each other with a right-handed twist along the long-axis [85] (Figure 1.1B). A filament is more accurately described as a single strand with a much tighter left-handed helix with repeating units of approximately 13 molecules occurring in six turns over approximately 35.9 nm. F-actin is polar with a fast-growing barbed end (subdomains one and three) and a slow-growing pointed end (subdomains two and four). The filament end names come from the initial discovery of filament polarity. Electron microscopy images of F-actin covered in myosin heads, which form arrowhead-shaped structures, showed uniform directionality of the arrows resulting in 'barbed' and 'pointed' ends [101]. G-actin that has been incorporated into F-actin has a slightly different structure than 'free' monomer. The outer domain (subdomains one and three) twist relative to the inner domain (subdomains three and four) 12-13°, while additional bending of subdomains two and four results in a final 16-18° and a much flatter structure [51]. The actin monomers within the filament form interactions on both the short- and long-pitch helices, but the longitudinal interactions within the separate protafilaments are strongest [34, 70]. The most notable intra-protafilament interaction is the DNase I binding loop (D-loop) in subdomain 2 inserting into the target binding cleft of the adjacent monomer [51].

Actin monomers bind adenosine triphosphate (ATP) or ADP tightly [107]. A divalent

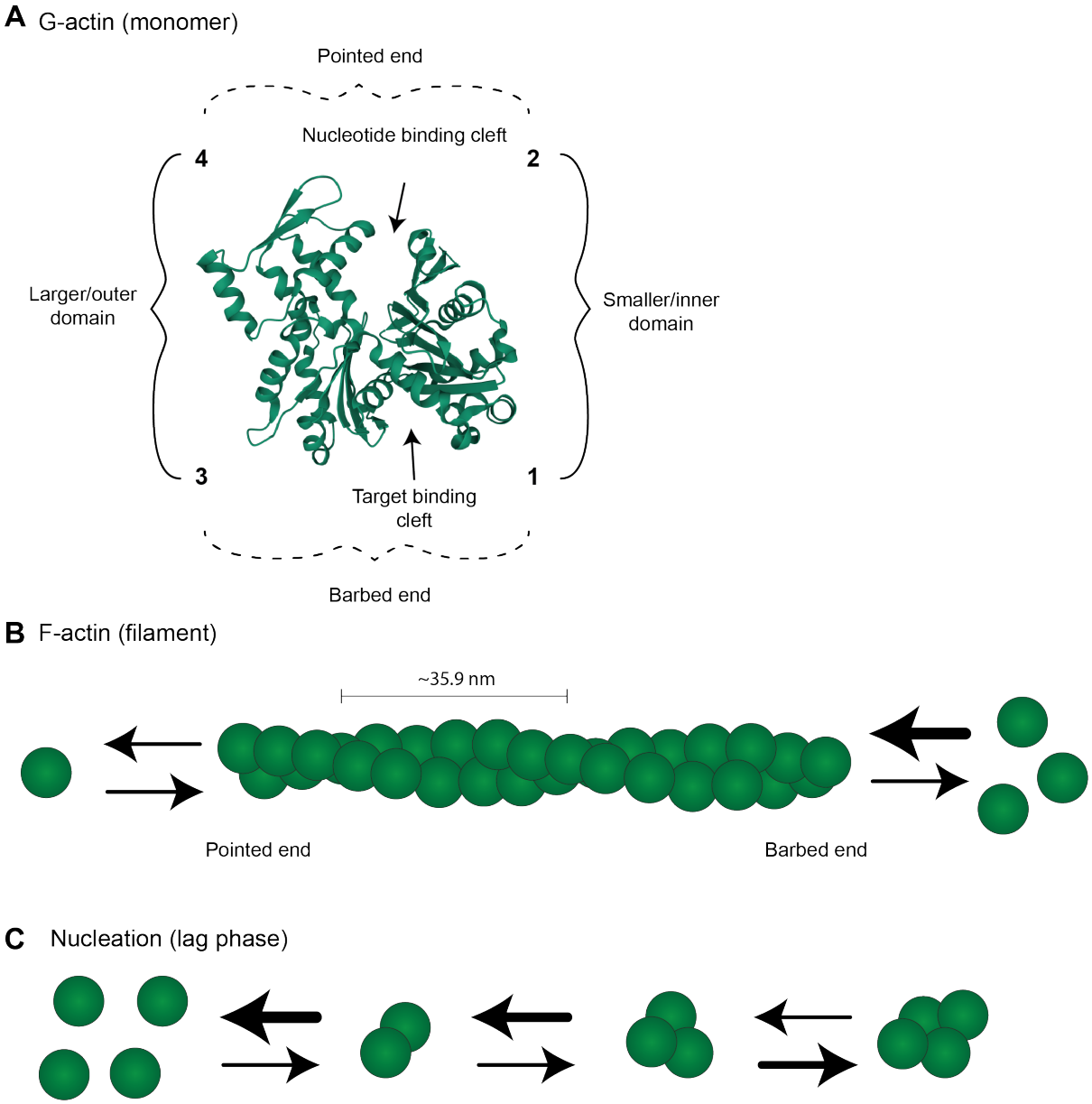

Figure 1.1: **Monomeric and filamentous actin. (A)** Monomeric actin (G-actin) (PDB: 1NWK) has four subdomains, and the polypeptide sequence starts and ends with the N- and C-terminus both in subdomain one. There are two main binding clefts in the monomer, nucleotide and target binding. **(B)** Actin monomers polymerize to form filamentous actin (F-actin). The polar filament has a fast growing barbed end and slow growing pointed end. While F-actin appears to be two protofilaments with right-handed twist, the overall structure is a single left-handed twist with a repeating unit of about 35.9 nm. **(C)** Actin nucleation is considered to be the lag phase as dimer and trimer formation is unfavorable. Tetramers are stable oligomers that are capable of elongation.

cation (Ca^{2+} or Mg^{2+}) associates with the β- or γ-phosphates of ATP and stabilizes the interaction with the monomer. Nucleotide-free monomers exist just briefly as the ATP affinity is in the nanomolar range, but monomers in the absence of bound nucleotides can denature within seconds [44]. While the bound nucleotide is essential for stabilizing the monomers, it is not required for filament polymerization [177]. Spontaneous polymerization occurs under physiological salt conditions with cations, which bind specific residues and promote interactions between monomers [110]. Spontaneous filament assembly begins with a slow nucleation step that is considered the lag phase (Figure 1.1C). Nucleation is limited by the unfavorable formation of dimers and then trimers [201, 38, 69]. The formation of a tetramer is an important transition step, as the oligomer is now a stable actin nucleus for elongation. Elongation rate depends on the available monomer and is the same for the freshly-established actin nucleus and the longer well-established actin filaments. However, filament polarity impacts elongation, as barbed ends elongate about 10 times faster than pointed ends. ATP-actin association at the barbed end occurs at the rapid rate of about 10 $\mu M^{-1} sec^{-1}$, while dissociation occurs at the slow rate of about 1 sec^{-1} [119]. The 'critical concentration' of monomer for barbed end elongation is 0.1 μM, while it is 0.6 μM for pointed end elongation.

The conformational change associated with an actin monomer incorporating into a filament increases the rate of ATP hydrolysis to 0.3 sec^{-1} [17]. Nucleotide hydrolysis most likely occurs randomly along the filament, but the nucleotide state of adjacent monomers may impact the rate [105, 116]. Although hydrolysis occurs rapidly, the γ-phosphate dissociates with a half-time of about six minutes [24]. While ADP-P_i-actin is behaviorally similar to ATP-actin, ADP-actin is much quicker to dissociate from both filament ends. The critical concentration at both filament ends is 1.8 μM for ADP-actin. Actin filaments maintain the ADP nucleotide and can exchange free phosphate with the surrounding buffer at a low rate of about 2 $M^{-1} sec^{-1}$ [24]. Pointed ends have a much lower affinity for phosphate than barbed

ends, and filament ends have a higher rate of phosphate dissociation than interior monomers. Therefore, the slow monomer association and dissociation rates at the pointed end lead to ADP-actin dissociating with the increased critical concentration. Therefore, the asymmetry of filament end polymerization is likely contributed to both the conformation and nucleotide state of the corresponding actin monomers.

The dynamics of actin filament polymerization have been well-studied with purified protein, but the behavior of actin in cells is much different [178]. The total cellular concentration of actin is 50-200 μM. At this concentration, purified actin would rapidly assemble until steady state. However, about half of the actin (25-100 μM) exists as monomer in cells, which is far beyond the critical concentration. Filaments also assemble and dissemble at much faster rates than *in vitro*. The difference is that cells contain an array of actin binding proteins (ABPs) that help regulate actin nucleation, elongation, severing, and bundling. Understanding ABPs is essential for understanding how distinct F-actin networks are assembled.

1.1.2 Actin Binding Proteins (ABPs)

There are many different actin binding proteins (ABPs) with a wide range of functions, but they all contribute to proper spatial, temporal, and structural assembly of F-actin networks in cells (Figure 1.2). Spontaneous random polymerization is prevented by a large pool of profiln-bound actin monomer. Profilin is a small protein with a high affinity for ATP-actin monomers (Kd = 0.1 μM) and a cellular concentration of 50-100 μM [177]. Profilin binds to the barbed end of a monomer, so incorporation at the pointed end is sterically inhibited. However, profilin-actin can be incorporated at the barbed end, and barbed end binding actually weakens the profilin association so the profilin quickly dissociates. Profilin also reduces the affinity for nucleotides, which facilitates the release of ADP from recently depolymerized monomers clearing the way for ATP to bind [132, 147]. Profilin also binds to the polypro-

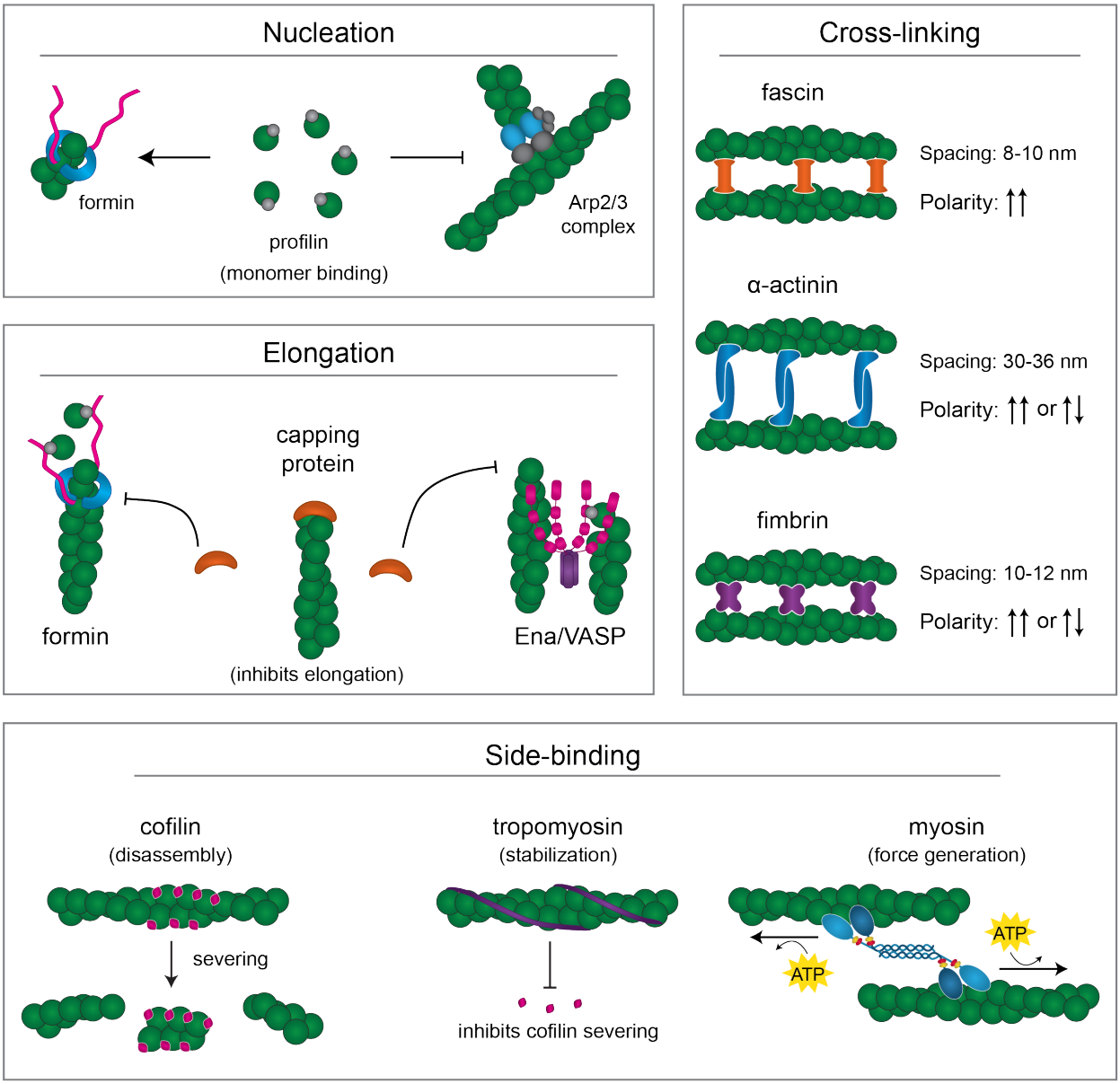

Figure 1.2: **A selection of actin binding proteins (ABPs).** Actin binding proteins (ABPs) determine many characteristic properties of F-actin networks. Profilin binds G-actin and inhibits spontaneous polymerization. Nucleation ABPs are activated by additional nucleation promoting factors (NPFs) and catalyze the slow nucleation step. Formin nucleates unbranched filaments and Arp2/3 complex nucleates branched filaments. Elongation factors (formin, Ena/VASP) increase the polymerization rate of F-actin and inhibit capping protein. Cross-linking proteins (fascin, α-actinin, fimbrin) create higher-order structures, including bundles with spacing and polarity corresponding to specific cross-linkers. Several ABPs bind to the sides of F-actin, including cofilin, tropomyosin, and myosin.

line regions of some actin elongation factors, which then promotes actin elongation from the barbed ends.

In vitro experiments revealed that nucleation is a slow step for actin assembly. Therefore, a whole class of ABPs catalyze nucleation to enable the quick assembly rates required in cells. The main actin nucleation factors are Arp2/3 complex, which produces branched filaments, and formins, which form unbranched filaments. Arp2/3 complex is composed of actin related protein 2 (Arp2), Arp3, and five additional proteins (ArpC1-5). Arp2/3 complex binds to an exisiting mother filament and nucleates a daughter filament to assemble as a branch forming 70° from the mother filament. Arp2/3 complex is intrinsically inactive and requires a nucleation promoting factor (NPF), like Wiskott-Aldrich syndrome protein (WASP) for activateion [194]. Two WASP molecules activate Arp2/3 complex and deliver two actin monomers to initiate the formation of the daughter filament [164]. Arp2/3 complex-mediated branched networks are ideal for producing pushing forces such as lamellipodia and endocytic patches.

Formins are a family of multidomain, homodimeric proteins. The formin homology domains (FH1 and FH2) are common domains among this family, while additional regulatory domains are more specified for the particular formin's cellular function. FH2 domains form head-to-tail dimers that interact with the barbed end of an actin filament, while the FH1 domain has proline-rich sequences that bind profilin-actin [161]. It was originally thought that FH2 domains stabilize actin dimers, which would indeed increase nucleation [257, 181, 168]. However, experiments showed that FH2 domains are inefficient nucleators of profilin-actin, which is the main source of available monomer in cells. It has been revealed that additional formin domains and NPFs may facilitate FH2 mediated profilin-actin nucleation [19]. Formin nucleated unbranched filaments are essential for contractile rings, stress fibers, and filopodia [91].

Formins are also important elongation factors and facilitate rapid actin elongation by

processivley associating with the growing barbed end via the FH2 domains and delivering profilin-actin via the FH1 domains [177]. Spontaneous actin assembly occurs at a rate of about 10 μM sec^{-1} [177], but some formins can elongate ten times faster. The tetrameric Enabled/Vasodilator stimulating phosphoprotein (Ena/VASP) interacts with the barbed end and delivers both profilin-actin and free actin monomers to facilitate increased F-actin elongation [64, 84]. Ena/VASP is not as processive or as efficient at elongating as many formins, but it is important for elongation of trailing filaments in bundles, especially during filopodia formation. Formin and Ena/Vasp both have an additional indirect effect on elongation rate by blocking capping protein. Capping protein binds an F-actin barbed end tightly and remains at the barbed end with a dissociation half-time of 30 minutes [56]. Capping protein inhibits elongation and monomer dissociation, which maintains the actin monomer pool and stabilizes actin filaments. Capping protein is essential for regulating the length of filaments, like Arp2/3 complex-mediated networks, where short branched filaments are needed to produce forces.

Many F-actin networks contain higher-order structures, including bundles, which are stabilized by cross-linking ABPs. The main characteristic of cross-linkers is the ability to bind two F-actin simultaneously with multiple actin binding domains (ABDs). ABDs typically consist of calponin-homology (CH) domains [18]. The spacing of ABDs and the structure of the cross-linker determines the higher-order organization of the actin filaments. Widely separated ABDs lead to cross-linking, where two filaments are connected at one point. Cross-linkers with ABDs relatively close together can bundle filaments by cross-linking multiple times to keep the filaments closely aligned. The orientation of actin filaments within a bundle can either be parallel or antiparallel and is an additional quality determined by the cross-linker. Fimbrin has tandem CH domains that facilitate the formation of narrow (10-12 nm) actin bundles that include both parallel and antiparallel filaments [83]. Monomers of α-actinin have one CH domain, so they must dimerize to create wider spaced bundles (30-36

nm) that also include antiparallel and parallel filaments [205]. Instead of CH domains, fascin contains β-trefoil domains that bind and bundle parallel filaments with very narrow spacing (8-10 nm) [103, 237]. Cross-linking ABPs are essential for building an array of complex F-actin networks in cells.

Both assembly and disassembly of F-actin in cells is much quicker than spontaneous actin dynamics *in vitro*. Actin filament disassembly rate is increased by severing proteins, like cofilin and gelsolin. Cofilin cooperatively binds to the sides of actin filaments and promotes γ-phosphate release to form ADP-actin polymers in seconds instead of minutes [16]. The expedited depolymerization facilitates rapid turnover of filaments in cells. Cell movement and division require F-actin networks with continuous turnover.

Additional actin binding proteins can bind to the sides of actin filaments. Tropomyosin is a coiled-coil protein that binds along the long-pitch helix, stabilizing the filament and protecting from cofilin mediated severing [135]. Tropomyosin is found in muscle cells, where it regulates myosin interactions. Myosins are motors that utilize ATP hydrolysis to exert force on F-actin via a bind and release cycle. There are many types of myosin that are classified by processivity, directionality, and force generation. Myosin are essential for transporting cargo along F-actin tracks, anchoring organelles, and mechanotransduction [87].

1.1.3 F-actin networks

In cells, actin filaments form distinct networks with specific structures and dynamics that drive many different cellular processes. Since the actin comes from the same pool of available monomer, the mechanistic properties of an F-actin network are determined by the associated actin binding proteins. *Schizosaccharomyces pombe* (fission yeast) cells have just one isoform of actin, but there are three distinct F-actin networks: endocytic patches, contractile ring, and polarizing cables [118]. Each of those distinct networks has a particular subset of ABPs that create the optimal architecture for the corresponding cellular process. In more complex

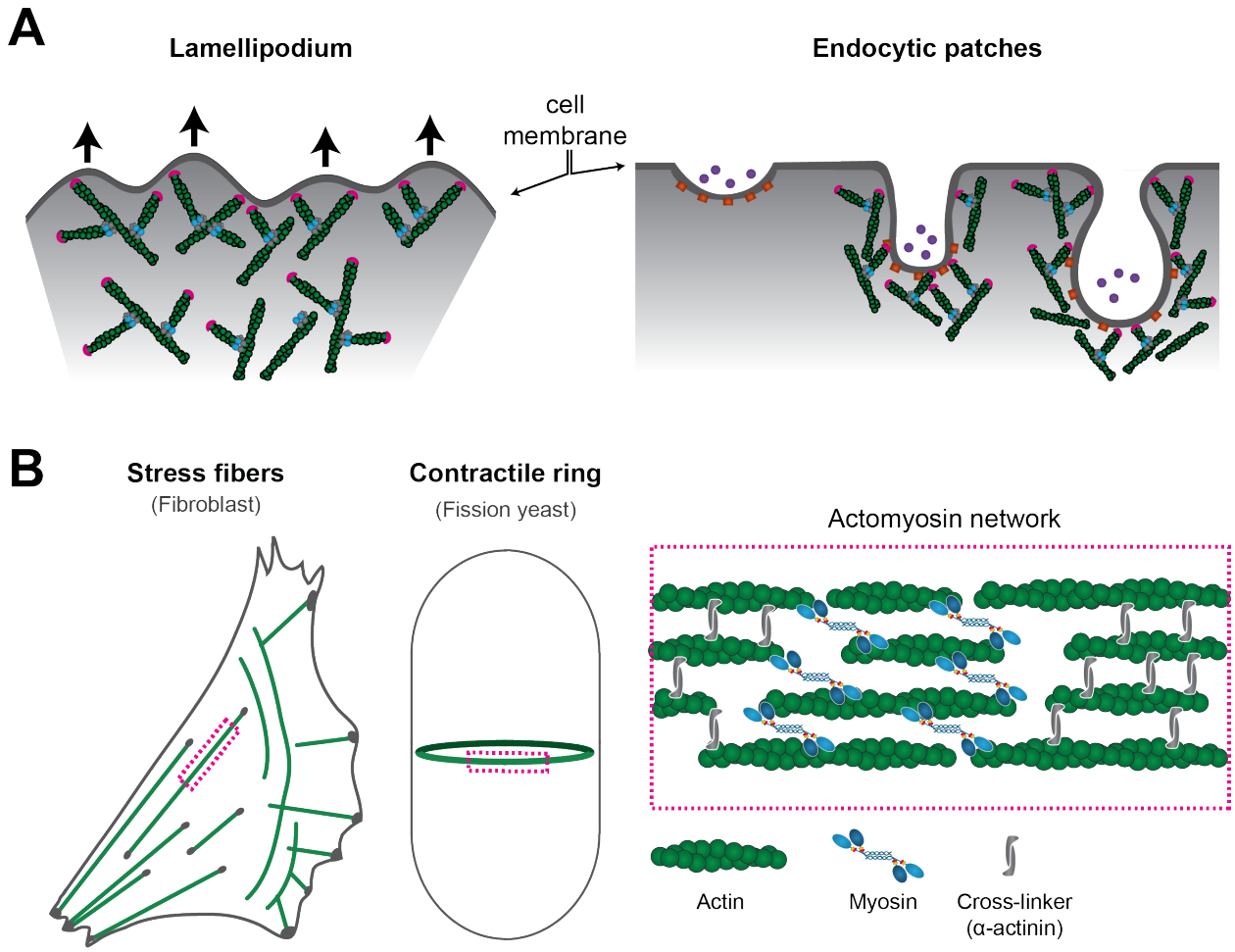

Figure 1.3: **Representative F-actin networks.** **(A)** Simple schematics of the short, branched F-actin networks that are ideal for pushing forces. The lamellipodium is a dense F-actin network that pushes the leading edge of the cell forward. Endocytic patches utilize branched F-actin networks to facilitate membrane invagination for intake of external substances. **(B)** Stress fibers and contractile rings have similar basic architectures of actomyosin networks. Each network is more complex and specialized, but the general principle of a contractile, bundled F-actin network is the same.

organisms, there are more actin binding proteins and more complex F-actin structures.

The lamellipodium is found at the leading edge of migrating cells. Cell motility is a basic process that is important for tissue remodeling, wound closure, and immune cell response. Migrating cells utilize actin polymerization of a dense short branched network to push the membrane of the leading edge forward (Figure 1.3). Actin filaments are nucleated by Arp2/3 complex near the membrane, and filament orientation is important as the elongation of the fast-growing barbed ends is directed toward the membrane and pushes it forward. Capping protein limits actin elongation and the resulting short branched filaments create a dense network ideal for the needed pushing force [178, 149]. Similar short, branched actin filaments are used for endocytosis, membrane invagination for intake of external substances.

Actin stress fibers (SF) are actomyosin networks that enable a cell to maintain mechanical homeostasis, as they are mechanosensitive load-bearing structures that also generate forces. SFs are generally anchored to focal adhesions (FA), which are force sensitive protein complexes that form a bridge between the extracellular matrix and actin cytoskeleton within cells. SFs are contractile actin bundles of 10-30 filaments with alternating regions of actin crosslinker α-actinin and non-muscle myosin [226, 41]. This pattern is reminiscent of less stringent muscle sarcomeres with mixed polarity actin filaments that span multiple regions. The less organized SF is built for continuous isometric contraction [23, 169]. SFs are further classified by their location and have slightly different morphologies. The most common SFs are ventral, which are anchored by FAs at both ends and are capable of generating forces [206]. Dorsal stress fibers are anchored to one FA and lack myosin and the ability to contract [226]. Transverse arcs are not anchored at either end but contain myosin. Dorsal SFs and transverse arcs are precursors to the more common ventral SFs [94].

Cytokinesis is the final step in the cell cycle and physically splits the cell into two. The contractile ring is an actomyosin structure that must assemble at the right time and location to ensure proper cell division. While the composition and organization varies between or-

ganisms, the general idea is organized chaos that involves formin elongated actin filaments, crosslinkers, myosins, membrane anchors, and assorted proteins [163, 179]. Tension is created by the myosin contractility and the contractile ring constricts and pulls the membrane inward.

1.2 Approaches to studying F-actin networks

1.2.1 Studying the actin cytoskeleton at the tissue level

The actin cytoskeleton is involved in a wide range of cellular processes, including structure, motility, division, endocytosis, and mechanotransduction. In multicellular organisms, the roles of actin at the cellular level impact the more complex levels of tissues and organs. Actin is expressed in essentially every eukaryotic cell, and there are several actin isoforms in humans that are differentially expressed throughout the body. The organismal level effects of actin and actin binding protein mutations have been studied and connected to a myriad of diseases [167]. Some actin mutations cause disorganization in cardiac muscle cells resulting in cardiac function defects [246]. Structural alterations to actin bundles that form the stereocilia, which are mechanosensing projections in the ear responsible for balance and hearing, can cause deafness [11]. Additionally, a number of mutations affect the motility, signaling, and proliferation of immune cells leading to immunodeficiency disorders [213]. Most actin studies done directly with complex organisms (e.g. humans, frogs, rats) use fixed and stained tissues to study the effects of gene mutations or drug treatments. Since F-actin networks are essential for many cellular functions, there are limitations to understanding the changes in F-actin network dynamics at the organ and tissue levels. The mutations could affect actin polymerization, depolymyerization, actin binding protein dynamics, or any actin property which would then impact the F-actin network and corresponding cellular function.

Tissue or cell cultures from complex organisms enable the direct visualization of cell

processes in real-time, which means understanding the dynamics. Cell cultures have been used to study the involvement of F-actin in wound healing, tissue homeostasis, endocytosis, and cell shape change [3, 59, 26]. The experimental drawbacks to cell cultures include the concern that the difference in cellular environment could affect cellular behavior. Methods have evolved to better mimic the corresponding environment in organisms. For instance, adherent cells (e.g. epithelial cells, fibroblasts) are plated on collagen or fibronectin. Cell cultures allow for manipulations that would be difficult to do with whole organisms. Laser ablation of cells initiates wound repair, and then the dynamics of repair by F-actin lamellipodia protrusions and the actomyosin purse string can be studied [3]. Simpler multicellular organisms (e.g. worms, fruit flies, zebrafish) can be studied similar to cell cultures but as embryos. Cell culture experiments are important for studying the involvement of F-actin networks in cellular processes that impact tissues within an organism. However, single cell experiments offer an even closer look at the F-actin network.

1.2.2 Studying F-actin networks at the cellular level

Most eukaryotic cells have multiple isoforms of actin and a multitude of different F-actin structures operating simultaneously, which makes it difficult to isolate the networks to study the formation and dynamics. Fission yeast (*Schizosacchormyces pombe*) is a single cell organism with one actin isoform and three distinct F-actin networks [118], which provides a simpler platform for studying F-actin networks *in vivo*. Decades of research have been dedicated to studying the composition, formation, and dynamics of the distinct F-actin networks in fission yeast. Genetic manipulation of fission yeast is relatively simple compared to more complex eukaryotic organisms. Fission yeast are generally haploid with a small genome with very little redundancy. Homologous recombination is used to directly target the genome to quickly engineer gene deletions, truncations, point mutations, inducible promoters, and fluorescent tags [118]. Directly altering the genome instead of using multi-copy

plasmids guarantees endogenous level expression of proteins. The genetic manipulation and fluorescent protein labeling enabled the discovery of the important proteins for the F-actin networks. Advances in precise imaging techniques have been important in investigating the dynamics of the F-actin networks. Single-molecule analysis of clathrin-mediated endocytosis revealed a detailed timeline of the recruitment and turnover of actin and actin binding proteins at endocytic patches [123].

Fission yeast cell studies have revealed a lot of information about the different F-actin networks, but there are still limitations. Genetic manipulation is a great cell tool, but the mutants can only be studied if the cells live. There are complex signaling pathways and overlapping cellular processes that make it impossible to completely isolate an F-actin network. Most cell experiments use drugs or mutations to perturb the cell, and the cellular response is typically F-actin network level. For instance, CK-666 eliminates F-actin patches [22]. The details of the F-actin networks are lost in the robust response. Live-cell fluorescent microscopy techniques have improved significantly, but the resolution is not quite single actin filament level.

1.2.3 Bypassing cell membranes to study F-actin networks

Breaking down the cell wall and membrane bypasses some of the constraints of the cell system. The simplest cell extract studies are sort of 'fishing' experiments for binding partners. A tagged target protein is incubated in the cell extract and then removed along with anything bound, which isolates the set of binding partners for analysis. Cell extracts were used by one group to study the dynamics of endocytic F-actin patches. Beads coated with the budding yeast Arp2/3 complex nucleation promoting factor Las17 (budding yeast WASP) were added to the cell extracts. Dynamic Arp2/3 complex F-actin networks assembled around the beads, which mimics comet tails and created motile beads [141]. The F-actin networks on the beads were then isolated and new binding interactions were discovered. The assay was extended to

cell extracts with mutations, and the involvement of different ABPs in regulation of F-actin elongation in Arp2/3 complex networks was investigated [143]. Another approach was used to isolate the function of contractile ring assembly from ring contraction. The two processes were separated by removing the cell wall and membrane after contractile ring assembly [145]. The contractile ring remained in a 'cell ghost' without any remaining cytoplasmic structures. The research group was able to determine that while myosin contractility is essential, F-actin depolymerization and severing are not important for contractile ring constriction *in vitro*.

1.2.4 Minimal reconstitution of F-actin networks in vitro

Cell experiments have been crucial for understanding F-actin networks, but the question remaining is how particular combinations of actin binding proteins interact to construct diverse F-actin networks with distinct structures and dynamics. *In vitro* reconstitution biochemistry removes the constraints of a cell system to study specific protein interactions. Reconstitution is a bottom-up approach that studies the properties of the individual parts and applies that knowledge to the whole. F-actin networks are formed in the presence of numerous proteins and signaling pathways in cells. Reconstitution allows the researcher to control the 'ingredients' in a reaction which eliminates the unknowns.

Reconstitution has been used since the 1940's to characterize the mechanistic and structural properties of F-actin and the many ABPs in exhaustive detail (reviewed in [73]). The assembly and disassembly properties of actin are known in immense detail. The binding and bundling efficiencies of the cross-linkers have been studied. The directionality and rates of the myosins have been recorded. More recent reconstitution biochemistry research has shifted to focus on rebuilding F-actin networks *in vitro* with minimal components. These experimental setups bridge the gap between characterizing the ABPs and the complex F-actin networks in cells. Minimal reconstitution has been used to study network homeostasis, ABP sorting, actin cable formation, and contractile ring constriction [216, 173, 258, 35].

Our lab used minimal reconstitution to determine how distinct F-actin networks are simultaneously assembled in the same cytoplasm and how specific sets of ABPs sort to particular networks. Competition for G-actin regulates the size and density of the simultaneous F-actin networks. However, the F-actin patches have nearly 15,000 Arp2/3 complexes and consume about 50% of the G-actin, while approximately 1,000 formins use about 20% of the G-actin [204, 252, 118]. Minimal reconstitution of the monomer competition between formins and Arp2/3 complexes revealed that profilin inhibits Arp2/3 complex mediated actin assembly [216]. Therefore, profilin enables formin to effectively compete with the higher number of Arp2/3 complexes to maintain network homeostasis.

The F-actin networks in the cell are associated with specifice sets of ABPs, but how the ABPs sort between the networks was not well understood. Minimal *in vitro* reconstitution assays showed competitive and cooperative interactions between tropomyosin, cofilin, α-actinin, and fimbrin create distinct F-actin networks within the same *in vitro* reaction [35, 36]. These experiments revealed that ABP sorting can be attributed to the interactions between the ABPs in the absence of any signaling pathways. These interactions likely contribute to sorting within fission yeast F-actin networks, as fimbrin and cofilin keep short, bundled networks at endocytic patches, while tropomyosin and α-actinin associate with the contractile ring. The *in vitro* reconstitution experiments were able to test different combinations of ABPs and directly visualize the sorting of the ABPs between networks.

In vitro results should be considered in parallel to *in vivo* observations to determine how the *in vitro* findings complement, confirm, and refine the molecular models of the cell F-actin networks. This comparison is important to ensure the *in vitro* results are relevant to cellular processes and not artifacts. *In vitro* biochemistry encompasses a wide range of assays that utilize purified proteins to carefully characterize their interactions with purified actin. A major benefit of purified proteins is being able to test a range of concentrations in assays, which then allows for calculations of binding affinities. The limited number of

variables within reconstitution assays also makes them ideal for mathematical modeling. The timescale of *in vitro* experiments are much shorter than cell experiments, so multiple variables can be tested in one afternoon. Protein mutations that might not be viable in cells can often be purified and characterized *in vitro*, and that can offer an idea of why those mutants are lethal to cells. Single molecule fluorescent microsocopy provides excellent resolution for visualizing direct binding of ABPs with actin filaments. Overall, *in vitro* biochemistry offers detailed understanding of protein interactions that can help elucidate the bigger picture within cells.

Of course, there are some drawbacks to *in vitro* biochemistry assays. As noted earlier, reconstitution assay results could be artifacts. *In vitro* assays take the proteins out of the cell environment, which could certainly result in altered behavior. However, *in vitro* assays utilize buffers, concentrations, and experimental designs inspired by cells. Then the *in vitro* results are compared to cell observations to understand how the *in vitro* results fit into our understanding of cells. Repetition is also key throughout experimental research. F-actin has been characterized repetitively in the past, and those numbers give a guideline to actin behavior *in vitro*. Repetition within experiments also helps average out any 'outlier' trial points. *In vitro* biochemistry involves a lot of troubleshooting to create functioning purified proteins and repeatable assays.

1.3 *In vitro* biochemistry troubleshooting

1.3.1 Protein purification troubleshooting

The biggest hurdle to overcome with *in vitro* experiments is protein purification troubleshooting. When creating new protein constructs for *in vitro*, there are many things to consider: (1) whether a truncated protein amino acid sequence is best; (2) what purification method would produce the highest yield (e.g. affinity tag); (3) whether a fluorescent tag is necessary;

(4) what buffers or conditions would result in stable protein. Many ABPs are often auto-inhibited or contain other regulatory domains. Since *in vitro* experiments bypass signaling pathways, the regulatory domains could be a hindrance. Therefore, unless the regulatory domains are relevant to the experiment, protein truncations are often used *in vitro*.

With the exception of some proteins, most proteins are expressed and purified from *E. coli*. Protein complexes or proteins that require post-translational modifcations are purified from more complex systems. Fission yeast Arp2/3 complex is purified directly from fission yeast cultures [203]. Actin requires post-translational modifications, so it is purified from chicken or rabbit [214]. Bacterial protein expression systems are simpler and often produce high protein yields. Plasmids containing the protein sequence are transformed into a codon optimized *E. coli* strain. Large cell cultures are then grown prior to inducing expression of the protein, and then the bacteria cells are easy to break open to purify the protein.

The affinity tag on a protein is how the construct is isolated from the bacteria 'cell soup', and the different tags each offer their own benefits and drawbacks (reviewed in [114]). Maltose binding protein (MBP) binds amylose resin and is eluted with maltose. MBP is bulky (45 kDa) and maltose is difficult to remove if a second round of resin is required, but MBP increases expression and solubility of a construct preventing it from ending up in the 'cell junk' pellet. Glutathione S-transferase (GST) is a smaller (26 kDa) tag that binds glutathione sepharose and is eluted with glutathione. GST expresses well in bacteria, but the tag dimerizes in solution and can alter a protein's function. GST tags are often used to mimic the dimerization of full protein constructs but with smaller sequences like dimerizing the VCA truncations of WASP. Polyhistidine tags (His-tag) typically consist of two to ten hisitidine residues, but six is the most common length. His-tags bind to immobilized transition metal ions (e.g Ni^{2+}, Zn^{2+}, Ca^{2+}, Co^{2+}, Cu^{2+}, Fe^{3+}). Most resins use immobilized Ni^{2+}, and elution is done with the addition of imidazole to compete for the metal ions and release the His-tag. His-tags are the most common method with the small size and high expression

(reviewed in [114]). However, the use of imidazole is not recommended for purification of proteins that bind metal ions. There are many other affinity tags that could be used for purification, but these three are the most common and used in our lab frequently.

The placement of the affinity tag can affect the protein's activity, so it may be necessary to test constructs with N- or C-terminally tagged proteins. By designing a protein construct with a protein cleavage site between the protein and tag sequences, the affinity tag can be removed following purification. Tobacco Etch Virus protease (TEV) is commonly used [114]. Protease cleavage can be done after elution or often times done on the affinity resin column to elute the protein. Additional column separation (affinity or chromatography) steps must be taken to separate the protein from the tag and protease.

In order for proteins to be seen in fluorescent microscopy, a fluorescent tag must be added. Fluorescent tags can be bulky, so the benefits of visualization must be considered along with the possibility of affecting protein activity. Fluorescent proteins (e.g. GFP, mCherry, mNeonGreen, mKate) produce luminescent light and can be used for both *in vivo* and *in vitro* tracking. However, there are some spectral limitations and photo-bleaching concerns for single-molecule imaging (reviewed in [129]). The most common fluorescent tags used in our lab our actually self-labelling enzymes: SNAP-tag and HaloTag. SNAP-tag (New England Biolabs) is an O^6-alkylguanine-DNA-alkyltransferase that reacts with O6-benzylguanine derivatives, and HaloTag (Promega) is a haloalkane dehalogenase that reacts irreversibly with primary alkylhalides. The fluorescent ligands for these enzymes have been precisely developed to be bright and photostable. A major advantage to using the self-labeling enzymes over the fluorescent proteins is the ability to label portions of the same protein prep with different fluorophores. There are also methods to directly label the proteins, including lysine (amine-reactive reagents) or cysteine (thiol-reactive reagents) labeling. Direct labeling is more convenient, but there has to be an available cysteine or lysine on the surface of the protein. Direct labeling could also cause some issues with

protein activity. There are a lot of decisions when determining whether to fluorescently label a protein.

The final major concern with purified proteins is stability. Buffer composition (e.g. pH, salt concentrations, glycerol) can affect proteins differently. There are general recipes for extraction, elution, and storage buffers that typically work for most proteins. Small alterations to these buffers might be necessary to determine the best conditions for specific proteins.

1.3.2 Troubleshooting and developing in vitro assays

Protein purification is the first round of troubleshooting for *in vitro* biochemistry. There are a lot of biochemistry assay options, and the appropriate assay(s) for the scientific questions must be chosen. Similar to purification, there are general experimental designs. However, the assays must be optimized for the particular question and proteins. This may require alterations to concentrations, timing, or buffers. The experiments must also be reproducible for consistent results. Often times, the scientific question requires an experimental design that differs more than just a few tweaks from the 'cookie cutter' guidelines. Designing a new assay can be as equally exciting as it is frustrating. This dissertation involves the design of new biochemical assays.

1.4 *In vitro* reconstitution assays for biochemical characterization of ABPs

1.4.1 'Bulk' pyrene assembly assays

While this dissertation includes cell level assays, the most direct approach for studying the interactions of ABPs with actin filaments (F-actin) is *in vitro* reconstitution assays. I focused on *in vitro* assays for the majority of my thesis research. Purified proteins are used

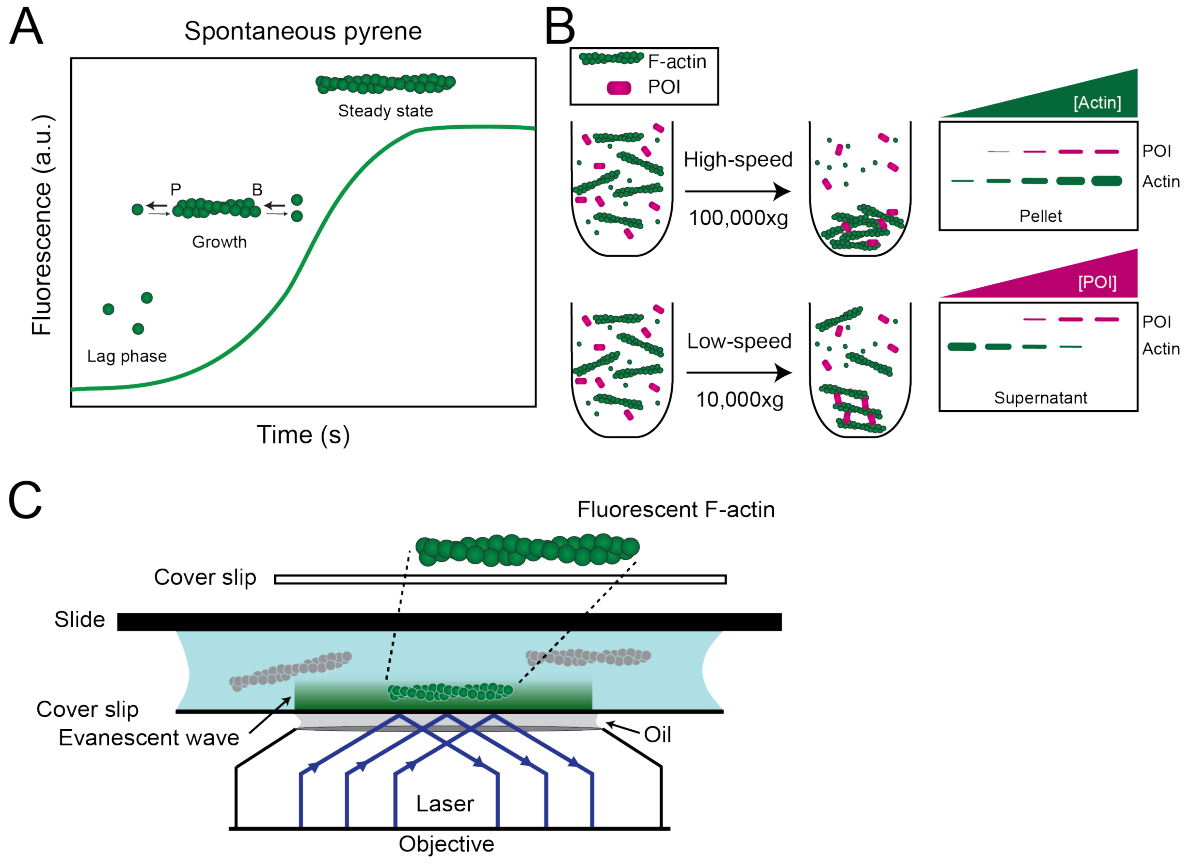

Figure 1.4: ***In vitro* biochemical actin assays. (A)** Schematic of a spontaneous pyrene assembly curve. Actin assembly occurs in three main stages: lag, growth, and steady state. **(B)** Schematic of sedimentation assays. The protein of interest (POI) is incubated with preassembled actin filaments, and the tubes are spun at either a high (100,000xg) or low (10,000xg) speed. The supernatants and pellets are run on an SDS-PAGE gel. **(C)** Schematic of Total Internal Reflection Fluorescence Microscopy (TIRFM) of single fluorescent actin filaments. Flourophores in the flow chamber are illuminated by a laser at a critical angle that enables total internal reflection of the laser within the glass coverslip. This incident light generates an exponentially decaying evanescent wave that only excites fluorescent molecules close to the probe surface (within 200 nm), allowing imaging with high signal-to-noise ratio and reduced background fluorescence [65, 5].

to minimally reconstitute the same F-actin networks that are assembled in cells, but the complexities of additional proteins and signalling pathways are irrelevant for *in vitro* assays. 'Bulk' kinetic assays are an easy way to analyze F-actin assembly and ABP binding. Pyrene assembly assays utilize fluorescent N-(1-pyrenyl)iodoacetamide (pyrene) labeled actin monomer (G-actin) (reviewed in [52]). The fluorescent signal increases/decreases proportionally to F-actin assembly/disassembly. Spontaneous pyrene assays begin with all G-actin, and the resulting assembly curve shows the three stages of actin growth: lag phase (nucleation), growth (elongation), and steady state (Figure 1.4A). These assays are best for comparing actin nucleators. Seeded pyrene assays begin with preassembled dark actin filaments, which then surpasses the lag phase and allows for easier comparison of effects on elongation rate. The kinetic results for 'bulk' assays can be complicated since the assembly curve includes elongation from both the pointed and barbed ends and also nucleation of new filaments from solution. Another limitation of pyrene assays is that changes in assembly and/or disassembly rates is the only readout.

1.4.2 'Bulk' sedimentation binding assays

Pyrene is essential for analyzing how ABPs affect nucleation and/or elongation. However, sedimentation allows for 'bulk' analysis of ABPs that either bind or cross-link F-actin [215]. The protein of interest (POI) is incubated with preassembled actin filaments, and then the tubes are spun at either a high or low speed (Figure 1.4B). High-speed sedimentation pellets polymerized actin, and any protein that is bound to the F-actin will pellet. Typically, a constant concentration of the POI is incubated with an increasing concentration of F-actin. Low-speed sedimentation pellets cross-linked F-actin, and the supernatant reveals depletion of F-actin with an increasing concentration of the POI. Sedimentation assays are used to determine the actin binding affinities and for competition assays.

1.4.3 Total Internal Reflection Fluorescence Microscopy (TIRFM)

Total internal reflection fluorescence microscopy (TIRFM), unlike the 'bulk' assays, allows for direct visualization of ABPs and F-actin. TIRFM was originally developed to image the contact regions of a growing cell culture and the glass surface. With additional modifications and the use of lasers, the method was adapted for fluorescent microscopy of fluorescent molecules within an aqueous solution [5, 65]. TIRFM is a type of microscopy that relies on a special objective, distinct low incidence angles of the incoming excitation laser, and an interface between two media with different refractive indices. Typically an aqueous reaction is added to a glass chamber. Excitation light is totally internally reflected within the glass coverslip, and an elctromagnetic field (evanescent wave) is created at the interface of the glass coverslip and the aqueous reaction. The evanescent wave is exponentially decaying, and therefore, only fluorophores within 200 nm of the coverslip are excited. The benefits of this small illumination volume include: (1) background 2,000-fold lower than normal epifluorescence, resulting in a much higher signal-to-noise ratio; (2) low light exposure, which lowers risk of photobleaching (Figure 1.4C) [5].

TIRFM is a very useful tool for visualizing single molecules, and our lab uses it to study fluorescently labeled actin filaments and interactions with ABPs. We can watch actin assembly in real time and investigate the kinetics of ABP with F-actin. Unlike 'bulk' biochemical assays, TIRFM allows us to visualize individual interactions, and we can distinguish between nucleation and elongation of actin filaments. Therefore, the combination of bulk assays and TIRFM can reveal a lot of information about F-actin and ABP dynamics. Thus, we can take advantage of *in vitro* biochemistry assays to investigate the molecular mechanisms of isolated F-actin structures and apply those results to cell observations to further our understanding of how distinct F-actin networks assemble simultaneously.

1.5 Summary

There are diverse F-actin networks within a cell that have specific roles in cell processes, and the dynamics of those F-actin networks can be studied both *in vivo* and *in vitro* with benefits and drawbacks to both approaches. *In vitro* biochemistry offers a bottom up approach to investigating F-actin networks. It is imperative to understand the characteristics of each individual component of the network to understand how the elements assemble to form specific F-actin networks with appropriate structural and dynamic properties essential for the corresponding cellular function. Minimal reconstitution assays utilize the well-characterized ABPs to rebuild F-actin structures with the fundamental components. Reconstitution offers a method to study the F-actin networks found in cells without the complications of unknown variables. These reconstitution *in vitro* approaches have contributed to our understanding of how distinct F-actin networks are built from the same pool of proteins and coincide in the same cytoplasm simultaneously.

The studies included in this dissertation utilized a wide range of experiments, but I focused on *in vitro* minimal reconstitution of F-actin networks to study the localization and mechanistic properties of different ABPs. My primary project was investigating the mechanosensitive LIM domain proteins. How actin binding proteins (ABPs) respond to mechanical forces is a relatively new question in cell biology. Recent research has shown that mechanical forces alter the actin binding affinity of several different ABPs [106]. LIM domain proteins make up a large fraction of the recently identified mechanosensitive ABPs. The main focus of my thesis research was to further understand how LIM domain proteins localize to stressed F-actin networks. My secondary project was investigating the branching pathway of Arp2/3 complex by purifiying and fluorescently labeling Arp2/3 complex from fission yeast. Through a combination of *in vivo* cell biology and *in vitro* reconstitution assays, this dissertation investigates the mechanosensitive recruitment of LIM domain proteins to

stressed F-actin networks and the branching pathway of Arp2/3 complex.

CHAPTER 2

LIM DOMAIN PROTEINS IN MECHANOBIOLOGY

Preface

This chapter is a recently accepted review for *Cytoskeleton* journal titled "LIM domain proteins in mechanobiology." The review covers the previous research about LIM domain protein mechanosensitivity. We included the most recent work from our group (Chapter 3: "Evolutionarily diverse LIM domain-containing proteins bind stressed actin filaments through a conserved mechanism") and the Alushin lab. I wrote the majority of the review with additional information and edits added by the other authors: David Kovar, Margaret Gardel, and Jon Winkelman.

2.1 Abstract

The actin cytoskeleton is important for maintaining mechanical homeostasis in adherent cells, largely through its regulation of adhesion and cortical tension. The LIM (Lin-11, Isl1, MEC-3) domain-containing proteins are involved in a myriad of cellular mechanosensitive pathways. Recent work has discovered that LIM domains bind to mechanically-stressed actin filaments, suggesting a novel and widely conserved mechanism of mechanosensing. This review summarizes the current state of knowledge of LIM protein mechanosensitivity.

2.2 Cells sense and respond to mechanical forces

Mechanical force plays an essential role in the control of cell shape and motion and serves as a key input in mechanotransduction pathways controlling cell survival, growth, and fate. Cells are subject to a myriad of external forces (e.g. tension, compression, shear), including those from neighboring cells, fluid flow, or osmolarity. In addition to these, mechanoenzymes

within the cell interior generate forces that are transmitted across cellular scales via the cytoskeleton. These internally generated forces enable cell shape change and are critical to cellular mechanosensing (e.g. environmental stiffness sensing) [228]. Cells sense and convert mechanical stimuli into chemical signals to initiate downstream signaling pathways [241]. Examples of force-sensitive chemistries of cytoplasmic proteins include force-dependent changes in binding affinity (e.g. integrins, actin binding proteins) or enzymatic activity (e.g. myosin II) [78, 106]. These molecular-scale transducers can then give rise to mechanical sensitivities of cytoskeletal arrays and/or regulate signaling and transcriptional pathways.

The ability to sense and respond to these forces directs many cellular processes, and any defects in mechanotransduction can lead to problems for those same cellular processes. Blood vessels experience shear stress and tension from the flow and pressure of the blood, and the biochemical response is expression of a corresponding set of genes that help maintain the integrity of the vascular system [28, 160, 131]. Medical conditions, like diabetes and hypertension, alter the blood vessel stiffness which negatively affects the mechanotransduction pathway and increases likelihood of cardiovascular diseases [2, 195]. Epithelial tissue homeostasis is also controlled by tensile and compressive forces. Cell stretching drives cell division and subsequently proliferation, while overcrowding compresses cells and results in cell extrusion [183, 97, 81]. The tissue level response to these forces maintains the cell number and prevents tumors [60]. While mechanotransduction pathways are well appreciated in cell physiology, we are just beginning to understand the diversity of force-sensing mechanisms within the cytoskeleton.

2.3 Mechanosensing in adherent cells

The actin cytoskeleton is a common component between sensing, transmitting, and producing mechanical forces. Cells are mechanically coupled to their local environment through adhesions to the extracellular matrix (ECM) (e.g. focal adhesions, FAs) and surrounding

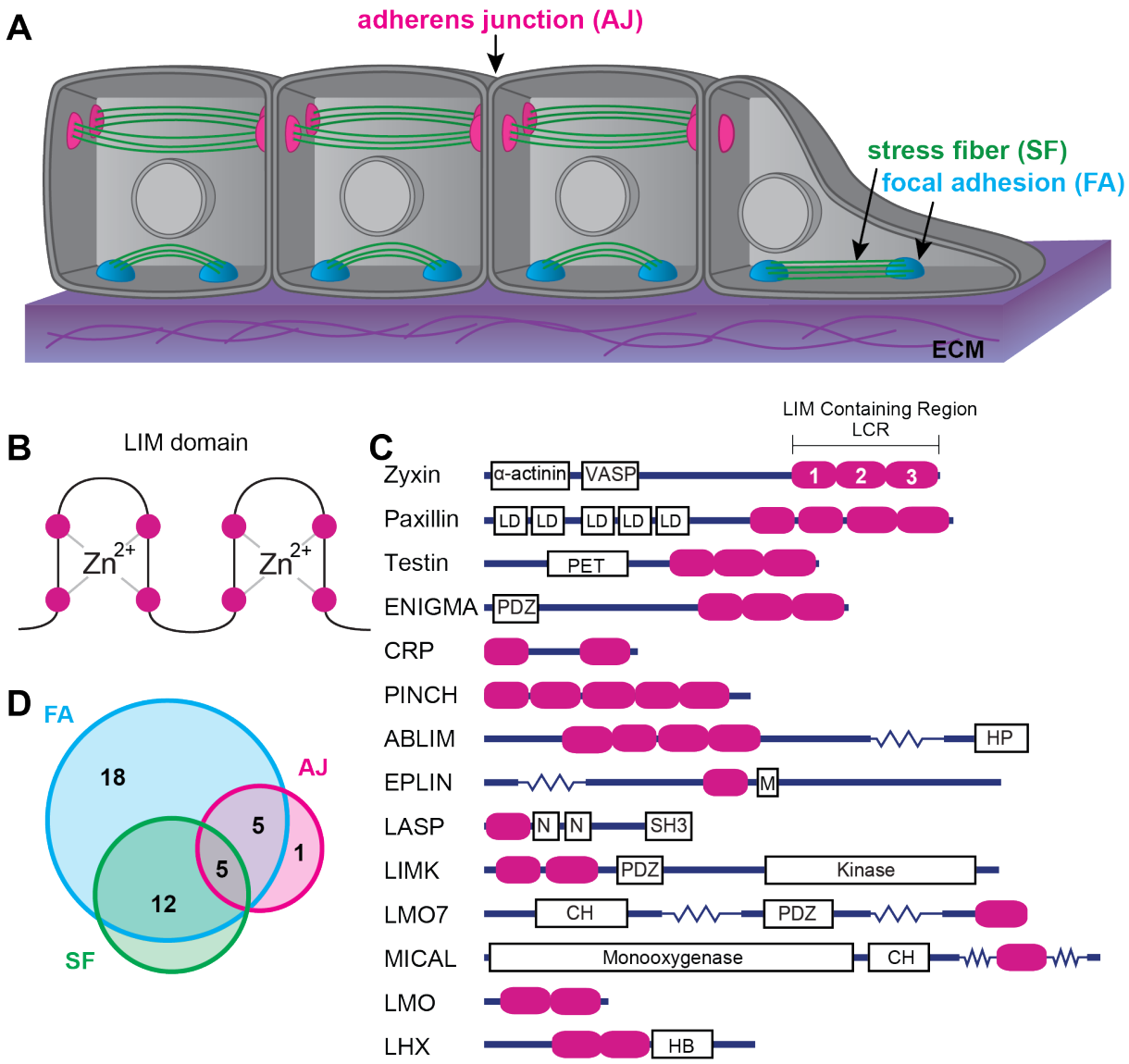

Figure 2.1: **Mechanically stressed cells and LIM domain proteins.** **(A)** Schematic of a layer of epithelial cells on top of an extracellular matrix (ECM). **(B)** Simple schematic of a LIM domain: two zinc finger motifs. The magenta circles represent the well-conserved residues (typically cysteine or histidine) that chelate the zinc molecules. The remaining amino acid sequence varies between LIM domains. **(C)** Domain organization of the fourteen classes of LIM domain proteins. Magenta ovals represent individual LIM domains. Zigzag lines are used to abbreviate a few rather long structures. Other domain abbreviations: leucine rich aspartate domains (LD), Prickle, espinas, testin (PET), membrane anchoring domain (PDZ), headpiece domain for F-actin binding (HP), Myo5B interacting domain (M), nebulin (N), Src homology 3 (SH3), calponin homology (CH), and homeobox (HB). **(D)** Venn diagram showing the overlap of LIM domain proteins that associate with the 3 main networks: focal adhesions (FA), adhesion junctions (AJ), and stress fibers (SF).

cells (e.g. adherens junctions, AJs) (Figure 2.1A). The actin cytoskeleton connects adhesions and transmits forces across the cell. Force sensitivity of adherent cells underlies adhesion regulation, cellular force generation, and mechanical properties of cells and tissues [13, 40, 66, 150, 159, 240, 254, 256]. The mechanical properties of a cell's environment are reflected by the actin cytoskeleton architecture. For example, F-actin networks in cells that are growing on rigid matrices, or within tissues that are being stretched, respond by self-organizing into thick bundles and larger FAs, which is thought to be important for generating and withstanding increased force [210, 253].

The actin cytoskeleton includes many different actin filament (F-actin)-based networks that vary in organization and composition. The architecture of FAs and AJs is comprised of stratified layers of distinct proteins that work together to transmit forces sensed by membrane-spanning adhesion receptors to actin filaments [30, 67, 109, 255]. Both FAs and AJs exhibit force-dependent changes to their composition and size, which is typically mediated by myosin-II activity within the actin cytoskeleton but can also be driven by external force [121, 189].

Stress fibers (SFs) are contractile bundles of 10-30 actin filaments of mixed polarity and alternating regions of the crosslinker α-actinin and non-muscle myosin, reminiscent of the sarcomeric organization in striated myofibrils [41, 94, 226]. While sarcomere architecture allows for recurring contraction and relaxation cycles, the less organized SF is built for continuous isometric contraction [23, 169]. SF formation, growth, orientation, and maintenance are sensitive to both externally and internally generated forces [37]. The constant tension makes SFs susceptible to damage, and localized damaged regions form spontaneously or in response to the application of external forces [210]. Thus, repair of such SF strain sites (SFSS) is important for maintaining the mechanical homeostasis of the actin cytoskeleton, allowing cells to maintain their integrity and adapt to force fluctuations. It is likely that the rearrangements of actin cytoskeleton networks in response to external force may also

be driven by a similar force-induced remodeling. For instance, repeated cycles of uniaxial stretch results in both SF thickening and reorientation perpendicular to the stretch axis [113, 253].

Recent progress has elucidated the force-dependent biochemistry of actin binding proteins (e.g. cadherins, vinculin, talin, alpha-catenin) [21, 96, 100, 140, 238]. These studies have primarily considered how forces applied to actin binding proteins (ABPs) alter their binding affinity to F-actin. However, the actin filament itself can twist, stretch, and compress, which may also alter the binding affinity of ABPs [71]. In this scenario, the actin filament itself is the force responsive element and could confer mechanical information about the cell and its environment to various signaling and transcriptional pathways [47, 62].

2.4 LIM domain proteins in mechanotransduction pathways

Proteomic screens of mechanotransduction pathways have revealed an abundance of proteins that contain one or more LIM (Lin-11, Isl1, MEC-3) domains [68, 111, 243]. The LIM domain is a 60 amino acid sequence that forms a double zinc finger protein-protein or protein-DNA binding interface [144] (Figure 2.1B). LIM domains occur in diverse multidomain protein organizations and are found in a wide range of eukaryotic proteins (LIM proteins), including 70 human genes that can be divided into 14 classes (Figure 2.1C) [115]. Early in the evolution of animal multicellularity, there was a large expansion in the number of LIM proteins as well as LIM 'promiscuity', i.e. LIM has combined within multidomain proteins with many other domains of different structure and function [8, 115]. This domain promiscuity has resulted in a functionally diverse LIM protein family whose members play roles in a variety of biological processes but especially those implicated in generating and responding to mechanical forces (Figure 2.1C, Table 2.1) [108, 211].

There are 41 LIM proteins found to be enriched at cell adhesions and/or the actomyosin cytoskeleton [211] (Figure 2.1D). To date, 26 LIM proteins have been identified in FAs

LIM protein	**Localization**	**LCR-dependent**	**Binding partners**	**Mechanotransduction pathway**
Zyxin	FA, AJ, SF	Yes	α-actinin, VASP	Ena/Vasp
Paxillin	FA, SF	Yes	Vinculin, FAK, Src	Rho GTPases, Microtubules
LIMD1	AJ, FA	Yes	WTIP, LATS1	HIPPO
Ajuba	AJ	Yes	α-catenin, retinoic acid receptor	HIPPO, Rac
FHL2	FA	Yes	Integrin, actin, titin, β-catenin	Wnt, cell cycle, p21
Testin	FA		Calcium sensing receptor	Rho kinase
Prickle	FA		CLASPs, LL5-β, Disheveled, membrane	Microtubules and CLASPs, Frizzled/Dischevelled, Wnt2
Pdlim5	FA		α-actinin, protein kinase C, protein kinase D, ID2	TGF-beta
Pdlim7	FA			YAP
TRP6	AJ		Vinculin, LATS1/2	

Table 2.1: **A subset of LIM domain proteins and their corresponding mechanotransduction pathways.** There is a wide range of information known about LIM domain proteins in mechanotransduction pathways: Zyxin [53, 92, 127, 185, 209, 230], Paxillin [20, 46, 57, 134, 229, 242, 245], LIMD1 [99, 102, 217], Ajuba [42, 95, 102, 138, 180, 184], FHL2 [104, 155], Testin [136, 211], Prickle [31, 128, 222, 234], Pdlim5 [32, 31, 120], Pdlim7 [61, 120], and TRP6 [55].

(including zyxin, paxillin, and LIMD1), and the localization of 21 of these is sensitive to myosin II activity [121, 197]. Similarly, at least 11 LIM proteins display force-sensitive localization to AJs. Numerous LIM proteins co-localize to both FAs and SFs, FAs and AJs, or all three organelles (Figure 2.1D). Some LIM proteins contain known actin binding

domains (e.g. the (CH) domain) that could drive their localization to F-actin networks. However, many that localize to the actin cytoskeleton lack these. Standard biochemical approaches have not found constitutive binding of LIM domains to actin filaments. One notable exception is the CRP class, which canonically binds and bundles actin filaments via their LIM domains [80, 224]. CRP is an ancient class as it is the only mammalian LIM protein class also found in plants, suggesting the possibility that canonical actin binding could be an ancestral function of the LIM domain. For instance, Muscle LIM protein (MLP) is a CRP class protein that has been implicated in mechanoresponse to muscle sarcomere stretching [231].

Several studies have implicated LIM proteins in cell signaling and gene expression mechanotransduction pathways [102, 139]. For instance, four-and-a-half LIM domains 2 (FHL2) is implicated in mechanical regulation of the cell cycle. On a soft matrix, FHL2 dissociates from F-actin networks and becomes more concentrated in the nucleus where it acts as a transcriptional cofactor to increase p21 gene expression, which regulates cell cycle progression and inhibits growth [155]. Most force-sensitive LIM proteins display nuclear shuttling raising questions as to whether detection of forces via LIM proteins is connected to localization and function inside the nucleus (Figure 2.2A). Similarly, several LIM proteins in the Ajuba/Zyxin classes exhibit force-dependent binding to AJs to regulate hippo and Yap/Taz signaling pathways [182, 183].

2.5 Force-sensitive localization of LIM proteins in adherent cells

The LIM domain-containing region (LCR) has been found to drive the subcellular localization for a large number of LIM proteins [20, 92, 209]. This has been dissected most carefully for the LIM protein zyxin, which localizes to SFs, FAs, and AJs in a force-dependent manner. Zyxin is necessary for stretch-mediated SF remodeling, SFSS repair, and FA maturation [92, 209, 211, 253]. The LCR of zyxin resides at the C-terminus and contains three LIM

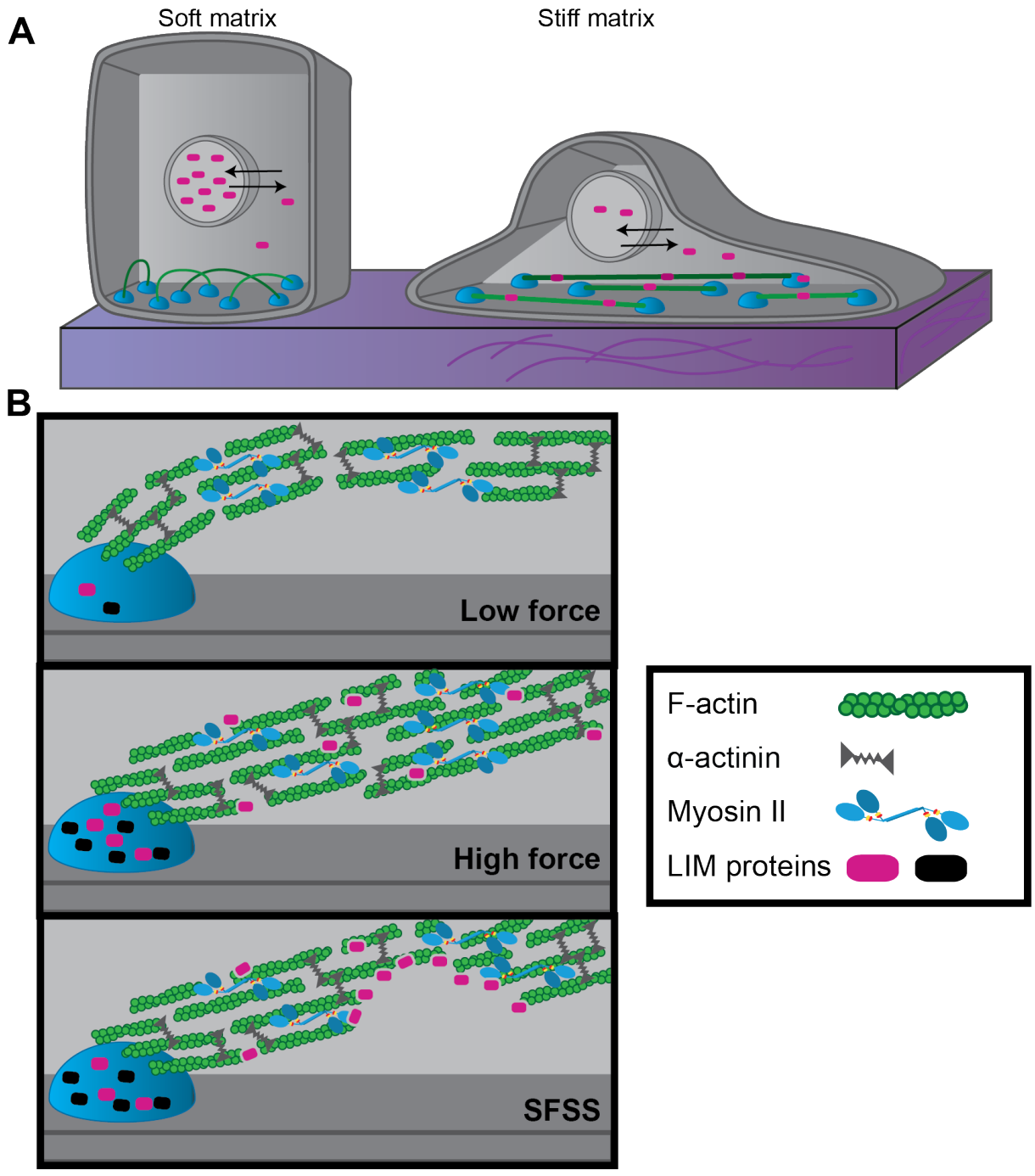

Figure 2.2: **Schematic of LIM domain protein localization in cells. (A)** Nuclear shuttling of LIM domain proteins (magenta ovals) occurs when cells spread out on stiff matrices. **(B)** LIM domain proteins (black and magenta ovals) localize to FAs and SFs under high tension. A subset of LIM domain proteins localizes to stress fiber strain sites (SFSS).

domains in tandem separated by short unstructured linkers. The LCR is required for zyxin recruitment to SFSS and FAs. For full length zyxin, any one of the individual LIM domains are not sufficient for its localization [230]. Recent results demonstrate that at least two tandem repeats of LIM1 or LIM3 are sufficient for LCR localization to SFSS [247], but further work is needed to demonstrate this sufficiency for the full-length protein. Once localized, zyxin's N-terminal functionality mediates SFSS repair by recruiting factors that promote actin filament polymerization (Ena/VASP) and crosslinking (α-actinin) [211]. Therefore, the LCR regulates force-sensitive recruitment, while the functional role is dependent on the additional domains [210].

2.6 LIM domains from diverse proteins bind stressed actin filaments

Recent research has made progress in understanding the mechanism of LIM protein force-sensitive localization to the actin cytoskeleton. Two studies used complementary experimental approaches to screen LIM proteins for force-sensitivity in cells. One employed cell stretching experiments to systematically quantify the enrichment of full length and LCR constructs of LIM proteins on stretched SFs [218], while the other quantified LCR recruitment to SFSS [247]. Together, these studies identified force-sensitive LCRs in 18 LIM proteins from Zyxin, Paxillin, Tes, and Enigma classes from both animals and yeasts [218, 247]. These complementary experimental approaches revealed that cytoskeletal strain sensing via the LIM domains is widespread in cells and existed in the last common ancestor of yeasts and animals.

To isolate the force-sensitive substrate of LIM, both groups used *in vitro* approaches to reconstitute force-sensitive recruitment with a minimal set of purified components [218, 247]. Two types of *in vitro* reconstitution assays were utilized to test the stress sensitivity of a subset of LIM proteins, and both showed localized recruitment of LIM domains directly

to mechanically stressed regions of F-actin. Sun et al. applied tensile stresses to actin filaments with a modified gliding filament assay. Single filaments were pulled in opposite directions via surface-attached myosins with barbed (myosin V) and pointed (myosin VI) end directionality. LIM proteins localize to actin filaments only after initiation of myosin activity facilitates tensed filaments. Actin filament breakage, coinciding with stress relief, results in LIM protein dissociation. Similarly, Winkelman et al. reconstituted contractile actin networks comprised of F-actin, α-actinin, and myosin II. After addition of myosin II to initiate contraction, LCRs localize to stressed regions of the network due to contractile forces, particularly to bundle sites just prior to their rupture, after which the LCR dissociates from the actin filaments.

To understand the mechanism by which LIM domains bind F-actin, these studies identified particular amino acids and LIM domain architectures that are necessary for binding. With the exception of eight well-conserved residues (cysteine and histidine) responsible for Zn^{2+} chelation, the sequence of LIM domains is highly variable. However, a phenylalanine resides at a similar position in all strain sensing LIM domains and was found to be necessary for force sensitivity [218]. Additionally, force-sensitive LCR all have three or more LIM domains in tandem, each separated by a short linker. Alterations to this organization in the LIM protein zyxin revealed that multiple LIM domains, when organized in tandem and connected by short linkers (serial), but not when oligomerized (parallel), contribute additively to stressed F-actin binding [218, 247]. Together, these data lead to a hypothesis that multiple LIM domains that are appropriately positioned interact via a hydrophobic interaction with a strained actin filament (Figure 2.3).

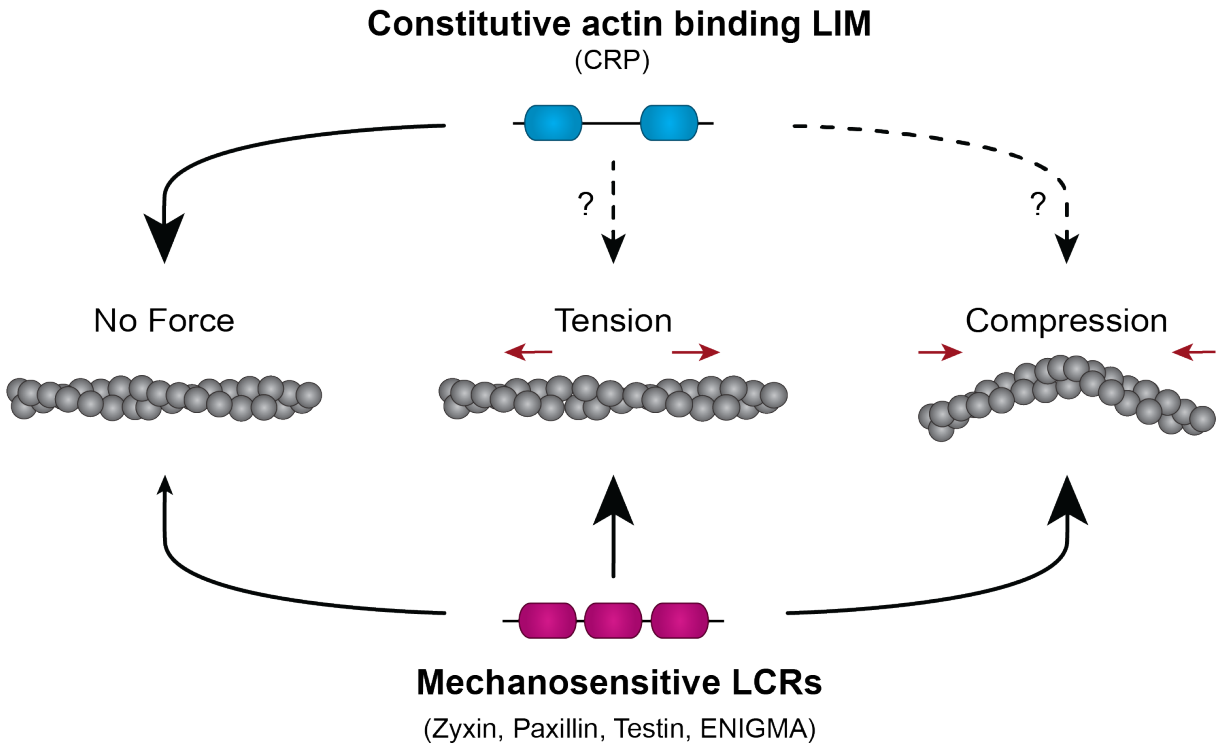

Figure 2.3: **Schematic of mechanosensitive LCR localization to stressed actin filaments.** The constitutive actin binding CRP class LIM proteins bind actin filaments in the absence or presence of force. The dashed lines indicate that CRP localization is suspected to occur for stressed actin filaments but has not been fully investigated. Mechanosensitive LIM domain protein LCR constructs bind with high affinity to actin filaments under tension or compression but with low affinity to relaxed filaments (adapted from [247]).

2.7 Evolutionarily conserved mechanism of LIM domain-based force sensing

Interestingly, despite the lack of sequence conservation in strain sensing LIMs, binding to stressed actin filaments appears to be an ancient function of the LIM domain. Strain sensing LIM domains may have a conserved tertiary structure despite primary sequence variability, similar to other well studied protein folds [49]. For instance, the LCR of the fission yeast paxillin 1 (Pxl1) binds to both SFSS in mammalian cells and purified strained vertebrate F-actin in vitro [247]. Fission yeast do not have stress fibers (or SFSS), but there is a phenomenon analogous to SFSS that occurs within the yeast cell. Pxl1 localizes to the cytokinetic contractile ring (CR), and its deletion results in fragmentation of the ring during contraction [74]. The rupture of the contractile ring in Pxl1 mutants is reminiscent of increase rupturing of stress fibers observed in zyxin null cells [210]. Indeed, there are many interesting parallels between CRs and SFs. Both are composed of similar molecular components and are arranged in an architecturally similar way: antiparallel bundled actin filaments crosslinked by α-actinin and pulled on by myosin II. Both may also display a rough sarcomeric pattern where α-actinin and myosin form complementary domains [226]. The contractility of these networks must be regulated so that they remain tense but do not rip themselves apart. While SFs remain roughly the same length, the CR must shorten during constriction to pinch the mother cell into two daughters. The organization of the CR, SF, and muscle sarcomere may be a coincidence or belie a common origin. Since we first see clear versions of myosin II, α-actinin, and strain-sensing LIM proteins in the unikont branch of eukaryotes, the ancestral version of these contractile networks may have emerged near this branch.

Once contractile machinery arose in evolution, the cell must have evolved regulatory mechanisms for their maintenance and repair. The strain sensing LIM domain may represent one way in which cells learned to detect stressed F-actin. Other domains may be added to

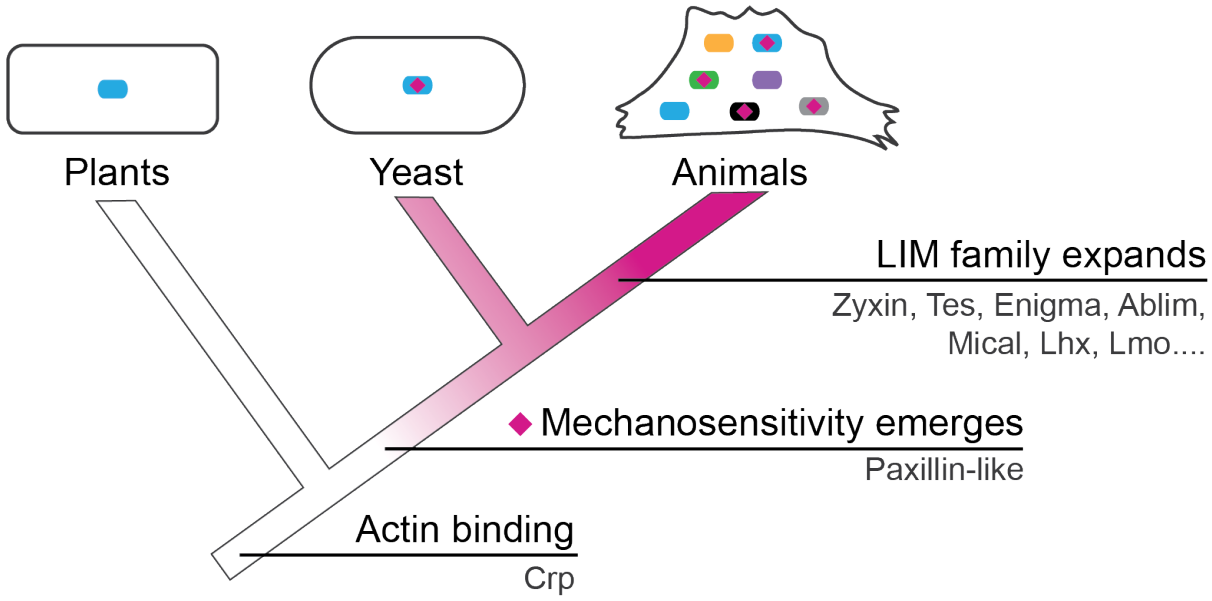

Figure 2.4: **Evolution of LIM domain proteins.** LIM domains have evolved over time to become mechanosensitive. The family then expanded to include a diverse population of proteins in mammals (adapted from [247]).

this LIM containing protein to tailor responses to LIM-detected stress, for example, some LIM proteins contain domains that bind actin assembly factors that enable these proteins to recruit actin assembly factors to sites of mechanical stress that has been detected by LIM [92, 210]. One hypothesis for the development of strain sensitive LIM domains is that general actin binding by LIM was tinkered with by evolution to tune it to bind strained actin filaments. The most ancient and widespread LIM proteins are in the CRP family and have been shown in multiple studies to bind unstressed actin filaments [80, 244], suggesting the possibility that generic actin binding may be an ancestral function of LIM domains that was tuned to bind strained F-actin (Figure 2.4).

2.8 The actin filament is a substrate for force-sensitive binding

The load dependent mechanical response of F-actin networks is likely to arise from force-sensitive biochemistry of ABPs. A recent review summarizes evidence for force-sensitivity

for several ABPs (e.g. Arp2/3 complex, cofilin, alpha-catenin) [106]. Filament curvature promotes the binding of Arp2/3 complex binding to F-actin, while tension decreases the stability of an Arp2/3 complex-mediated daughter branch [166, 188]. There are conflicting reports of how tension may impact the binding of F-actin depolymerizing factor cofilin [88, 250], while additional research suggests torsion may impact cofilin's F-actin severing rate [146, 250]. Low tension applied directly to an actin filament increases the binding of alpha-catenin to adjacent actin subunits, and the force detection is attributed to a 35 amino acid region at the C-terminus [140]. We hypothesize that similar sensing may occur in LIM protein, but will require further investigations.

As a common component in these mechanosensitive networks, it is likely that the actin filament itself is a force sensor whereby the force-induced conformation of actin filaments affects the binding interactions of the ABPs. There are many studies and hypotheses about how mechanical forces may alter filament conformation, but there is no explicit structural data comparing stressed and unstressed actin filaments [71]. Modeling has shown that due to the twist of an actin filament, strain is not distributed homogenously throughout the filament, and localized regions of strain may result [198]. Therefore, the filament level force can impact the conformation of and interactions between adjacent subunits. These subunit level alterations could possibly reveal additional binding sites for ABPs. We hypothesize that LCRs recognize a binding site along an actin filament that is revealed under tensile or compressive stress [247]. Additional research will be required to fully understand the binding interface of LCRs and mechanically stressed actin filaments. LIM domain proteins, and even isolated strain sensing LCRs, display overlapping but non-identical localization to stressed actin networks, raising the question of how specificity for particular networks arise. Additionally, stressed actin binding is distributed across several protein families involved in diverse cellular processes. Lastly, an important remaining question that will require extensive investigation is how binding by LIM to stressed actin filaments might regulate these diverse

cellular processes.

CHAPTER 3

EVOLUTIONARILY DIVERSE LIM DOMAIN-CONTAINING PROTEINS BIND STRESSED ACTIN FILAMENTS THROUGH A CONSERVED MECHANISM

Preface

The work in the following chapter was done in collaboration with Jon Winkelman, a previous graduate student of the Kovar lab and current postdoc in the Gardel lab. The project was initiated by Jon, and I became a part of the project while he mentored me during a rotation in the Gardel lab. Jon completed the *in vivo* portion of the project and some analysis of the the *in vitro* work. I was responsible for the majority of the *in vitro* work, including construct creation, biochemical characterization, troubleshooting, and the TIRFM contractile assays. Cristian Suarez collaborated with us to to add my protein constructs into his motile bead assay. Jon took the lead in writing the manuscript, and I was responsible for merging our styles to create consistent and presentable figures.

3.1 Abstract

The actin cytoskeleton assembles into diverse load-bearing networks including stress fibers, muscle sarcomeres, and the cytokinetic ring to both generate and sense mechanical forces. The LIM (Lin11, Isl- 1 & Mec-3) domain family is functionally diverse, but most members can associate with the actin cytoskeleton with apparent force-sensitivity. Zyxin rapidly localizes via its LIM domains to failing stress fibers in cells, known as strain sites, to initiate stress fiber repair and maintain mechanical homeostasis. The mechanism by which these LIM domains associate with stress fiber strain sites is not known. Additionally, it is unknown how widespread strain sensing is within the LIM protein family. We identified the

LIM domain-containing region of 18 proteins from the Zyxin, Paxillin, Tes, and Enigma proteins accumulate to stress fiber strain sites. Moreover, the LIM domain-containing region from the fission yeast protein paxillin like 1 (Pxl1) also localizes to stress fiber strain sites in mammalian cells, suggesting that the strain sensing mechanism is ancient and highly conserved. We then use sequence and domain analysis to demonstrate that tandem LIM domains contribute additively, for sensing stress fiber strain sites. Employing *in vitro* reconstitution, we show that the LIM domain-containing region from mammalian zyxin and fission yeast Pxl1 bind to mechanically stressed F-actin networks but do not associate with relaxed actin filaments. We propose that tandem LIM domains recognize an F-actin conformation that is rare in the relaxed state but is enriched in the presence of mechanical stress.

3.2 Introduction

Cells are subject to a wide range of omnipresent mechanical stimuli, which play essential physiological roles. Epithelial tissue stretch modulates cell proliferation [183, 97], blood pressure regulates the contractility of endothelial cells within blood vessels [28, 160], and muscle contraction shapes connective tissue remodeling [25]. Such mechanotransduction pathways allow for the integration of mechanical cues with the biochemical and genetic circuitry of the cell. While much progress has been made to elucidate the importance of mechanical stimuli in cell physiology, the underlying force-sensing mechanisms and organizational logic of many mechanotransduction pathways are unknown. To respond to mechanical cues and dynamically modulate cell mechanics, the actin cytoskeleton exploits force-sensitive biochemistry to construct actin filament (F-actin)-based network assemblies. Focal adhesions, the adhesive organelles between cells and their external matrix, can change in composition and size under varied mechanical load [219]. At the molecular scale, these focal adhesion changes arise primarily from force-dependent modulation of constituent proteins [219, 121, 197]. The force-dependent association of the focal adhesion proteins, vinculin and talin, to actin filaments

is sensitive to filament polarity [162, 96], providing a mechanism to guide local cytoskeletal architecture under load. Protrusive forces at the leading edge of migrating cells are generated by actin polymerization into short-branched F-actin networks [174]. Compressive stress increases the actin filament density, which, in turn, alters its force generation potential [13]. At the molecular scale, this mechanical adaptation of lamellipodial networks may arise from increased branch formation efficiency by the actin nucleator Arp2/3 complex on extensionally strained sides of bent actin filaments [188]. Although cofilin was reported to have a reduced affinity for tensed actin filaments [88], this has recently been called into question [250]. While direct evidence for detection of stressed actin by actin binding proteins is still scant, the structural polymorphism in actin filaments suggests that force-induced conformations exist and could be recognized by actin binding proteins [71]. There may be information about the mechanical state of the cell stored within these actin filament conformations available to be read by actin binding proteins that regulate various mechanotransduction pathways.

Within adherent cells, F-actin bundles known as stress fibers (SFs) generate contractile force across the cell and, via focal adhesions, are coupled to the extracellular matrix. SFs dynamically re-arrange over long (hour) time scales in response to forces applied to the extracellular matrix [92], and this remodeling process requires zyxin and paxillin [92, 209, 253, 210, 211]. At short times, mechanical failure of the SF can occur either spontaneously or in response to applied force [209, 210]. At such damage sites, the SF is locally weaker, leading to a localized retraction to create a stress fiber strain site (SFSS) [210] (Figure 3.1A). Rather than irreversible failure, a repair process at the SFSS is initiated by the rapid accumulation of zyxin and followed by the recruitment of binding partners VASP and α-actinin to promote actin assembly and cross-linking to repair the SF and maintain mechanical homeostasis [210] (Figure 3.1A). The recruitment of VASP and α-actinin require known interactions at the zyxin N-terminus [211]. However, the recruitment of zyxin to SFSS occurs through a region near the C-terminus that contains three tandem Lin11, Isl-1 & Mec-3 (LIM) domains

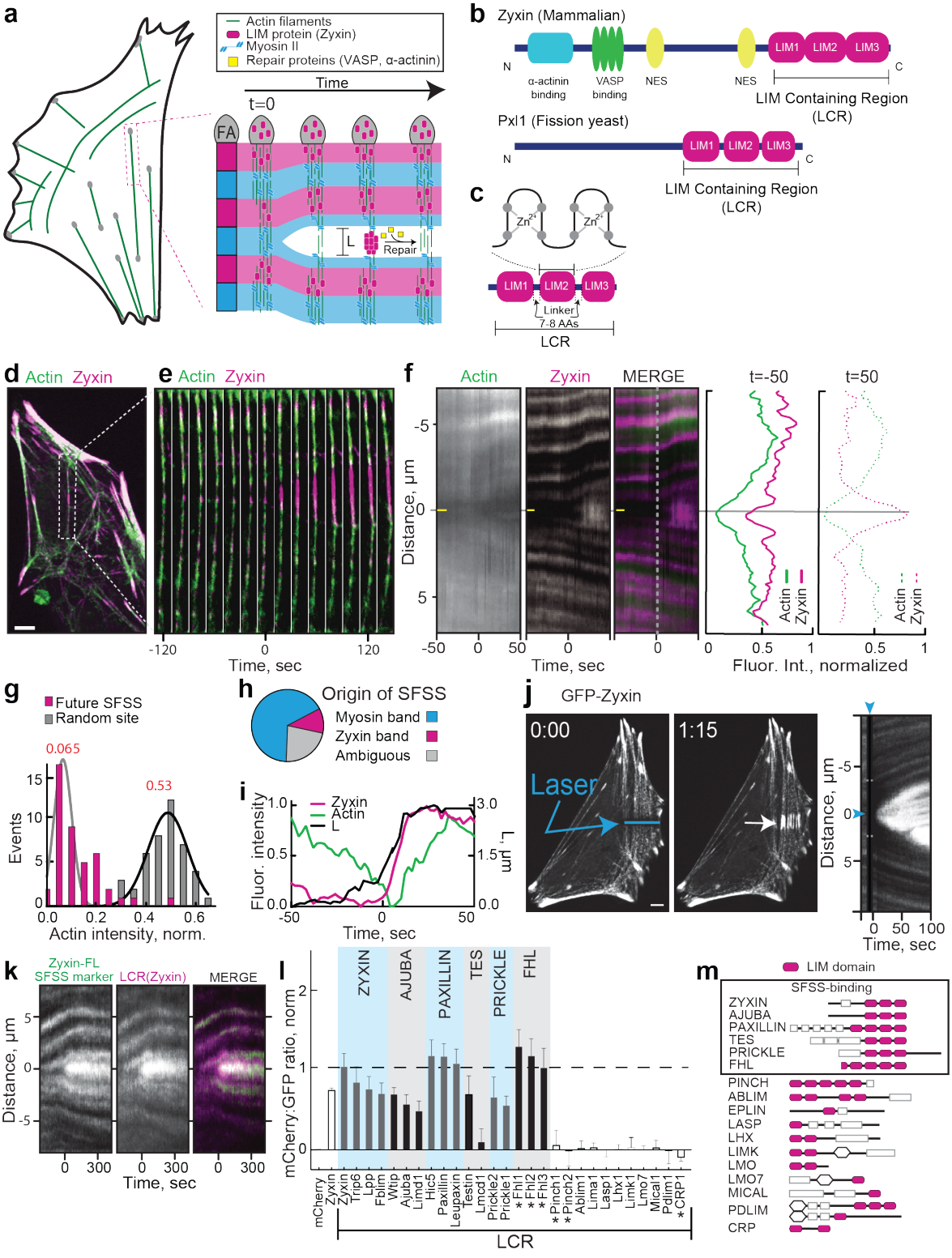

Figure 3.1: **Diverse LIM domains localize to SFSS.**

Figure 3.1: (continued) **(A)** Cartoon of a fibroblast cell with actin stress fibers. Schematic of the development and repair of a stress fiber strain site (SFSS). FA=Focal adhesion. L is distance across the SFSS. **(B)** Domain organization of the LIM domain (pink ovals)-containing proteins mammalian zyxin and fission yeast Pxl1. Zyxin also contains binding sites for α-actinin (F-actin crosslinker) and VASP (F-actin elongation factor), and two nuclear export sequences (NES). LIM containing regions (LCR) are indicated. **(C)** Each LIM domain contains two zinc finger binding domains with conserved residues (cysteine/histidine, grey circles) to chelate the zinc, but the remaining sequence varies between different LIM domains. The linker length between adjacent LIM domains is 7-8 amino acids. **(D-I)** Analysis of SFSS in mouse embryo fibroblasts (MEF) with stably integrated GFP-zyxin and transfected mApple-actin. Scale bar=5 μm. **(D-E)** Fluorescent micrograph (D) and associated montage (E) of a representative stress fiber over time showing accumulation of zyxin on a developing SFSS. **(F, left)** Kymographs of the same event: actin channel (left), zyxin channel (middle), and a merged image (right). The future SSFS (horizontal yellow line) indicates where background measurements for (G) and a later screen will be taken. Vertical dotted line indicates when strain has begun at t=0. **(F, right)** Average fluorescence intensity line scans of 74 SFSS, measured 50 seconds before and after initiation. **(G)** Histogram of actin intensities at a future SFSS (about 50 seconds prior) and random sites on the same stress fiber. **(H)** Pie chart showing the distribution of where SFSS occurred. **(I)** Kinetics of zyxin accumulation and actin depletion and reassembly (left y-axis), and distance across the SFSS indicated as L in (A) (right y-axis), for a representative SFSS. **(J)** Left, fluorescent micrographs showing laser induction of a SFSS in a representative MEF cell with stably integrated GFP-zyxin. Blue line shows where light was targeted, and white arrow denotes developing SFSS. Scale bar= 5 μm. Right, kymograph showing this event over time, with blue arrowheads indicating time and location of laser light. **(K)** Representative kymograph of the laser-induced SFSS screen, from a cell expressing GFP-zyxin and LCR(zyxin)-mCherry. **(L)** Screen of 28 LIM domain proteins from Mus musculus. Y-axis is the mCherry:GFP ratio at the strain site, error bars=95% CI. LCR constructs were used for all but those marked with *, for which the whole protein sequence was used. **(M)** Domain organizations of LIM families in mammals. Box denotes the families that bound to SFSS.

separated by two short 7-8 residue-length unstructured linkers (Figure 3.1B,C) [210]. While this LIM domain-containing region (LCR) is necessary and sufficient for localization to SFSS, the underlying mechanism is not known. It has been speculated that the signal within SFSS that the LCR senses may arise from new F-actin barbed ends, conformational changes to an actin binding protein, or post-translational modifications of actin or zyxin's binding partners [211]. Moreover, the focal adhesion protein paxillin also localizes to SFSS through its LCR [209], suggesting that this apparent mechanosensing process may be more generally conserved.

The family of proteins that contain one or more LIM domains is large. In humans, there are 70 genes containing LIM domains that can be divided into 14 classes [115], many of which associate with load bearing elements of the cytoskeleton, such as focal adhesions, cell-cell adhesions, and stress fibers [211]. There are at least 26 LIM domain-containing proteins that localize to focal adhesions, many of which require cell contractility for proper localization [121, 197]. While LIM domain-containing proteins are ubiquitous in diverse mechanotransduction pathways, it is unknown whether these share a mechanism by which mechanical stimuli is transduced. Moreover, the mechanism by which the LCR is recruited to SFSS is unknown.

3.3 Results

3.3.1 LIM domain-containing regions (LCRs) from diverse mammalian proteins bind to SFSS

SFs are contractile bundles of 10-30 crosslinked actin filaments with alternating bands enriched with either myosin II motor or α-actinin, VASP, and zyxin (Figure 3.1A) [211], a structure similar to that in striated myofibrils [226]. SFSS develop when SFs mechanically fail, resulting in local elongation and thinning that compromise their force transmission [210]

(Figure 3.1A, D-F). Zyxin rapidly accumulates at the SFSS and recruits the actin assembly factor VASP and crosslinking protein α-actinin to repair and stabilize the damaged site (Figure 3.1A) [210]. Previous work identified the LCR of zyxin to be necessary and sufficient for accumulation on SFSS [209]. Measuring the fluorescence intensity of zyxin and actin along the SF prior to a SFSS reveals locally diminished intensity of both proteins at the future SFSS (Figure 3.1D-F). Examining the local actin intensity of a future SFSS, we find that the actin intensity is depleted five-fold as compared to regions of SFs that do not fail (Figure 3.1F,G). Moreover, we find that >65% of SFSS occur in a myosin-rich band (Figure 3.1H), and myosin II is displaced laterally from SFSS (Figure 3.2A-C). The filament density decreases as the SFSS expands [210], and zyxin recruitment occurs nearly simultaneously as the length L of the strain site increases (Figure 3.1I). For temporal alignment of data, we define t=0 as the time of zyxin accumulation (Figure 3.1F,I). These data suggest that SFSS occur at SF regions pre-disposed to failure because of lower actin density and depletion of actin assembly and cross-linking factors. We also found that SFSS can be induced by partially damaging the SF with high laser intensity (Figure 3.1J). The LCR of zyxin is recruited to laser-induced SFSS with similar kinetics to that of spontaneous SFSS (Figure 3.1K and Figure 3.2D). Considering force balance along the SF in either of these two scenarios, the reduced number of actin filaments at SFSS suggests filaments and crosslinks present there are under an increased load.

To assess whether localization to SFSS is a feature ubiquitous within the LIM family of proteins, we developed an assay to quantify their recruitment to either endogenous or induced SFSS. We cloned the LCR from one or more genes belonging to each LIM protein class [115] and generated mCherry-tagged mammalian expression constructs. Each of the 28 mCherry-tagged LCRs was transiently transfected into mouse embryo fibroblast (MEF) cells with GFP-zyxin stably integrated into the genome. Using the GFP-zyxin as a positive marker for SFSS, we then assessed the localization of the mCherry-tagged LCRs at the site

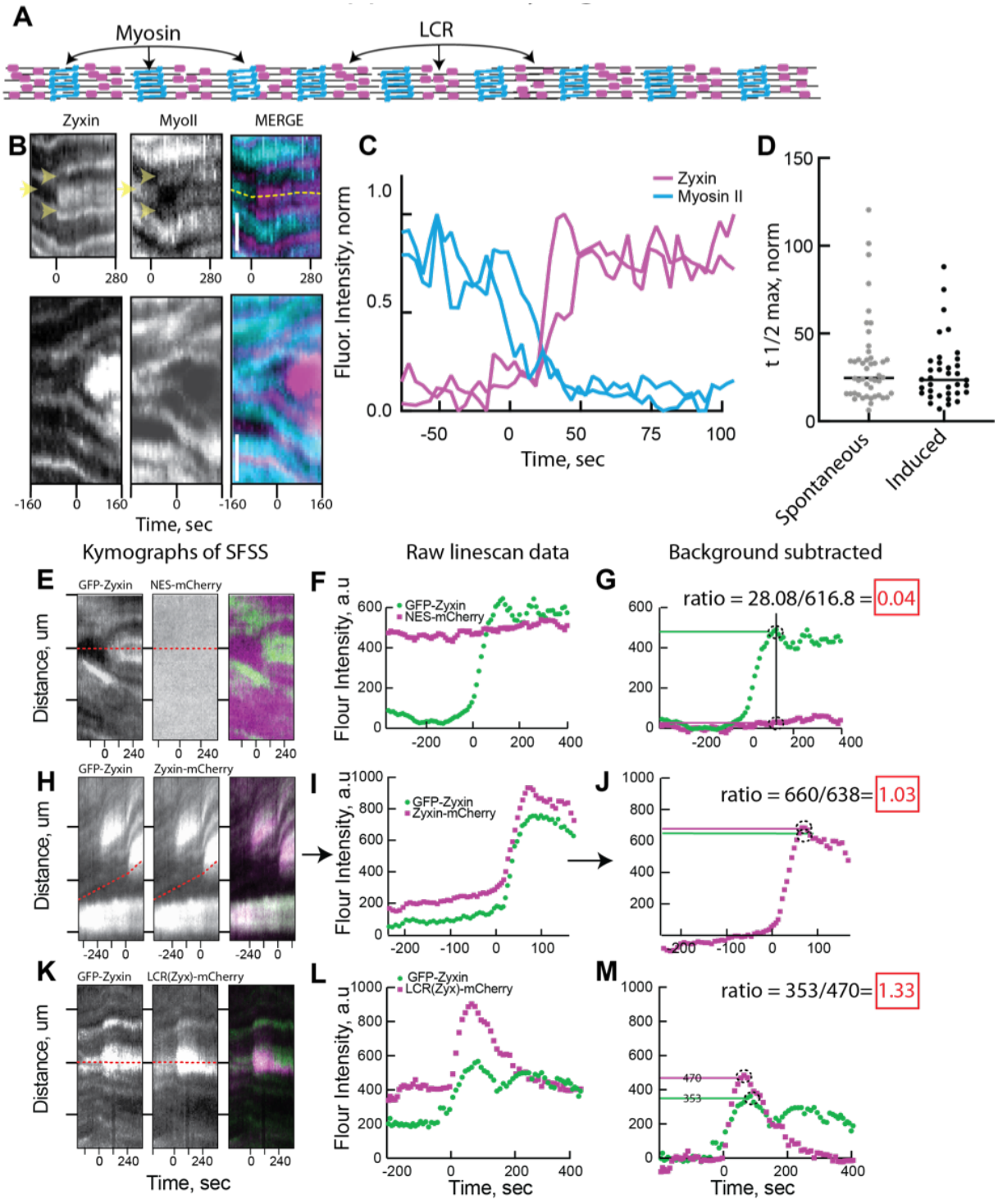

Figure 3.2: **Diverse LIM domains from mammals localize to SFSS.**

Figure 3.2: (continued) **(A)** Cartoon Schematic of a stress fiber showing the periodic, complementary banding pattern of Myosin and LCR. **(B-C)** Myosin behavior in SFSS. **(B)** Kymographs taken from a time-lapse confocal movie of 3T3 cell with the heavy chain of myosin II fused on its amino terminus with mApple (Cyan) and stably integrated. Zyxin-mCherry transiently transfected. (Scale bar=2 μm). **(C)** Linescans through kymographs such as those shown in (B), (yellow dotted line in merge) showing fluorescence intensity over time of myosin and zyxin. **(D)** Kinetics of Spontaneous and laser-induced SFSS. The time to reach half of the maximum fluorescence intensity (t1/2) was calculated by taking linescans through kymographs as done in B and C. **(E-M)** General SFSS quantification workflow using mouse embryo fibroblasts with integrated GFP-zyxin. Kymographs and corresponding linescan data generated from SFSS with the mCherry-zyxin as a positive control **(E-G)**, a negative control consisting of just a nuclear export signa tagged with mCherry **(H-J)**, and the LCR being assayed, here the LCR from zyxin (LCR(zyx)) is shown (K-M). **(G,J,M)** Background subtracted linescans. The signal before SFSS development is subtracted. From the background subtracted data, we determined the peak of each curve (dotted circles) and averaged the maximum with the two adjacent data points to determine the construct enrichment at the site. The enrichment of the mCherry construct was divided by the enrichment of GFP-zyxin to obtain the main metric, the mCherry:GFP fluorescence ratio.

(Figure 3.1K). As a control, the mCherry-tagged constructs of both full length zyxin and the LCR of zyxin, LCR(zyx), localize very similarly to GFP-zyxin (Figure 3.1K,L). At a SFSS, we generated kymographs (Figure 3.1K) and, from these, took linescans across the time axis at the center of the SFSS to generate a kinetic profile of SFSS accumulation for both GFP-zyxin and the transfected LCR-mCherry. From these profiles, the ratio of the LCR-mCherry to GFP-zyxin was determined and normalized (Figure 3.2E-N) such that a cytoplasmically expressed mCherry-tagged nuclear export signal (NES), which was added to all LCRs, is zero and mCherry-LCR(zyx) is one (Figure 3.1L). Ratio averages that were significantly above zero were scored as SFSS-binders. We observed SFSS localization of the LCRs from 18 proteins across 4 LIM classes: Zyxin, Paxillin, Tes, and Enigma (Figure 3.1l,M). SFSS-sensing is isolated to, but ubiquitous within, these classes. The LCRs of all but two protein sub-groups tested from these classes (Lmcd1 and Alp) localize to SFSS significantly above background. These results identify novel LIM domain protein-sensitivity to mechanical strain in the actin cytoskeleton and demonstrate its conserved function across diverse LIM domain containing proteins.

3.3.2 LIM domains from fission yeast bind to SFSS in mammalian cells via a conserved mechanism

To explore when SFSS-binding arose in LIM domain proteins along evolutionary lines and to determine the level of conservation, we looked for SFSS-binding homologues in more divergent species. The Paxillin class first appears in the unikonts (amoebas, yeasts, metazoans) while Tes, Zyxin, and Enigma classes arose later in the metazoans [115]. Reflecting a much simpler genome, the fission yeast *S. pombe* expresses five LIM domain-containing proteins: Rga1, Rga3, Rga4, Hel2, and Pxl1 (Figure 3.3A). The only contractile actin filament network in fission yeast is the cytokinetic ring, where myosin-rich nodes condense into an actomyosin bundle that constricts to drive cell division [252]. Time-lapse imaging of fission yeast Pxl1-GFP shows strong co-localization with myosin II at the contractile ring but only after the ring has assembled and begins to constrict (Figure 3.3B) [172, 74]. Although localization to the constricting contractile ring may suggest mechanosensitive localization, we could not easily manipulate the mechanics of the ring to directly test this possibility.

To determine whether SFSS localization found in mammalian LCRs is preserved in the fission yeast LIM domain-containing proteins, we used the SFSS-localization assay developed for mammalian cells. We transfected fission yeast LCRs tagged with mCherry into MEF cells containing stably integrated GFP-zyxin. The LCR of fission yeast Pxl1, LCR(Pxl1), localizes with the periodic z-bands in SFs but is largely absent from focal adhesions (Figure 3.3C). Surprisingly, LCR(Pxl1) exhibits strong SFSS localization, similar to that observed with LCR(zyx) (Figure 3.3C-E). Conversely, the LCR of fission yeast RhoGAPs and budding yeast Pxl1 did not display SFSS localization (Figure 3.3E). To determine if the fission yeast LCR(Pxl1) binds to the same target in SFSS as mammalian LCR(zyx), we compared their accumulation kinetics at SFSS (Figure 3.3F) and calculated the time to reach half of the maximum fluorescence intensity $t_{1/2}$. The $t_{1/2}$ of LCR(Pxl1) is nearly identical to

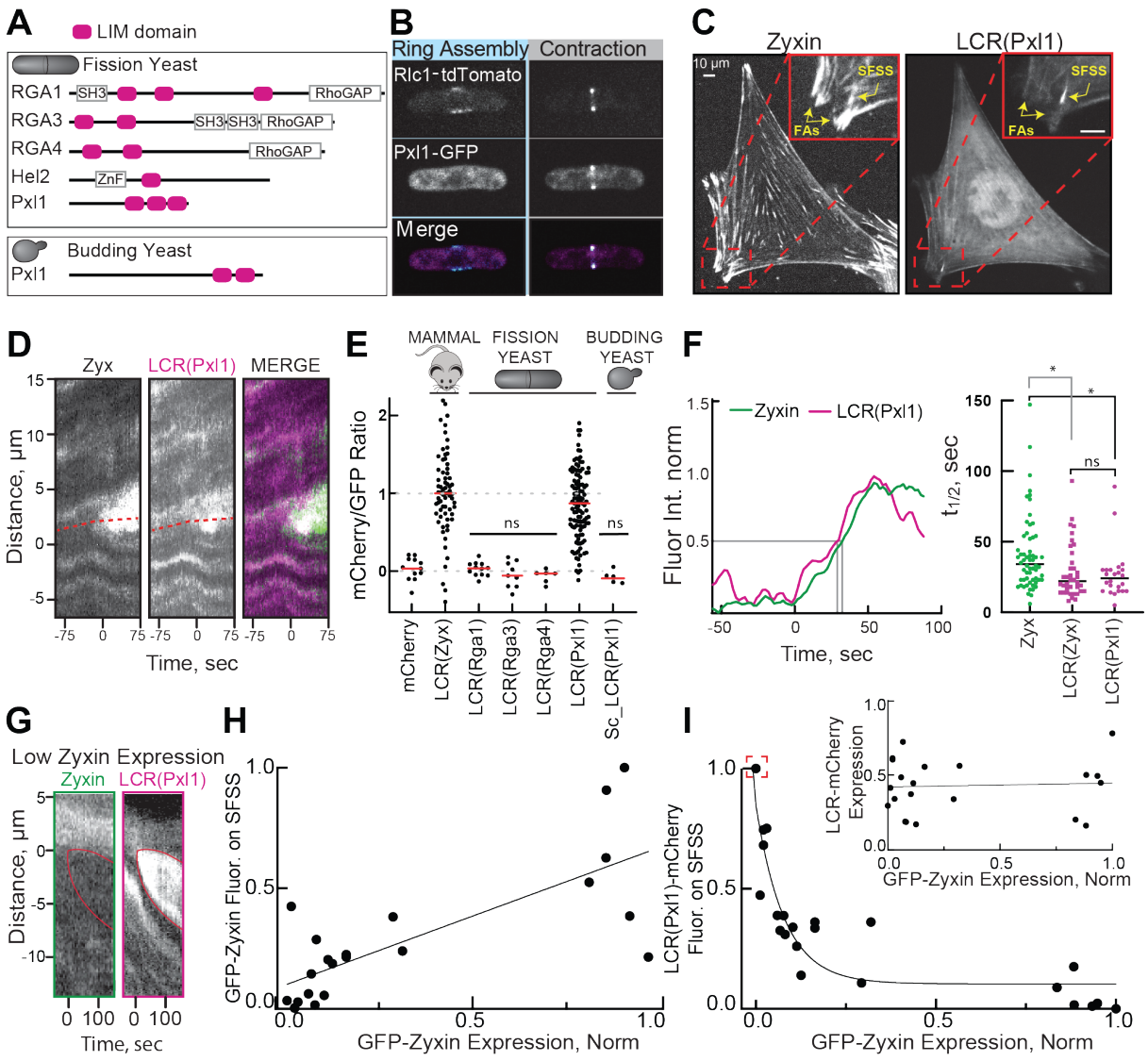

Figure 3.3: **LCR of fission yeast Pxl1 associates to SFSS and displays similar kinetics and competes at SFSS. (A)** Domain organization of *Schizosaccharomyces pombe* (fission yeast) LIM domain proteins and budding yeast Paxillin-like 1 (Pxl1). **(B)** Fluorescent micrographs of a fission yeast cell undergoing cytokinesis that is expressing myosin II regulatory light chain Rlc1-tdTomato and full length Pxl1-GFP. Contractile ring assembly (left panels) and beginning of contraction (right panels) are shown. **(C)** Mouse embryo fibroblast (MEF) cell expressing GFP-zyxin and the LIM domains of fission yeast Pxl1, LCR(Pxl1)-mCherry. Focal adhesions (FAs) and SFSS (yellow arrows) are labeled in the magnified inset image. **(D)** Kymograph of SFSS in the MEF cell from (C). **(E)** Screen for SFSS-association in fission yeast and budding yeast LCRs. Each LCR mCherry:GFP ratio was compared to background with ANOVA, ns=not significantly different. Each point represents individual SFSS ratio, n= average cellular ratio of 1 or more SFSS, 30>n>4 **(F, left)** Plot of the accumulation of GFP-zyxin and fission yeast LCR(Pxl1)-mCherry on SFSS over time. Grey lines indicate $t_{1/2}$ for GFP and mCherry.

Figure 3.3: (continued) **(F, right)** Plot of $t_{1/2}$ for accumulation on SFSS. Asterisks indicate statistical significance and ns = not significant as determined by ANOVA, n=60,24,38. **(G-I)** Fluorescence intensity of zyxin and LCR(Pxl1) at SFSS correlates with expression levels. **(G)** Kymograph showing competition of fission yeast LCR(Pxl1)-mCherry with GFP-zyxin at a MEF cell SFSS. Expression levels were estimated by measuring cytoplasmic intensity. **(H)** Fluorescence signal of fission yeast LCR(Pxl1)-mCherry or GFP-zyxin at SFSS as a function of estimated expression levels of the same construct. R^2=0.57, n=21. **(I)** Fluorescence signal of LCR(Pxl1) at SFSS as a function of estimated expression of GFP-zyxin. R^2=0.81. **(I, inset)** Estimated expression of LCR(Pxl1)-mCherry as a function of GFP-zyxin expression. R^2=0.003.

LCR(zyx) (Figure 3.3F), strongly suggesting that the two highly divergent LCRs use the same mechanism for SFSS association.

As a second test of whether LCR(Pxl1) and LCR(zyx) sense the same binding site to associate with SFSS, we assayed whether they compete for association to the same SFSS. For these experiments, we exploited natural variations in the expression of zyxin-GFP and LCR(Pxl1)-mCherry in our cell populations (Figure 3.3G-I). As expected, cells expressing high levels of zyxin showed more zyxin signal at SFSS (Figure 3.3H), which is also true for LCR(Pxl1) (Figure 3.4A). We also verified that expression of zyxin is not correlated with expression of LCR(Pxl1) (Figure 3.3I, inset). Importantly, high zyxin expression inversely correlates with reduced SFSS association of LCR(Pxl1) (Figure 3.3I). For instance, when expressed at low levels, zyxin accumulation at SFSS is nearly completely inhibited by LCR(Pxl1) (Figure 3.3G,I), and conversely, very little LCR(Pxl1) accumulates at SFSS in cells expressing high levels of zyxin (Figure 3.3I). The competitive relationship between zyxin and LCR(Pxl1) argues that these diverse LCRs (Figure 3.4B) are recruited to SFSS via the same mechanism. Although yeasts may not have canonical SFs, the contractile ring may still exhibit processes similar to SFSS [74, 29] that are recognized by Pxl1. Thus, although fission yeast do not contain SFs, a highly conserved molecular feature that exists in both fission yeast and mammalian SFSS is recognized by LCR(Pxl1). We conclude that the target of SFSS-sensing LCRs existed in the common ancestor of yeast and mammalian cells, and this association of LCRs with the actin cytoskeleton has likely been conserved since at

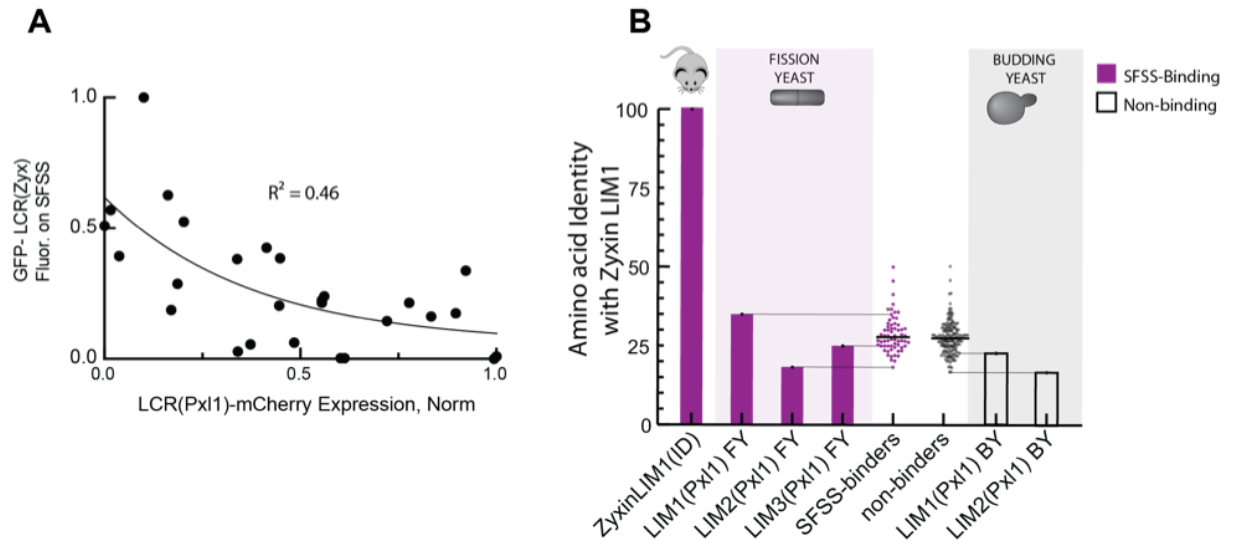

Figure 3.4: **LCR from fission yeast Pxl1 and zyxin compete for SFSS and display similar kinetics. (A)** The cytoplasmic signal of LCR(Pxl1) plotted against the LCR(Pxl1)-mCherry signal at the SFSS. Cytoplasmic signal was used as a proxy for expression level. **(B)** Diversity of LIM domains from fission yeast as compared with zyxin LIM domain 1, ID =Identity; zyxin LIM 1 is compared with itself here. The three LIM domains from fission (FY) and budding yeast (BY) Pxl1 were aligned with all other mammalian and Yeast LIM domains and a distance matrix was generated. The distances between zyxin LIM 1 and all other LIM domains were plotted.

least the divergence of yeasts and mammals.

3.3.3 Tandem LIM domains contribute additively to SFSS localization

Since LCRs from mammals and fission yeast appear to recognize a common target in SFSS, we speculated that conserved amino acid sequence signatures may be required for this function. Within the LCR of zyxin, there are three LIM domains (LIM1, LIM2, LIM3) separated by 2 short linkers (Figure 3.1C). Outside of the highly conserved amino acids that coordinate the zinc ions (Cys, His, or Asp), the sequences of individual LIM domains are highly variable. For instance, LIM2 and LIM3 share only 33% and 26% sequence identity to LIM1 (Figure 3.5A). Furthermore, LCRs from SFSS-binding and non-binding proteins show similar level of sequence identity (30% and 28%) to LIM1 of zyxin (Figure 3.5A). Despite this

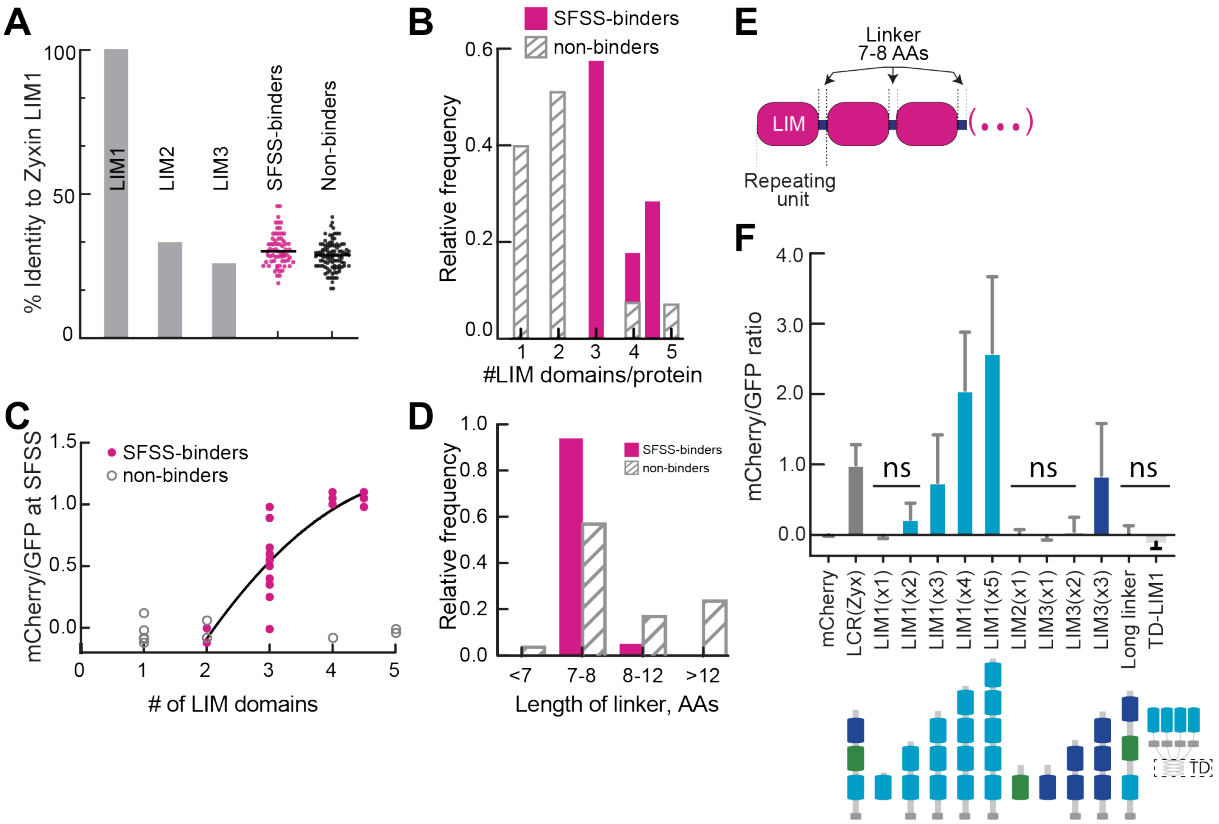

Figure 3.5: **LCRs bind to SFSS through multiple, precisely spaced domains organized in tandem.** **(A)** Amino acid identity to mammalian zyxin's first LIM domain (LIM1) of zyxin's other LIM domains (LIM2 and LIM3) and LIM domains from SFSS-binder and non-binder classes. **(B)** Histogram of the number of individual LIM domains in each SFSS-binder and non-binder protein. (C-E) Common organizational elements of LCRs in SFSS-binders. **(C)** Plot of SFSS-binding vs the number of LIM domains in the LCR construct. Data from LCRs within LIM binding classes was fit with a quadratic function using least squares. R^2=0.68. **(D)** Length distribution of linkers (in amino acids) connecting LIM domains in SFSS-binding (55 linkers) and non-binding classes (47 linkers) **(E)** Domain organization of a typical SFSS-binding LCR. There are typically 3 (or more) LIM domains separated by linkers of 7-8 residues. **(F)** SFSS-association screen of various organizations of zyxin's LCR. LIM1(X3) indicates the LIM1 is repeated 3 times. TD-LIM1 indicates the LIM1 domain was oligomerized by the addition of a modified GCN4 tetramerization domain (TD), ns = not significantly different from background as determined by ANOVA. 15>n>5, n= average cellular ratio of 1 or more SFSS.

sequence diversity, results complementary to ours show that a phenylalanine at position 66 (F66) of the LIM domains in Zyxin, Hic5, and FHL3 is necessary for localization to tensed actin filament networks both in cells and *in vitro* [218]. Among LIM domains from SFSS-sensors, only 75% of these contain F66 (Figure 3.6A-C); it is possible that proximal phenylalanine or tyrosine residues may be a suitable substitute (Figure 3.6B). However, 29% of the non-binders also have an F66, indicating that this amino acid is not sufficient for SFSS binding (Figure 3.6B,D). This led us to focus on other features of the LCR involved in SFSS-localization. We noticed common organizational elements of the LCR in SFSS-binders. First, all SFSS-binders contain three or more LIM domains in tandem organization, while 85% of non-binders have fewer than three LIM domains (Figure 3.5B). For all mammalian and yeast proteins in Zyxin, Paxillin, Tes, and Enigma classes, we plotted the level SFSS binding determined from the screens in (Figure 3.1M, Figure 3.3E) versus the number of LIM domains within the LCR. We found that the degree SFSS binding is weakly correlated ($R^2 = 0.7$) with the number of tandem LIM domains (Figure 3.5C). Furthermore, linkers from SFSS-binding proteins are 7-8 amino acids long, while linkers in non-binders range widely from 7- 200 amino acids (Figure 3.5D). These findings suggest a testable hypothesis that tandem LIM domains connected by a short linker is necessary for SFSS binding (Figure 3.5E).

We addressed these possibilities by exploring how alterations to LCR(zyx) organization impacts its localization to SFSS using the screening approach described previously. Constructs containing any one LIM domain of zyxin (LIM1(x1), LIM2(x1), or LIM3(x1)) do not localize to SFSS (Figure 3.5F). However, linkage of multiple LIM1 domains in tandem connected by a linker 8 AA long (See materials and methods) are recruited to SFSS (Figure 3.5F). Two tandemly linked LIM domains (Lim1(X2), LIM3(X2) and LIM1LIM2) weakly associate with SFSS (Figure 3.5F, Figure 3.7A,B). Additionally, three tandemly linked LIM domains (LIM1(x3)) or (LIM3(x3)), exhibit SFSS localization similarly well as LCR(zyx)

A.

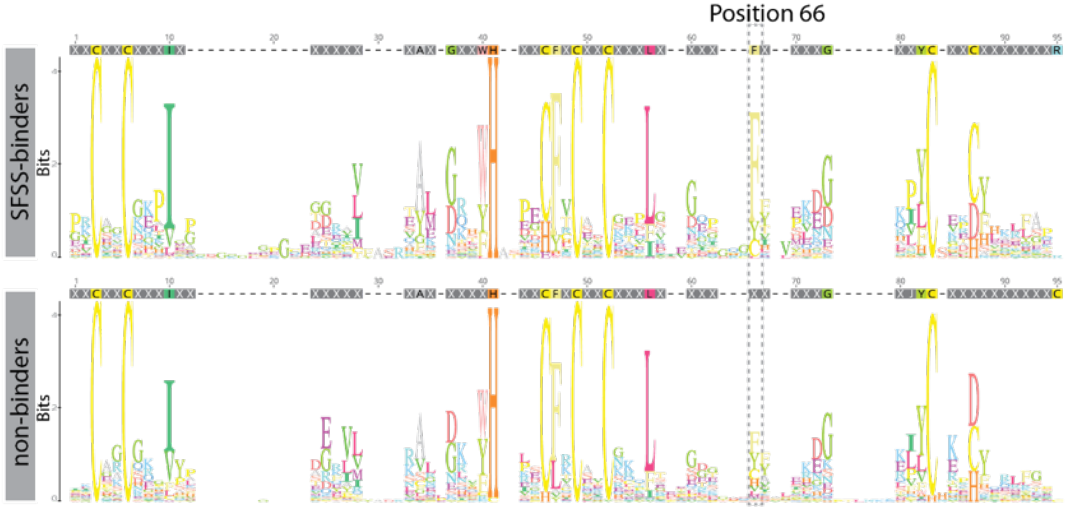

B.

	SFSS binders	non-binders
Total Sequences	70	95
F66	53 (75%)	28 (29%)
F66 or F67	60 (86%)	44 (46%)
F66 or Y66	62 (89%)	50 (53%)
F66, F67, Y66, Y67	69 (98%)	78 (82%)

C. SFSS-binders w/o F at pos 66

		66	67	70
Pxl1	LIM2	C	I	Y
Fblim1	LIM3	C	Y	P
Zyx	LIM3	C	F	P
Trip6	LIM3	C	Y	P
Lpp	LIM3	C	Y	P
Ajuba	LIM3	C	F	P
Limd1	LIM3	C	Y	P
Wtip	LIM3	C	Y	P
Prickle1	LIM1	Y	F	Y
Prickle2	LIM1	Y	F	Y
Tes	LIM1	Y	F	
Pxl1	LIM3	Y	F	
Tes	LIM2	Y	V	
Prickle1	LIM2	Y	I	
Prickle2	LIM2	Y	I	

D. Non-binders with F at pos 66

		# of LIMs	Linker length	Notes
Ablim1	LIM1	4	Long	third LIM has no Y or F in position 66-70
Ablim2	LIM1	4	Long	third LIM has no Y or F in position 66-70
Ablim3	LIM1	4	Long	third LIM has no Y or F in position 66-70
Pinch1	LIM1	5		
	LIM2			
	LIM5		Long	LIM3 has no Y or F in position 66-70
Pinch2	LIM1	5		
	LIM2			
	LIM5		Long	LIM3 has no Y or F in position 66-70
Isl1	LIM2	2		
Isl2	LIM2	2		
Lhx2	LIM2	2		
Lhx3	LIM2	2		
Lhx4	LIM2	2		
Lhx6	LIM2	2		
Lhx8	LIM2	2		
Lhx9	LIM2	2		
Lmo1	LIM2	2		
Lmo3	LIM2	2		
Lmo4	LIM2	2		
Lmx1a	LIM2	2		
Lmx1b	LIM2	2		
Mical2	LIM1	1		
Nrap	LIM1	1		
RGA3	LIM2	2		
RGA4	LIM1	2		
	LIM2			

Figure 3.6: **Phenylalanine (F) is enriched at position 66 in SFSS-binding LIM domains.** **(A)** Sequence Logos generated from multiple sequence alignments of all LIM domains from mammals and fission yeast. Logo generated from LIM domains extracted from SFSS-binding proteins (top) or non-binding protiens (bottom). Dashed box indicates position 66 where F is enriched in binders. **(B)** Absolute number and percentage (%) of LIM domains from SFSS-binding and non-binding proteins containing F at (1) position 66, (2) position 66 or 67, (3) F or Y at position 66, (4) F or Y at position 66 or 67.

Figure 3.6: (continued) **(C)** LIM domains from SFSS-binding proteins that do not have a F at postion 66 have an F or Y nearby. For example LIM domain 3 from the zyxin/ajuba family of protiens all have a cysteine (C) at 66, but F or Y at position 67. **(D)** Non-binders with a F at position 66 indicate that this amino acid is not sufficient to confer SFSS-binding. Most non-binders have less than 3 tandem LIM domains (column 2, red) except for Ablim and Pinch classes that have 4 and 5 tandem LIMs (column 2 green). Although Ablim and Pinch have >2 tandem LIMs, there are not >2 tandem LIMs with hydrophobic/aromatic F or Y in position 66-70 (Column 4). Aditionally, Ablim and Pinch classes both contain abnormally long linkers connecting LIMs together (column 3).

(Figure 3.5F). When the number of LIM1 repeats is increased to four (LIM1(x4)) or five (LIM1(x5)), the localization to SFSS further increases, exceeding LCR(zyx) by up to two-fold Figure (3.5F). These data suggest that each LIM domain alone may weakly bind the target within SFSS, but multiple interactions (at least for LIM1 and LIM3) contribute to the avidity of target binding. To determine whether the specific organization of LIM oligomerization matters, we clustered four LIM1 in parallel with a synthetic GCN4 tetramerization domain (TD) that drives the formation of a left handed coiled coil [86], TD-LIM1(x4). However, we did not observe SFSS localization with this construct (Figure 3.5F). Since the length of linkers in SFSS-binding LCRs is highly conserved Figure (3.5D), we tripled the linker lengths in LCR(zyx) from 8 to 24 amino acids (Long Linker), which abrogated SFSS localization (Figure 3.5F). Thus, full binding of LCR to the target within SFSS requires at least three tandem LIM domains connected with a short linker. We note that the Pinch and Ablim classes both contain more than three tandem LIM domains but fail to localize to SFSS in our screen. This could be explained by the fact that in both classes 1) two of the LIMs are connected by a longer (13-19 AAs) linker, and 2) the central LIM domain does not contain an F or similar amino acid at position 66-70. This supports the notion that a serial organization of multiple, appropriately-spaced LIM domains is necessary for SFSS binding.

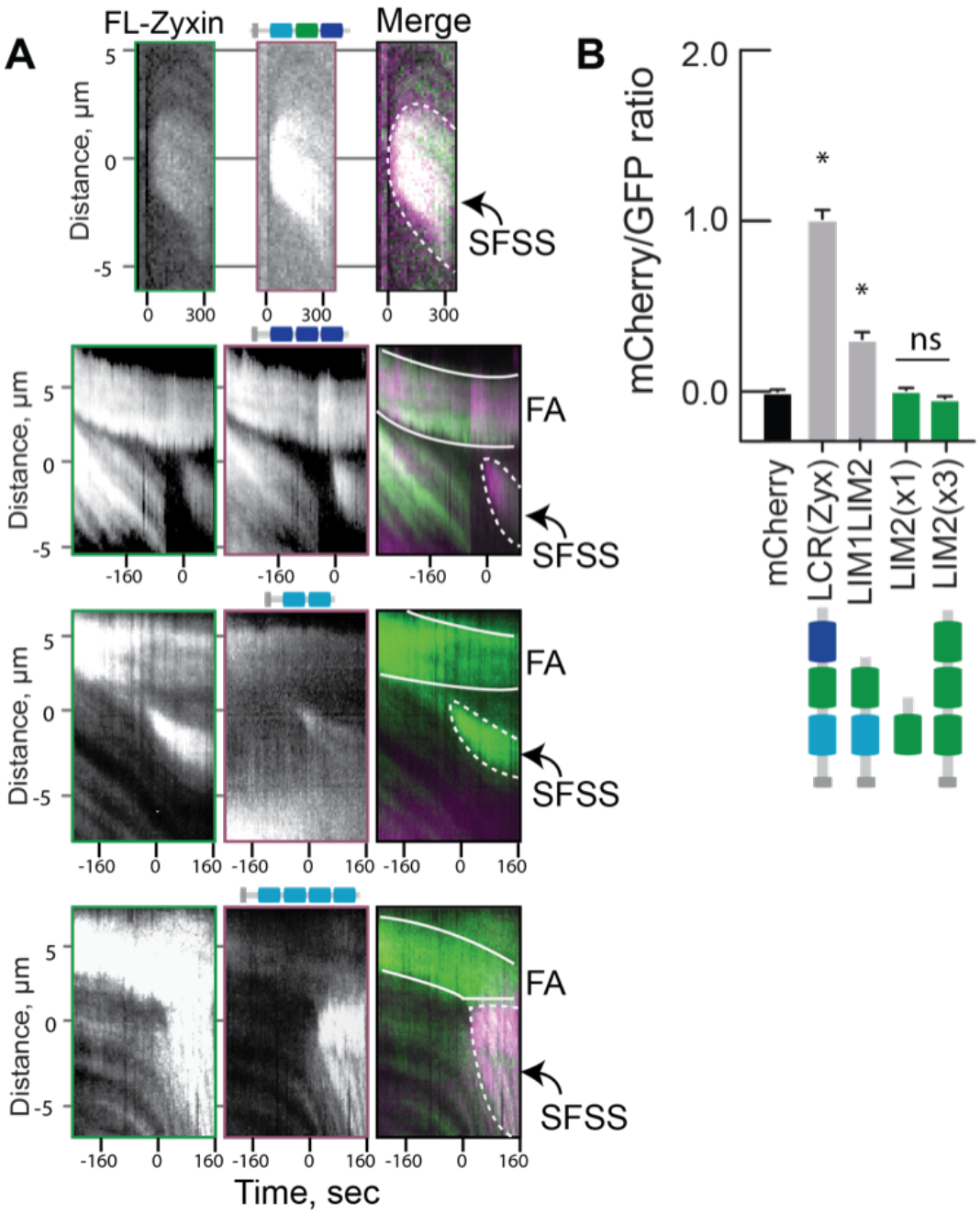

Figure 3.7: **Additional analysis of mutant LCR localization to SFSS. (A)** Representative kymographs taken from cells expressing various mutant constructs in MEFs with integrated GFP-zyxin. Top row is LCR(zyx)-mCherry, top-middle row is LIM3(x3), bottom middle row is LIM1(X2), and bottom row is LIM1(x4). FA=Focal adhesion. **(B)** SFSS binding by control LCR(zyx) compared to zyxin LIM2 constructs, n>5 cells, n = average of mCherry:GFP ratio from multiple SFSS in a single cell, error bars = SEM. Asterisks denote ratios that are significantly different from mCherry background using ANOVA test, ns = not significantly different.

3.3.4 In vitro reconstitution of LCR recruitment to contractile actomyosin bundles

While the above experiments identify organizational features of LCR required for association with SFSS, its binding target remains unclear. These experiments also indicate that LCR binding to SFSS is highly conserved from mammals to fission yeast, suggesting the binding target of LCR may be a core component of the eukaryotic contractile machinery. To identify the target within SFSS that is recognized by LCRs, we chose an *in vitro* reconstitution approach with a well-studied set of purified proteins. Untagged and SNAP-tagged LCR proteins SNAP-LCR(Pxl1) and SNAP-LCR(zyx) (Figure 3.8A and 3.9A) were purified from bacteria and the SNAP tag was fluorescently labeled with SNAP-surface 549 or 647 for single molecule imaging using total internal reflection fluorescence (TIRF) microscopy. Untagged and SNAP-tagged LCR(zyx) and LCR(Pxl1) elute from a gel filtration column as a stable monomer.

A leading hypothesis is that LCR(zyx) binds to actin filament barbed ends produced from filament breakage in SFSS [210]. We first tested whether LCR(zyx) or LCR(Pxl1) bind to actin filament sides or barbed ends in standard bulk assays (Figure 3.9B,C). Actin filament sedimentation assays revealed a barely detectable increase of either LCR in the pellet over a range of increasing actin filament concentrations, indicating an extremely weak affinity for actin filaments (Figure 3.9B). To query for F-actin barbed end binding, we utilized a seeded pyrene actin assembly assay to measure relative rates of elongation. Protein binding to assembling barbed ends usually modulates their elongation rates [174, 177], but we failed to detect any change in the presence of LCRs (Figure 3.9C). In support of these bulk biochemical assays, imaging of fluorescently labeled SNAP-LCR shows very minimal colocalization with actin filaments via TIRF microscopy (Figure 3.8G; -27 and -23 min). Thus, LCR appears to have a very low affinity to the sides or the barbed ends of relaxed actin filaments.

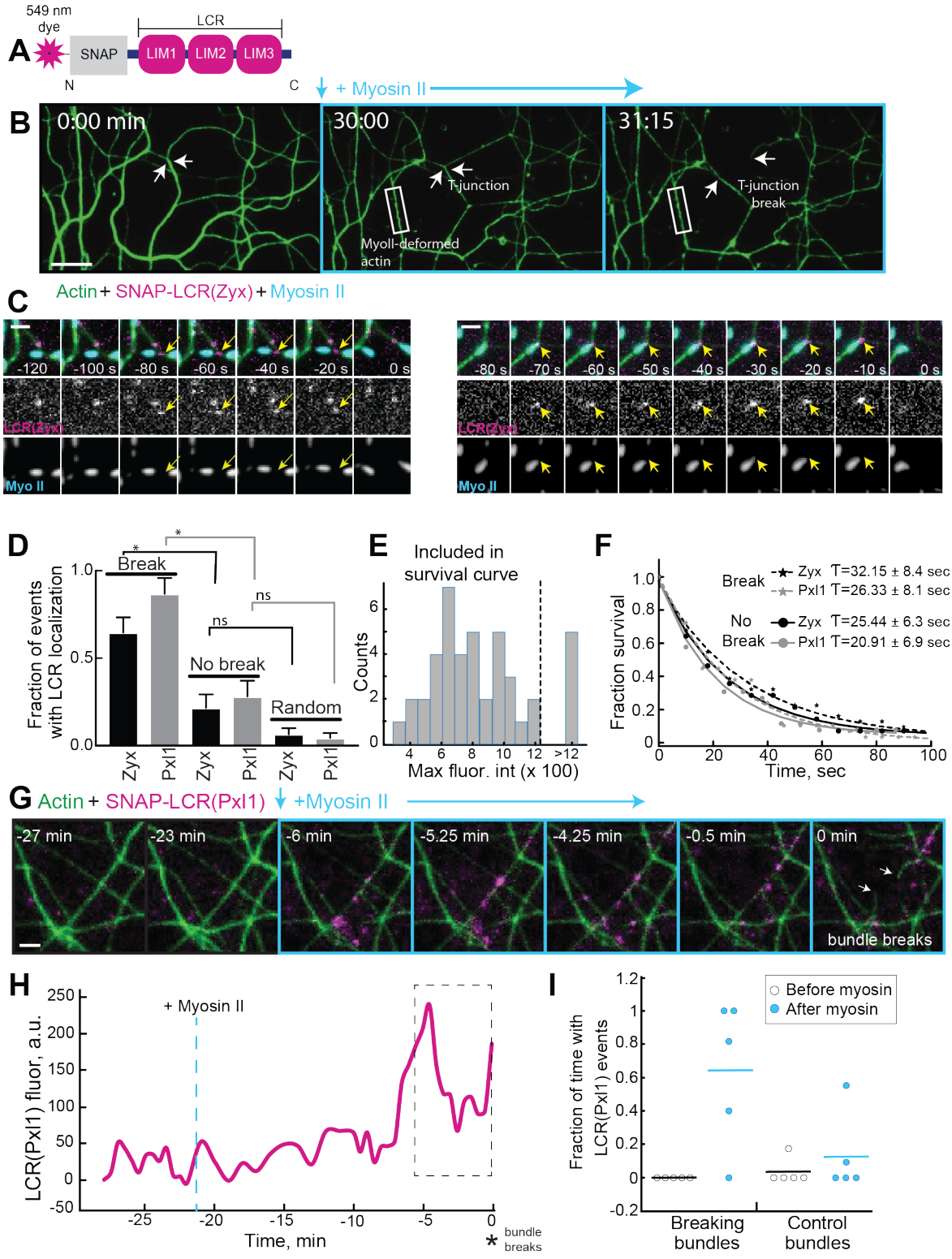

Figure 3.8: **Purified LCR of yeast Pxl1 and mammalian zyxin localized to stressed F-actin networks.**

Figure 3.8: (continued) **(A)** Schematic of the SNAP-tagged LCR protein constructs used for *in vitro* experiments. **(B-I)** TIRFM visualization of the recruitment of LCR protein constructs to actin filament networks. F-actin networks were preassembled with Mg-ATP-actin (10% Alexa488-labeled), α-actinin, and the indicated LCR construct (SNAP-549-tagged,) for 30-45 minutes. Network contraction was subsequently induced by flowing in polymerized myosin II with actin (0.1 μM) and the same initial concentrations of α-actinin and LCR. **(B)** A representative time-lapse of the *in vitro* contraction assay. After myosin is added to the preassembled bundled F-actin network, several types of network stresses occur, including T-junctions (white arrow) and myosin-induced F-actin deformations (white box). Scale bar = 10 μm. **(C-F)** LCR localization to T-junctions. **(C)** Representative time-lapse montage. A preassembled network was formed with 1.5 μM actin, 75 nM α-actinin, and 100 nM SNAP-LCR(zyx), followed by the addition of 100 nM myosin to induce network contraction. Yellow arrows show when LCR(zyx) localizes to the T-junction prior to break. Scale bar = 2 μm. **(D)** Quantification of fraction of events where LCR signal was observed: at T-junctions in the frame before breaking (break), at T-junctions that did not break (No break), or at random sites along bundles (Random). Error bars represent SEM, n>14 events for each condition. ns means p>0.05, asterisk = p<0.05 as determined by ANOVA. **(E)** Distribution of maximum fluorescence intensity of LCR on a T-junction. Data to the right of the dotted line were excluded from residence time calculations as shown in F. **(F)** Lifetime of LCR single molecules on T-junctions that broke (stars) or did not break (circles) average lifetimes derived from single exponential fits (lines)., error=95% CI calculated from curve fits, n = individual LCR binding event, n>14. **(G-I)** LCR localization to less common breaks along filament bundles. **(G)** Representative time-lapse montage of a preassembled network formed with 3.0 μM actin, 150 nM α-actinin, and 200 nM SNAP-LCR(Pxl1), followed by the addition of 75 nM skeletal muscle myosin II to induce network contraction. Scale bar = 2 μm. White arrows indicate broken ends of a bundle. **(H)** LCR(Pxl1) recruitment measured along the F-actin bundle in **(G)** that breaks at time 0. **(I)** LCR(Pxl1) fluorescence along bundles was measured similarly as in (H) for 5 bundle breaking events. Since LCR recruitment appears to be dynamic along the bundle, the fraction of frames with LCR localization during the 5 minutes just prior to break was measured.

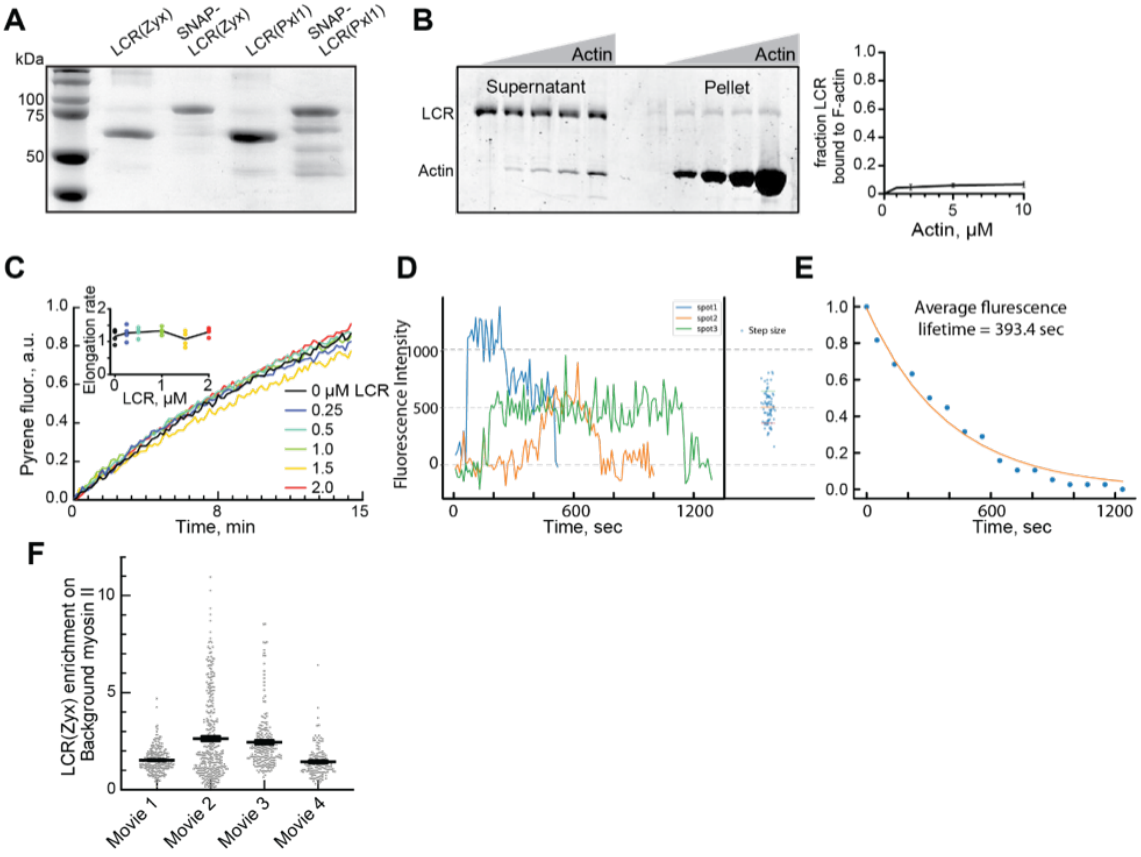

Figure 3.9: **Purified LIM domains have a low affinity for the sides and barbed ends of F-actin.** **(A)** SDS PAGE of Purified LCRs from mammalian zyxin and fission yeast paxillin Pxl1. **(B)** High-speed (100,000 x g) sedimentation assays of 0.5 μM LCR(zyx) with actin filaments preassembled from an increasing concentration (0, 1, 2, 5, 10 μM) of Mg-ATP actin monomer. **(B, left)** Coomassie stained gel of supernatants and pellets. **(B, right)** Graph of the percent of total LCR(zyx) observed in the pellet as a function of increasing actin concentration. **(C)** Seeded bulk actin assembly assay. Addition of 0.5 μM Mg-ATP actin monomers (20% pyrene labeled) onto 0.5 μM preassembled filaments in the presence of a range of LCR(zyx) concentrations (0-2 μM). **(C, inset)** Plot of initial slopes of the curves (proxy for elongation rate). **(D-E)** Bleaching analysis of SNAP-LCR(zyx). **(D)** Stepwise bleaching of SNAP-LCR(zyx) passively adsorbed to the coverslip surface. **(D, right)** Distribution of bleaching step sizes in one movie with mean and standard deviations marked. **(E)** To measure the magnitude of bleaching, the length of time a single fluorophore on SNAP-LCR(zyx) persisted without reduction in fluorescence intensity was measured. 1 -cumulative frequency plotted as a function of time and fit to a single exponential function to obtain the average lifetime (394 sec). **(F)** SNAP-LCR(zyx) fluorescence within myosin II puncta that were adhered to a PEG-passivated surface, but not associated with the F-actin network in the *in vitro* contraction assay. The average LCR fluorescence within the puncta was divided by the average local background signal to get an enrichment of LCR within Myosin puncta compared to background. Bars = mean, error bars = SEM.

Since Pxl1 and zyxin localize to diverse actomyosin contractile structures, we hypothesized that these LCRs bind to an element common to both fission yeast contractile rings and mammalian SFs. We reconstituted the core contractile machinery base on previously developed protocols [153, 152]. An F-actin network was assembled from actin monomers, α-actinin, and a SNAP-LCR (LCR(Zyx) or LCR(Pxl1)) within a buffer that contained 0.5% methylcellulose to crowd the network to a PEG-passivated glass coverslip surface. Individual actin filaments are mobile, but dynamics arrest as filaments elongate and are cross-linked by α-actinin into a network of mixed polarity bundles (Figure 3.8B; 0 min). When the network reached an appropriate density, we flowed in a fresh mixture containing the initial concentrations of SNAP-LCR and α-actinin, the critical concentration of actin monomers (0.1 μM) to prevent network disassembly, and pre-polymerized myosin II filaments (Figure 3.8B; 30 min). Myosin II activity on F-actin generates local stresses and deformations that remodel and contract the network. Gently curved bundles become taut, with many breaking over time (Figure 3.8B; 31 min). These failures usually occurred at bundle junctions ("T-junctions") and more rarely along the length of a single filament or bundle (about 10%). After rupture, bundle portions recoil and then compact into asters in which actin filaments are compressed, bent, and severed [153]. Thus, the myosin-driven contraction of a reconstituted F-actin network occurs with a build-up of both tensile and compressive stresses on the actin filaments that drive filament buckling and breaking [153].

Whereas LCR does not localize well to the networks initially, consistent with the 'bulk' F-actin sedimentation assays (Figure 3.9B), after the addition of myosin II, LCR accumulates on a subset of the network structures most likely to be under high contractile tension (Figure 3.8C-I). The majority (about 90%) of myosin II-induced breaks in the network occurred at T-junctions (Figure 3.8C,D) where actin filaments become highly distorted and break. Assuming the number of filaments in a bundle is constant and forces are balanced, there should not be increased tension at the T-junction compared to more distal sites along the

filament bundle. However, filaments at these junctions are highly curved, which could also be coupled to changes in filament twist [45]. Further work is needed to understand the underlying mechanism of LCR recruitment.

LCRs bind more frequently to T-junctions that break than to non-breaking T-junctions and random sites along the actin network (Figure 3.8C,D). A majority of the T-junction breaks appear to bind single molecules of LCR (Figure 3.8C, left), but there is a fraction of T-junctions that show increasing LCR fluorescence prior to breaking (Figure 3.8C, right). To verify that we are observing single molecules, we monitored LCR bleaching in our experiments and obtained the average fluorescence intensity of a single dye. 78% of the LCR puncta monitored disappeared in a single step (Figure 3.9D). A distribution of the maximum LCR fluorescence intensity suggests that most T-junction binding show fluorescence values consistent with that of sinlge molecules of LCR (Figure 3.8E).To get a sense of the affinity of LIM domains for sites of stressed F-actin, we measured the residence time of LCR single molecule fluorescence on the two T-junction populations (breaking and non-breaking). We monitored the residence time of LCR puncta on T-junctions that displayed fluorescence intensities consistent with single LCR molecules (Figure 3.9D, right). LCRs associate for an average of 30 sec but LCR signal disappears from the network coincident (at our 10 s imaging interval) with breaking of a T-junction (Figure 3.8F). Since the average bleaching time is over 10-fold higher than the measured residence time, we conclude that the disappearance of signal at the T-junction is due to LCR dissociation rather than bleaching (Figure 3.9E). An assumption that LCR association rate is between 106 – 107 $M^{-1}s^{-1}$ [176] and the measured off rate of approximately 0.038 s^{-1} (1/residence time) (Figure 3.8F) suggests that LCR may have low nanomolar affinity for actin filament conformations that are enriched at T-junctions.

Compared to T-junctions, myosin-induced breaks along the F-actin bundle are much rarer. However, when these breaks occur, SNAP-LCR(Pxl1) binding to the bundles appears

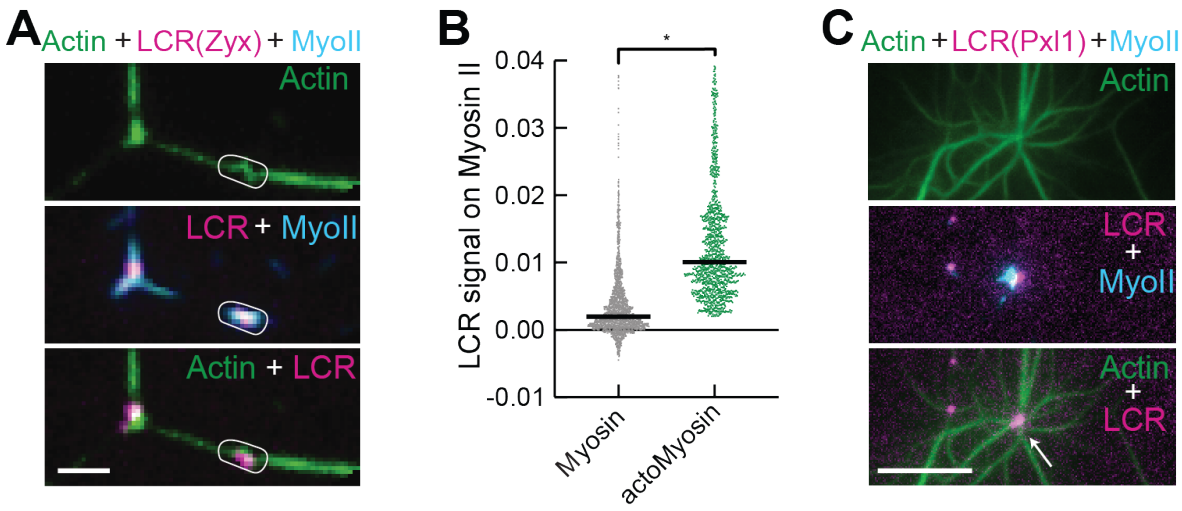

Figure 3.10: **Purified LCRs localizes to stressed F-actin networks where myosin deforms F-actin bundles. (A)** Representative fluorescent image of LCR(zyx) localizing with myosin II along the network. Ovals indicate myosin on the F-actin network or on the glass. Scale bar = 2 μm. **(B)** Quantification of LCR localization with myosin or myosin associated with actin (actomyosin). n = individual myosin puncta in four different movies, n>300, bar indicates mean, asterisk indicates p<0.05 as determined from t-test. **(C)** Representative fluorescent images of a large aster that forms from a preassembled network with 3.0 μM actin and 200 nM SNAP-LCR(Pxl1) in the absence of α-actinin, followed by the addition of 90 nM myosin II (Alexa 647 labeled). Scale bar = 10 μm. LCR(Pxl1) localizes to the center of these asters with the myosin (white arrow).

dynamic with most localization occurring within 5 minutes prior to breaking at t=0 min (Figure 3.8G,H). While the exact localization site varies between breaking events, SNAP-LCR signal is detected for an average of 60% of the 5 minutes prior to bundle breakage (Figure 3.8I). LCR is also observed along control bundles that do not break throughout the course of the movie, but for only an average of 20% of the 5 minutes (Figure 3.8I). LCR(Pxl1) only associates to the network after myosin addition, remaining on filament portions for several minutes prior to breaking at t=0 min (Figure 3.8H,I).

LCR also co-localizes with myosin II, especially in areas with highly deformed F-actin networks (Figure 3.10A-C). While SNAP-LCR is detected above background on isolated myosin II (Figure 3.9F), LCR binding is 5-fold higher when myosin is localized on the F-actin network, suggesting this colocalization is a result of LCR binding to myosin-induced

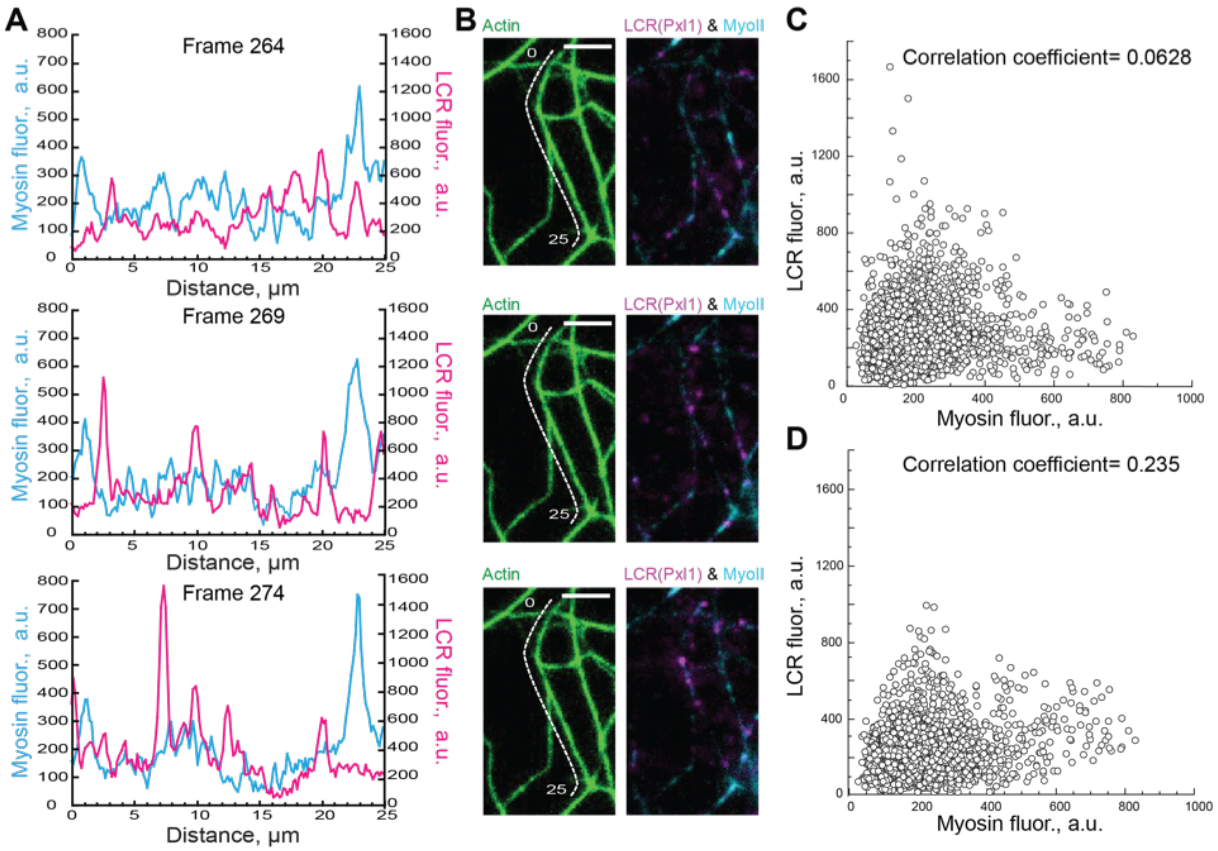

Figure 3.11: **LCR(Pxl1) localization along reconstituted F-actin networks does not correlate with myosin localization.** **(A-C)** Quantitative analysis of LCR(Pxl1) and myosin localization along an F-actin bundle in the *in vitro* contraction assay described in Fig. 3.8. A preassembled network was formed with 3 μM actin, 200 nM α-actinin, and 200 nM SNAP-LCR(zyx), followed by the addition of 300 nM myosin to induce network contraction. The network was imaged every 15 sec. **(A)** Myosin (cyan, left y-axis) and LCR(Pxl1) (magenta, right y-axis) linescans taken along a single F-actin bundle over time. Linescans for frames 75 sec apart are shown here. **(B)** The corresponding images for the linescans in (A). White lines indicate the bundle starting at 0 μm and ending at 25 μm. Scale bar = 5 μm. **(C-D)** Plots of LCR fluorescence vs myosin fluorescence for the bundle in (B) over 20 frames. **(C)** The Pearson's correlation coefficient was calculated for the relationship between LCR and myosin, 0.0628. **(D)** As a control, the LCR channel was rotated 90 to the right, and new values for the same ROIs in (C) were plotted against the same myosin values in (C). The Pearson's correlation coefficient is 0.235 for this plot.

actin filament deformations rather than directly to myosin (Figure 3.10B). Line scans of a bundle over time show that the majority of LCR localization is independent of myosin localization (Figure 3.11). This further indicates that colocalization of LCR and myosin II along the network is due to LCR binding to actin filament deformations instead of myosin II directly (Figure 3.10A,B). In actomyosin contraction assays that lack the cross-linker α-actinin, myosin drives contraction of the F-actin network into asters, which are dense clusters of actin and myosin II. Previous work has shown that these so-called asters are sites where filaments are buckled and broken due to compressive forces [153]. We observe that SNAP-LCR localizes to these asters, suggesting that LCR localization does not require the cross-linker α-actinin and localizes to highly compacted actomyosin (Figure 3.10C). These data show that myosin II-generated forces on actin filaments is necessary and sufficient to drive LIM localization to actin filaments.

3.3.5 Polymerization-generated stress is sufficient for LCR localization to actin

To determine whether LCR localization can occur by alternate means of applying force to actin filaments, we employed a well-established reconstitution assay that serves as a model for actin-based motion [130, 43]. Here, 2 μm polystyrene beads were coated with the Arp2/3 complex nucleation promoting factor pWa (Figure 3.12). Mixing the beads with actin monomers, Arp2/3 complex, and capping protein drives the assembly of a branched network of short actin filaments at the bead surface [1], which can be visualized by imaging of fluorescently labeled actin. In the expanding actin shell, the outer network continuously stretches as it is displaced outward by continuous assembly of new actin at the bead surface. Forces generated by actin polymerization result in the buildup of circumferential tension along the outer part of the actin shell, resulting in network tearing that breaks the symmetrical shell. After symmetry breaking, the so-called comet tail drives directed bead motion

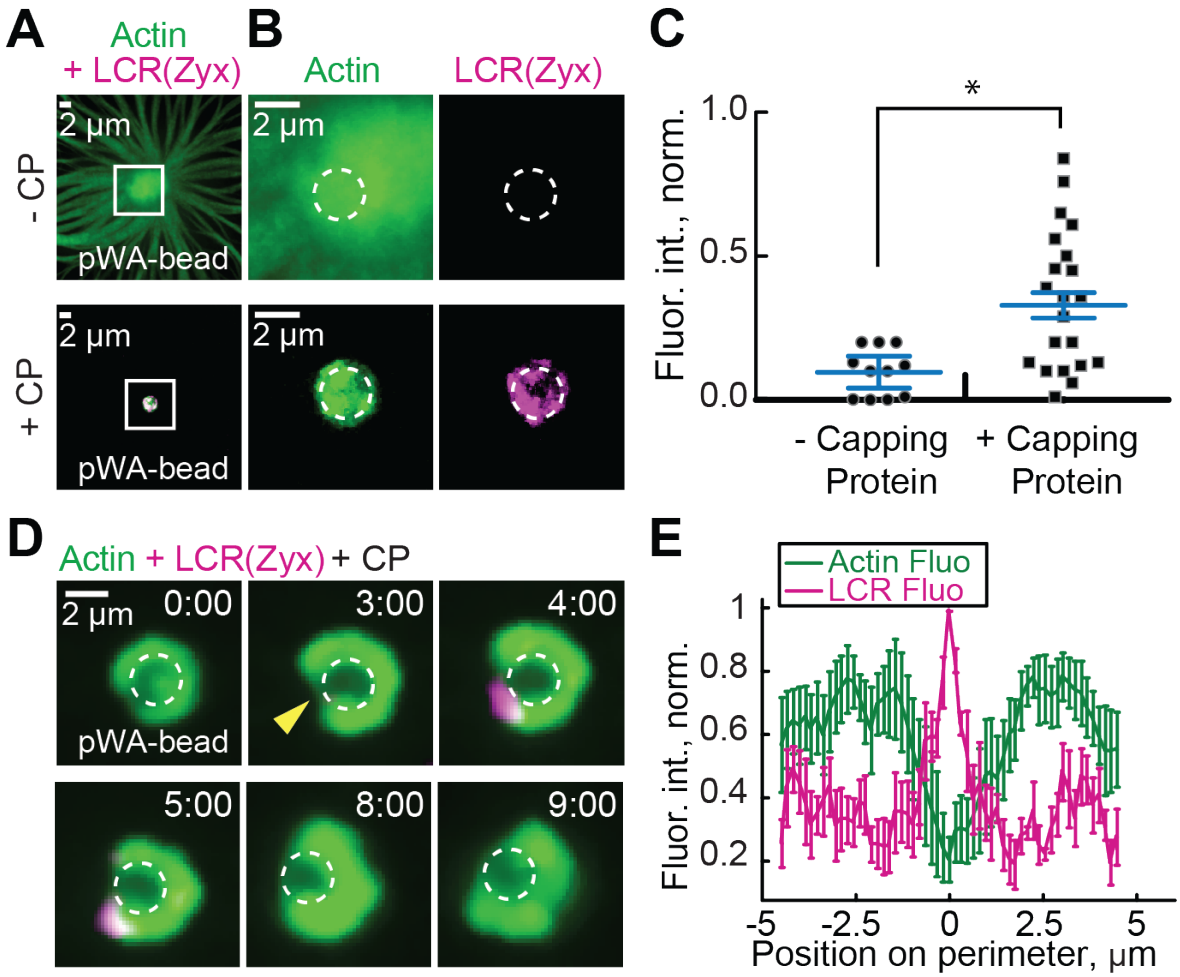

Figure 3.12: **SNAP-LCR(zyx) localizes to branched F-actin networks during symmetry breaking (A-C)** LCR(zyx) localizes to capped F-actin networks in motile bead assays. **(A)** Confocal images taken from a motile bead assay, where the Arp2/3 complex activator pWa is electrostatically bound to the surface of polystyrene beads. The beads are mixed with 4 μM actin monomer (5% Alexa-488 labeled), 100 nM Arp2/3 complex, 12 μM profilin, and 400 nM LCR(zyx) in polymerization buffer in the presence or absence of 200 nM capping protein. **(B)** Zoomed images from the white boxed region of (A). White circle traces the beads. **(C)** LCR fluorescence on the actin networks in (A) in the absence or presence of capping protein. Normalization was done relative to the total actin fluorescence on the bead. n>10, error bars=SEM, asterisk indicates p<0.05 as determined from t-test. **(D-E)** Halo-LCR(zyx) localizes to symmetry breaking events in motile bead assays. The pWa beads are mixed with 2 μM actin monomer (5% Alexa-488 labeled), 100 nM Arp2/3 complex, 100-200 nM LCR(zyx), and 42 nM capping protein. **(D)** Confocal time-lapse of a representative symmetry breaking event. White circle indicates the beads, and the yellow arrow shows where symmetry breaks. (E) Linescans of LCR (magenta) and actin (green) fluorescence on the circumference of the F-actin network from reactions where beads break symmetry. Linescans are the average of 5 beads and were aligned by setting the peak LCR intensity to position zero. Error bars=SEM.

[130]. Previous work has demonstrated that capping protein (CP) facilitates symmetry breaking, as short-capped filaments are more effective in force generation [12, 43, 148].

In the absence of capping protein, large amounts of actin are assembled from the bead that elongates away from the bead surface. While the overall actin signal is much higher in the absence of capping protein, LCR binds only slightly above background detection (Figure 3.12A-C). Conversely, in the presence of capping protein, we observed a wide distribution of LCR binding to the shell. A subset of beads has high LCR intensity associated with the actin shell (about 50%), while others display levels of LCR binding similar to controls without capping protein (Figure 3.12C). However, in this set of assays, the high concentration of capping protein inhibits formation of a complete actin shell on the bead, and we witness no instances of symmetry breaking. In confocal sections taken through the center of beads in the presence of a lower concentration of capping protein, LCR localizes where the actin signal is weakest (Figure 3.12D,E). We speculate this is because symmetry begins to break at these sites and the F-actin network thins as it is strained. To look more closely at this phenomenon, we took confocal time-lapse movies of beads going through the process of symmetry breaking. We observed LCR localizing most intensely to the actin shell during the period of most rapid straining as the shell ruptures (Figure 3.12D).

3.4 Discussion

Here we show that the mechanism by which zyxin is recruited to SFSS is through binding of its LCR exclusively to mechanically strained actin filaments and note that a parallel study has come to the same conclusion independently [218]. We identify 18 proteins from four different LIM domain protein classes with LCRs that localize to SFSS, indicating that this force-sensitive interaction may function as an input into diverse cellular processes. While SFSS are a particular feature within adherent fibroblasts, mechanical stresses are ubiquitous within the actin cytoskeleton. Force-sensitive biochemistry is inherent to mechanical regulation of the

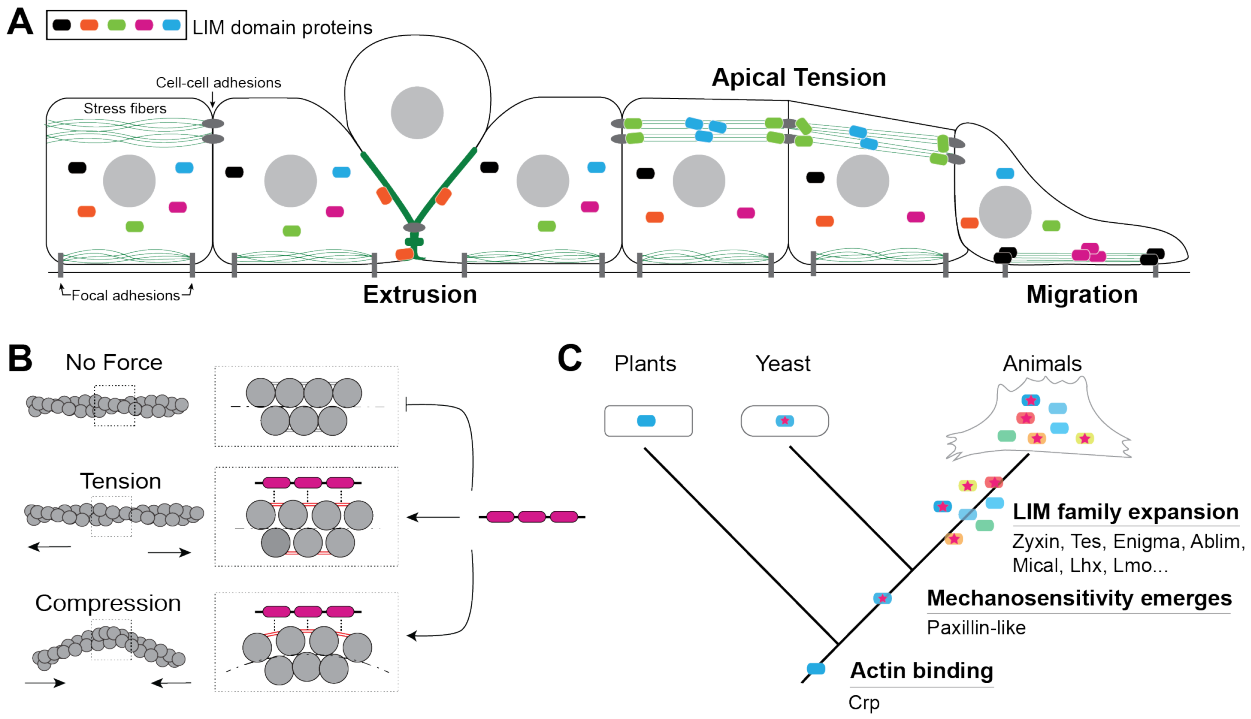

Figure 3.13: **Model of LCR mechanosensing. (A)** Cartoon of an epithelial tissue layer with different examples of mechanical stress that cells experience (extrusion, apical tension, and migration). LIM domains bind the different mechanically stressed F-actin networks. **(B)** Actin filament experiencing different forces: tension (middle) or bending due to compression (bottom) which is likely coupled to changes in filament twist. The box indicates the zoomed in diagram showing the bonds between actin subunits. The grey lines indicate regions of low stress while the red lines indicate high stress due to tension, compression, or twist-bend coupling. LIM domain proteins likely localize through their LCR to the regions of high stress. **(C)** Phylogenetic tree showing emergence of strained actin filament binding by paxillin class of LIM domain proteins and later expansion of LIM family in the metazoan stem lineage.

cytoskeleton and, we suspect, also a means for transmitting information about the mechanical status of the cell to the nucleus. The tension in SFs tends to reflect the mechanics of the environment in which cells are embedded. Cells growing in rigid matrices or within tissues that are being stretched build F-actin networks under increased tension [253, 183, 122]. Recent work suggests that matrix mechanics and the resulting actin networks control nuclear localization of the LIM protein FHL2 [155, 218]. Interestingly, a majority of SFSS-binding LIM proteins display nuclear shuttling [108], suggesting a model by which LCR binding to stressed F-actin networks blocks nuclear import. Our data raises the possibility that detection of cytoskeletal mechanics by LCRs from four different LIM classes [115], Zyxin, Paxillin, Tes, and Enigma may underlie regulation of diverse transcriptional pathways they are part of, including YAP/TAZ, Hippo, p21 signaling, and planer cell polarity. While much work has demonstrated these to be mechanically regulated [183, 155, 54, 235], our work implicates interactions between the LCR with strained actin filaments in diverse cytoskeletal assemblies as a potential mechanism. We anticipate that understanding the details of how and why diverse LIM domain containing proteins differentially localize to strained actin filaments at focal adhesions, cell-cell adhesions, and the actin cytoskeleton will yield insight into the regulation and architecture of these mechanotransduction pathways (Figure 3.13A).

In vitro data from both this and a parallel study [218] indicate that the LCR can be recruited to highly tensed or compressed actin filaments, suggesting that these two distinct force-induced filament conformations may expose a similar actin filament structure that has high affinity for LCR (Figure 3.13B). The maximum distortion that may occur within a highly bent filament before it breaks is estimated to be approximately 1.5A of displacement/subunit [4]. An attractive hypothesis is that mechanical stretch, compression, or twist exposes a site within the actin filament that is weakly recognized by each LIM domain. Future work is needed to understand the full mechanism of the force-dependent interaction. A parallel study identified a phenylalanine within each LIM domain that was necessary for force-dependent

association with actin filaments [218]. Both [218] and our data demonstrate this site is not sufficient, as tandem LIM domains are required. Our work suggests that 3 tandem domains connected by linkers of a precise length, each contribute to binding a strained-induced feature on an actin filament. We suspect the linker length may act as a ruler that positions individual LIM domains to optimally bind a stress-induced feature on the actin filament (Figure 3.13B).

We show that this force-sensitivity is found in fission yeast LIM protein Pxl1. The fact that Pxl1 both localizes to the contractile ring in fission yeast and to SFSS in animal cells suggests that myosin II-induced strained actin filament conformations are a common feature in contractile networks. Despite large evolutionary distances, this interaction has been conserved, indicating that there is significant selective pressure to maintain it. Actin is one of the most highly conserved proteins in Eukaryotes with 90.4% amino acid sequence identity between fission yeast and mammals, so it is not surprising that the LCR of Pxl1 from fission yeast binds to a strained F-actin structure in mammals. The oldest LIM domain protein found in plants and animals, CRP [115], binds and bundles actin filaments via its LIM domains in the absence of mechanical stress [244, 227, 80]. We hypothesize that duplication and divergence of an ancestral CRP-like LIM domain resulted in a modification to its actin binding mechanism that favored a strained conformation of F-actin (Figure 3.13C). The other core components of the contractile machinery, myosin II and α-actinin, have not been found in plants but are clearly present in the unikonts [187, 126] and may have appeared around similar times. We hypothesize that the emergence of contractile F-actin machinery coincided with, or required proteins that could report on the stresses present there. The oldest SFSS binding class from our screen appears to be paxillin [115], which is involved in mechanical homeostasis of contractile networks in yeast [74]and mammals [209]. F-actin strain sensing via LIM may have been co-opted by other signaling pathways later on during the LIM family expansion that originated in the stem lineage of metazoan (Figure 3.13C) [115].

Zinc finger proteins have diverse functionality from regulation of cell cycle, transcription, and protein folding through interactions with DNA, lipid, and proteins [124]. Our data demonstrate that mechanically stressed actin filaments are an additional substrate for a subset of zinc finger proteins. The extent to which mechanical forces may regulate interactions with other known substrates is an opportunity to be explored. The use of the actin filament itself as a force sensor, or mechanophore, within the actin cytoskeleton is a particularly attractive one as means to control mechanotransduction pathways. Both its abundance and the different types of force (twist, compression, extension) that can be sensed could provide a wealth of control of mechanotransduction pathways. Moreover, our work suggests the possibility of other biomolecules that exclusively bind to mechanically stressed filaments that may not be have been isolated by traditional biochemical studies.

3.5 Materials and Methods

3.5.1 Cell culture and transfection

NIH 3T3 fibroblasts (American Type Culture Collection, Manassas, VA) and mouse embryo fibroblasts (MEFs) were cultured in DMEM media (Mediatech, Herndon, VA) and supplemented with 10% fetal bovine serum (HyClone; ThermoFisher Scientific, Hampton, NH), 2 mM L-glutamine (Invitrogen, Caarlsbad, CA), and penicillin–streptomycin (Invitrogen). Zyxin(-/-) and zyxin(-/-)+EGFP-zyxin MEFs cells were a gift of Mary Beckerle's laboratory (University of Utah, Salt Lake City, UT) and have been described previously [92, 93]. All cells were transiently transfected via electroporation before experiments using a Neon transfection system (ThermoFisher Scientific). 1-2 μg of plasmid DNA was used per transfection. Following transfection, cells were plated in 8-well μ-slide chambers (Ibidi USA, inc.) and imaged 12-24 hours later.

3.5.2 Live-cell imaging and SFSS induction

Cells were grown in 8-well μ-slide chambers with culture media supplemented with 10 mM HEPES and maintained at 37°C. Cells were imaged on an inverted Nikon Ti-E microscope (Nikon, Melville, NY) with a Yokogawa CSU-X confocal scanhead (Yokogawa Electric, Tokyo, Japan) and laser merge module containing 491, 561 and 642 nm laser lines (Spectral Applied Research, Ontario, Canada). Images were collected on Zyla 4.2 sCMOS Camera (Andor, Belfast, UK). A 405 nm laser coupled to a Mosaic digital micromirror device (Andor) was used to locally damage SF. A small area targeting a region of a SF was drawn in MetaMorph and illuminated by the 405 nm laser for ˚∼5 seconds. Images were collected using a 60x 1.49 NA ApoTIRF oil immersion objective (Nikon). All hardware was controlled using MetaMorph Automation and Image Analysis Software (Molecular Devices, Sunnyvale, CA). Cells were imaged in the 491 and 561 channel at various time intervals ranging from 2 – 20 seconds.

3.5.3 Image processing and analysis for LCR Screening Assay

SFSS were analyzed by measuring the ratio of the mean fluorescence of transiently transfected mCherry-tagged LCR to the stably integrated EGFP-zyxin fluorescence as so: Ratio = (LCR SFSS – LCR background) / (zyxin SFSS – zyxin background). Several images of the cell culture media region without cells was captured in each channel before an imaging experiment to obtain the background signal from camera noise, media fluorescence. These images were averaged and subtracted. On a day of imaging, care was taken to keep imaging settings constant. Each new day, at least two different transfections of LCR(zyx) were used as a control to adjust for day to day differences in imaging conditions. Kymographs were generated with imageJ reslice function, or if stress fibers moved significantly, a python script written in imageJ from user-drawn line segments was used. Background was considered to be

the location on the stress fiber where the SFSS eventually developed. A linescan was drawn across the kymograph (through the time axis) to generate a profile. The signal immediately prior to SFSS development was subtracted from both channels. The maximum fluorescence signal was found and averaged with the two adjacent points to obtain the enrichment value for each channel. If there was no obvious signal for the LCR being tested, then the time point at which GFP-zyxin signal was maximal was used in measuring the mCherry-LCR signal. The enrichment of mCherry was divided by the enrichment of GFP-zyxin to obtain the fluorescence. To determine statistical significance, ANOVA was used to compare the mCherry:GFP ratio of each construct to background signal (mCherry tag alone). alpha was set 0.05.

3.5.4 Data analysis

Data analysis: Cells presented in figures are representative samples of the population behavior. Error bars represent the s.d., s.e.m or 95% confidence interval as indicated and were computed in graphpad prism (version 8.0d, GraphPad Software, Inc., La Jolla, CA) or from python's pandas, matplotlib and scipy libraries. Statistical significance was determined using ANOVA or independent two-sample Student's t-test of the mean as noted.

3.5.5 Single molecule analysis

LCR puncta on T-junctions were assumed to be single molecules If the fluorescence signal appeared and disappeared in a single step with the fluorescence intensity remaining constant over the lifetime of the interaction. Additionally, we determined the fluorescence intensity of single fluorphores by performing stepwise bleaching. The size of the steps in bleaching followed a gaussian distribution. Puncta that appeared on the network and corresponded to the mean step size were assumed to be single molecules of LCR. Bleaching in the LCR channel was measured over the time course of the movie and the average time to bleach a

fluorophore was greater than 10-fold the measured residence time of Zyxin and Pxl1 LCRs. We therefore concluded that loss of LCR signal at T-junctions was largely due to dissociation rather than bleaching. The fraction of LCR molecules bound at was determined by fitting 1-cumulative frequency to a single expontial equation f(x)=$x_0 * exp^{(-x/T)}$.

3.5.6 Plasmid constructs for SFSS screens and protein purification

LIM domains can be roughly defined by the following sequence motif: [C][X]2[C][X]13-20[H][X]2[C][X]2[C][X] 2 [C][X]13-20[C][X]2[C], where the zinc coordinating residue [C] is usually cysteine but less frequently H, D, or E, and X is any amino acid. To identify LIM domain containing proteins, the LIM hidden Markov model (HMM PF00412.22) from pFam was used to scan mouse, fission and budding yeasts proteomes using hmmsearch (EMBL-EBI). Primers were designed to PCR amplify LIM domains from cDNAs generated from mouse embryo fibroblasts or fission yeast cells. 15 nucleotide overlaps were included in primers for infusion cloning (Clontech, Mountain View, CA). Where this failed, or for generating synthetic constructs as in (Figure 3.5F), synthetic gBlock DNAs from IDT (Integrated DNA Technologies, Inc.; Coralville, IA) were designed, optimizing codons for expression and to reduce DNA repeat sequences. If possible, eight amino acids on either side of the first and last zinc coordinating residues were included in the LCR clones for the screen. In synthetic construct where one of LIM domains was repeated, 4 amino acids before and after the first and last zinc-coordinating residues were included, comprising an 8 amino acid hybrid linker. Several initial LCR clones localized strongly to the nucleus. To ensure that LCRs were cytoplasmic, a nuclear export sequence l (NES) of zyxin was included on the amino terminal end of the LCR clones. A vector containing CMV promoter, zyxin's NES, BsmBI and BamHI sites, GGSGGS linker, and mCherry. LCRs were cloned into the BsmBI/BamHI cut vectors. BsmBI removes its own recognition sequence, so no additional residues were added in the NES-LCR ORF. For purification constructs, zyxin (residues 381-572) and *S.*

pombe Paxillin-like protein (Pxl1; residues 256-438) PCR products were either inserted into pET21a-MBP-TEV at EcoRI/HindIII or into pET21a-MBP-TEV-SNAP at XmaI/NotI with a flexible linker (GGSGGS) in the forward primer following the SNAP sequence.

3.5.7 LIM protein expression in fission yeast

For expression in fission yeast, full length sequences were cloned into genomic integration vectors pJK210-41xnmt-[LIM domain protein]-GFP::ura4+ that targeted a ura4 region in cells containing a ura4-294 loss of function point mutant, and restored the ability to grow in the absence of uracil when successful integration had occurred. Successful integration was secondarily screened by PCR and sequencing of the ura4 genomic region.

3.5.8 Protein purification and labeling

Zyxin and Pxl1 LCR plasmids were transformed via heat shock into the *Escherichia coli* strain BL21-Codon Plus (DE3)-RP (Agilent Technologies, Santa Clara, CA) and grown on LB Agar plates + selection antibiotics (ampicillin and chloramphenicol). Small cultures (5 mL in culture tubes) were grown overnight shaking at 37°C in TB + salts + antibiotics. The next morning, the small cultures were added to 50 mL of TB media with antibiotics in a 250 mL beveled flask, and this culture was grown for 3 hours shaking at 37°C. Finally, 5-10 mL of that culture was added to 500 mL of TB media with antibiotics in a 2 L beveled flask. This large culture was incubated shaking at 30°C until the OD = 0.6-0.8. Protein expression was then induced with the addition of 0.5 mM isopropyl -D-1-thiogalactopyranoside and left to shake for 16 hr at 16°C.

Cells were lysed with rounds of sonication (Branson Sonifier; ultrasonic probe sonicator) and high pressure homogenization (Emulsi-Flex-C3; Avestin, Ottawa, Canada) in extraction buffer [10 mM HEPES (pH 7.4), 150nM NaCl, 0.02% NaN_3, 0.1 mM DTT] with EDTA-free Protease Inhibitor Cocktail (Roche, Basel, Switzerland). The addition of 50 μM $ZnCl_2$ to

the extraction buffers and subsequent buffers during later protein purifications resulted in an increased protein yield. The extract was clarified into the 'cell junk pellet' and 'soluble protein supernatant' fractions via centrifugation. The supernatant was incubated for 1 hr rocking at 4°C with amylose resin (New England Biolabs, Ipswich, MA). The resin was loaded onto a disposable column and washed with extraction buffer until Bradford reagent indicated clean washes. Protein was eluted with extraction buffer + 30 mM maltose, and the Bradford blue fractions were loaded onto a SDS-PAGE gel for confirmation. The fractions with protein were pooled and dialyzed against SNAP buffer [20 mM Hepes (pH 7.4), 200 mM KCl, 0.01% NaN_3, 10% glycerol, and 1 mM DTT]. SNAP-tagged proteins were filtered on a Superdex 200 10/300 GL or Superose 6 Increase 10/300 GL column (GE Healthcare, Little Chalfont, UK) and then labeled with SNAP-surface-549 (New England Biolabs, Ipswich, MA) overnight at 4°C following the manufacturers' protocols. LIM proteins were flash-frozen in liquid nitrogen and stored at -80°C. Protein concentrations were calculated with the absorbance at 280 nm and extinction coefficients (Table 3.1).

Actin was purified from chicken skeletal muscle acetone powder by a cycle of polymerization and depolymerization and gel filtration [214]. Gel-filtered actin was labeled with Alexa 488 carboxylic acid succinimidyl ester (Life Technologies) on lysine residues [112, 237]. Pyrene actin was labeled on Cys374 with N-(1-Pyrene)Iodoacetamide. The actin concentrations were calculated with the absorbances at 290 and corresponding wavelengths for each label (Alexa-488: 491; Pyrene: 344). Black actin concentration is found with the equation: A_{290} x 38.5 μM. Alexa-488 actin concentration is found with the equations: total = [A_{290} - (0.11 x A_{491})] x 38.5 μM; labeled = $A_{491}/0.071$ μM^{-1}. Finally, pyrene actin concentration is calculated with the equations: total = [A_{290} - (0.1277 x A_{344})] x 38.5 μM; labeled = A_{344} x 45 μM.

Human α-actinin IV was expressed in bacteria and purified as described [248]. Skeletal muscle myosin II was purified from chicken breast and labeled with Alexa 647 as de-

scribed. Dark myosin concentation (mg/mL) is calculated by (A_{280}-A_{320})/0.52, and dividing by the molecular weight (260,789 Da) converts the concentration to M. Labeled myosin concentration uses the correction factor (0.03), extinction coefficient (265,000 $M^{-1}cm^{-1}$), and absorbance wavelength (651) for the fluorescent dye to adjust. Total myosin (mg/mL)= [(A_{280}-A_{320}) -(0.03 x A_{651})]/0.52. Labeled myosin (M) = A_{651}/265,000. Arp2/3 complex was purified from calf thymus by WASp(VCA) affinity chromatography [186]. WASP fragment construct GST-human WASp pWA was purified by Glutathione-Sepharose affinity chromatography.

Protein	**KV #**	**Wavelength (nm)**	**Extinction coefficient (M^{-1} cm^{-1})**
LCR(zyxin)	1081	280	78,270
SNAP-LCR(zyxin)	1092	280	99,240
LCR(Pxl1)	1094	280	99,240
SNAP-LCR(Pxl1)	1095	280	120,210
α-actinin IV (human)	749	280	125,550

Table 3.1: ***In vitro* protein construct extinction coefficients.** Protein information for the *in vitro* constructs. KV # indicates the plasmid number in the lab database. The wavelength is for absorbance, and the extinction coefficient is used to calculate protein concentration.

3.5.9 High-speed sedimentation

20 μM Mg-ATP actin monomers were spontaneously assembled in [10 mM imidazole (pH 7.0), 50 mM KCl, 6 mM $MgCl_2$, 1.2 mM ethylene glycol tetraacetic acid (EGTA), 50 mM dithiothreitol (DTT), 0.2 mM ATP, 50 M $CaCl_2$] for 1 hr to produce F-actin. A range of F-actin (0-10 μM) was then incubated with 0.5 μM LCR construct for 20 min at 25°C. The mixture was spun at 100,000 g for 20 min, and the supernatant and pellet were separated by 12.5% SDS PAGE, stained with Coomassie Blue, destained, and analyzed via densiometry with ImageJ.

3.5.10 Seeded pyrene

Pyrene assembly assays were conducted in 96-well plates in an Infinite M200 Pro (Tecan Systems, Inc., San Jose, CA) fluorescent plate reader to measure the fluorescence of pyrene-actin (excitation at 367 nm and emission at 407 nm. For seeded assembly, a 5 μM stock of unlabeled Mg-ATP actin monomers was preassembled, followed by the addition of 100x anti-foam, 10x KMEI [500 mM KCl, 10 mM $MgCl_2$, 10 mM EGTA, 100 mM imidazole (pH 7.0)], and a range of LCR(zyx) (0-2 μM). The final concentration of F-actin unlabeled seeds was 0.5 μM for each well. Actin monomers (20% pyrene-labeled) were added to another row of wells, and mixing the monomer row with the preassembled actin filament row initiated the reactions.

3.5.11 In vitro contractility assay

Time-lapse TIRFM movies were taken using a cellTIRF 4Line system (Olympus, Center Valley, PA) fitted to an Olympus IX-71 microscope with through-the-objective TIRF illumination and an iXon EMCCD camera (Andor Technology, Belfast, UK). The bundled actin networks consisted of F-actin (1.5 or 3 μM, 10% Alexa 488 labeled), α-actinin (100-200 nM), LCR (50-200 nM), and polymerization TIRF buffer [10 mM imidazole (pH 7.0), 50 mM KCl, 1 mM $MgCl_2$, 1 mM EGTA, 50 mM DTT, 0.2 mM ATP, 50 μM CaCl2, 15 mM glucose, 20 μg/ml catalase, 100 μg/ml glucose oxidase, and 0.5% (400 cP) methylcellulose]. Based on the glass and imaging conditions, the specific protein concentrations varied within a set range to create contractile networks. The protein mixture was transferred to a flow chamber, and the network was allowed to preassemble for 30-45 minutes (Figure 3.14). Simultaneously, monomeric myosin II was polymerized separately in a low salt buffer [10 mM imidazole (pH 7.0), 1 mM $MgCl_2$, 1 mM EGTA, 0.3 mM ATP]. To induce network contraction, polymerized myosin (50-150 nM) was flowed into the chamber. The flow mixture also contained the

critical concentration of actin (0.1 μM) and the same initial concentrations of α-actinin and LCR. Images were then acquired at either 10 or 15 s intervals at room temperature.

3.5.12 Bead symmetry breaking assay

Polystyrene microspheres (Polysciences, Eppelheim, Germany) were coated with GST-pWA [186]. Motile beads were imaged after 15 minutes of polymerization on an inverted microscope (Ti-E; Nikon, Melville, NY) with a confocal scan head (CSU-X; Yokogawa Electric, Musashino, Tokyo, Japan), 491, 561, and 642 laser lines (Spectral Applied Research, Richmond Hill, Ontario, Canada) and an HQ2 CCD camera (Roper Scientific, Trenton, NJ). Z-stacks were acquired, reconstructed and analyzed using ImageJ. Fluorescence ratios were determined using the central, single plane of motile beads. Background-subtracted fluorescence values were measured for each fluorescent protein in the comet tail region and in the protrusion region.

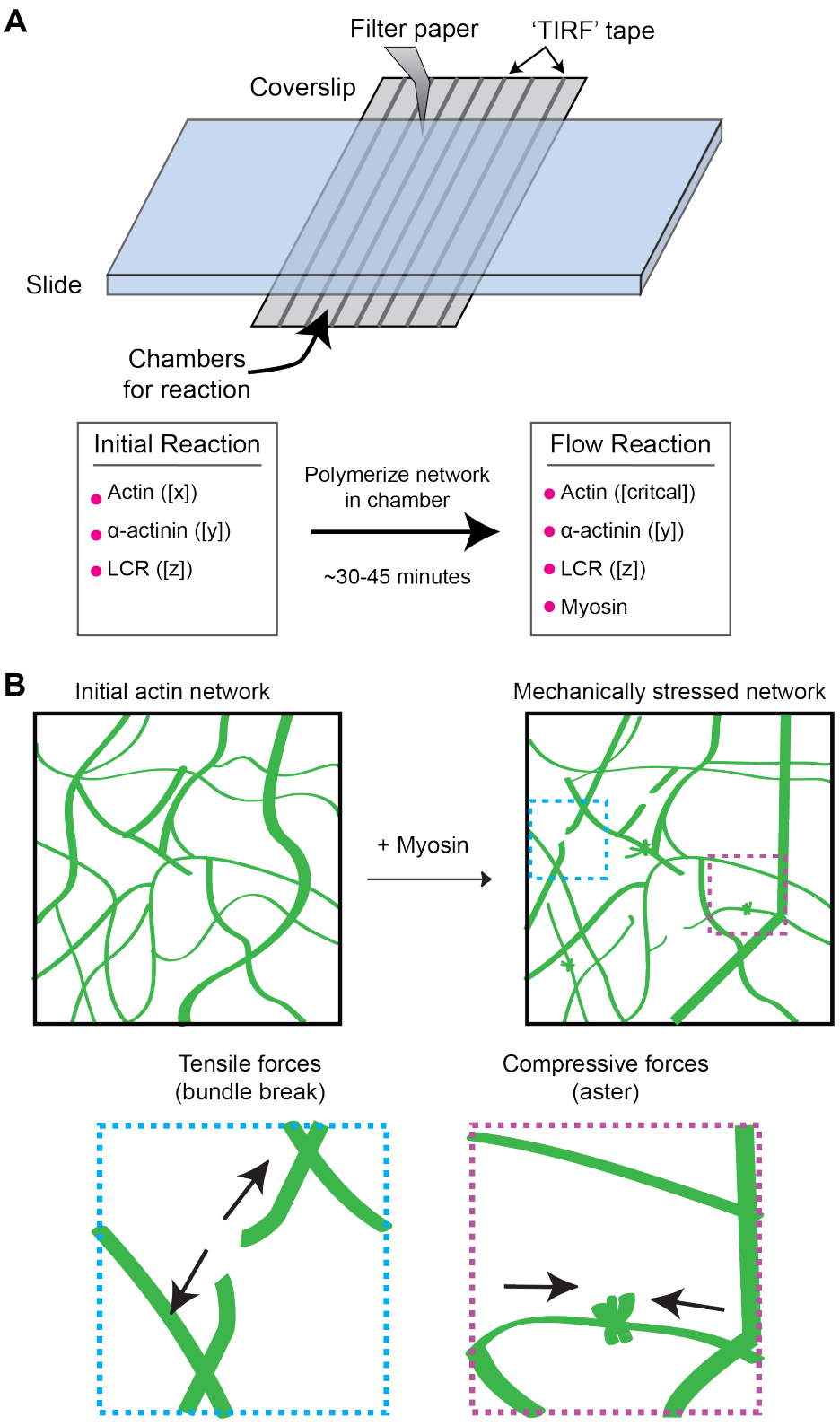

Figure 3.14: ***In vitro* contractility assay setup.**

Figure 3.14: (continued) **(A)** Simple schematic of the flow chamber setup. Double-sided 'TIRF' tape is used to make long chambers between the coverslip and slide. The initial reaction is flowed into the chamber, and the 'flow in' reaction is added by using filter paper to wick the liquid from the other side. The 'flow in' reaction is added 30-45 minutes after network assembly and essentially maintains the initial reaction with the same concentrations of α-actinin and LCR and the criticial concentration of actin monomer. The addition of myosin in the 'flow in' reaction initiates network contraction. **(B)** Simple cartoon of bundled F-actin network assembly and myosin induced contractility. Major myosin forces are tension and compression, which deform the network.

CHAPTER 4

ENGINEERING A FLUORESCENTLY-LABELED FISSION YEAST ARP2/3 COMPLEX FOR SINGLE MOLECULE MECHANISTIC INVESTIGATIONS *IN VITRO*

Preface

The work in this chapter is currently in progress to complete for submission in a few months. Meghan O'Connell, Cristian Suarez, Vilmos Zsolnay, and David Kovar have contributed to the work in this chapter so far. I initiated the project, cloned and troubleshooted the fluorescent Arp2/3 complex constructs, conducted pyrene assays, did some TIRFM, formatted all figures, and wrote the first manuscript draft. Meghan did all the cell work, most TIRFM, and most analysis. Vilmos did the more complex computational analysis for Arp2/3 complex binding. Additional data for the manuscript will be provided by Michael James and Vladmir Sirotkin (State University of New York (SUNY) Upstate Medical University) for patch dynamics analysis.

4.1 Abstract

Arp2/3 (actin-related protein 2/3) complex is a seven-component protein complex that binds to a 'mother' actin filament and nucleates a branched new 'daughter' filament. Arp2/3 complex is activated by a nucleation promoting factor (e.g. WASp/Scar family proteins), and the mechanism and pathway of Arp2/3 complex activation and branch formation has been well-studied with limited direct visualization. Here, we have successfully engineered and purified a fluorescently-labeled fission yeast Arp2/3 complex and visualize Arp2/3 complex binding and branch formation in single molecule TIRF microscopy. We have made progress into fully understanding the pathway of Arp2/3 complex-mediated branch formation.

4.2 Introduction

Cells assemble and maintain diverse actin filament (F-actin) networks with unique architectures and dynamics that are best suited to facilitate their corresponding cellular processes [15, 142]. In fission yeast, the F-actin networks are assembled by two nucleators: formins (Cdc12, For3, Fus1) and Arp2/3 (actin-related protein 2/3) complex [175]. Formins assemble straight filaments that form polarizing actin cables (For3), the contractile ring (Cdc12) in dividing cells, and the fusion focus (Fus1), whereas Arp2/3 complex nucleates branched filaments for endocytic actin patches [27, 63, 118]. The different actin networks exist in homeostasis as they compete for available actin monomers (G-actin) to maintain their density and size [22]. The G-actin binding protein profilin favors formin-mediated actin filament (F-actin) elongation and directly inhibits Arp2/3 complex-mediated actin assembly [216, 117, 193, 58, 90, 192].

Arp2/3 complex is essential for creating short branched actin networks that are ideal for generating forces, including the lamellipodia in motile cells, endocytic patches in budding and fission yeast, and actin tail formation and propelling movement of pathogenic listeria [178]. Arp2/3 complex binds to an existing mother filament and mediates daughter branch formation (Figure 4.1A). Arp2/3 complex consists of two actin related proteins (Arp2 & Arp3) and five additional subunits (ArpC1-5), which together form the intrinsically inactive complex [221, 14] (Figure 4.1B). Nucleation promoting factors (NPFs) are required to activate Arp2/3 complex. The most well-studied NPFs are the Wiskott-Aldrich syndrome protein (WASp) and Scar/WAVE protein families. These NPFs have a C-terminal VCA (Verpolin, Central, Acidic) region that is responsible for Arp2/3 complex activation [165]. The different VCA (also known as WCA) components have separate roles, as VC binds G-actin and CA associates with Arp2/3 complex [137, 33]. Therefore, VCA initiates the interaction of the Arp2/3 complex and the first subunit of the daughter filament. This creates a trimer

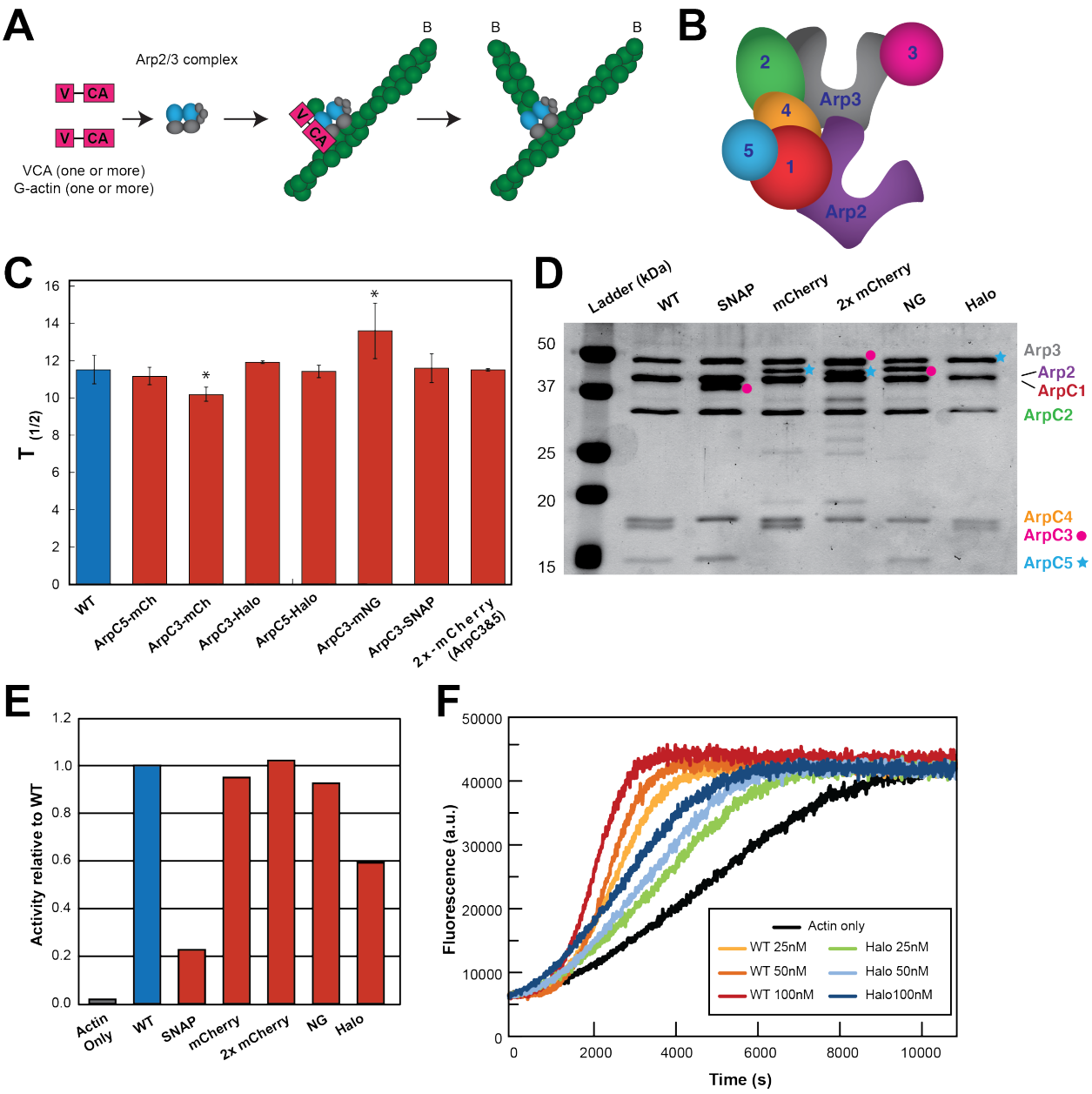

Figure 4.1: **Determining the optimal labeled Arp2/3 complex.** **(A)** Simplified schematic of the pathway of Arp2/3 complex-mediated branch formation. Typically, one or more VCA containing proteins brings one or more actin monomers to the Arp2/3 complex and initiates binding and branch nucleation. 'B' labels the barbed end of the filaments **(B)** Cartoon of the seven-component organization of Arp2/3 complex (Arp2, Arp3, ArpC1-5). **(C)** Calculated $t_{1/2}$ for fission yeast growth assays of tagged Arp2/3 complex strains. n = 3 replicates for all strains except WT, where n = 6, error bars = s.d. One-tailed t-test with unequal variance comparing each strain to WT yielded significantly different p-values for ArpC3-mCh (0.0288) and ArpC3-mNG (0.0235).

Figure 4.1: (continued) **(D)** SDS-PAGE gel showing 0.6 μg of each purified Arp2/3 complex construct. The components are labeled along the right side of the gel. Pink circles and blue stars indicate shifts in ArpC3 (SNAP, NG) and ArpC5 (mCherry, Halo) with fluorescent tags, respectively. These are the only constructs discussed any further so the abbreviations are: SNAP (ArpC3-SNAP), mCherry (ArpC5-mCherry), 2x-mCherry (ArpC3-mCherry; ArpC5-mCherry), NG (ArpC3-mNeonGreen), and Halo (ArpC5-Halo). **(E)** Relative activity of each Arp2/3 complex construct in bulk spontaneous pyrene assays containing 1 μM actin, 100 nM Arp2/3 complex, and 100 nM VCA. The $t_{1/2}$ for each construct was normalized and compared to WT (1) and actin only (0). **(F)** A representative trial of spontaneous pyrene with a range (25 nM, 50 nM, 100 nM) of wildtype or ArpC5-Halo with 100 nM VCA.

structure that is more energetically stable than a trimer formed from three actin monomers. It has been proposed that two WASP proteins function as dimers and actually deliver two monomers to Arp2/3 complex [164]. In addition to VCA containing nucleation promoting factors (NPFs), the WISH/DIP/SPIN90 (WDS) family of NPFs utilize an armadillo repeat to activate Arp2/3 complex [133, 202]. WDS proteins don't require a pre-existing mother filament and instead nucleate linear actin filaments [239].

The formation of a ternary structure of Arp2/3 complex, VCA (one or more), and G-actin (one or more) is one step in the pathway leading to successful nucleation of an Arp2/3 complex-mediated branch. Arp2/3 complex must also bind ATP and conformationally change to bring Arp2 closer to Arp3 [9, 158]. The precise order and rates of the Arp2/3 complex-mediated branch formation pathway have been studied extensively over the years [137, 10]. While there is much known on how Arp2/3 complex branching occurs, there has been limited direct visualization of the branching pathway. Smith et al. [207, 208] visualized the pathway with fluorescently labeled *Saccharomyces cerevisiae* (budding yeast) Arp2/3 complex and WASp. However, *S. cerevisiae* Arp2/3 complex has a minimal base level of activity in the absence of WASp (reviewed in [77]). In *Schizosaccromyces pombe* (fission yeast) and mammalian systems, Arp2/3 complex remains fully inactive in the absence of an NPF. Additionally, fission yeast is a long-standing model system for understanding the mechanisms and functions of the actin cytoskeleton and its associated actin binding proteins.

Therefore, we engineered a fluorescently labeled *S. pombe* (fission yeast) Arp2/3 complex and Wsp1-VCA constructs to further characterize the branching pathway with fission yeast proteins. These engineered tools can now be used for further investigation into understanding the formation and regulation of Arp2/3 complex-mediated F-actin networks in cells.

4.3 Results

4.3.1 Engineering an optimal fluorescently-labeled Arp2/3 complex for in vitro experiments

To visualize Arp2/3 complex at the single molecule level *in vitro*, we initially needed to engineer and purify an optimally functional fluorescently-tagged Arp2/3 complex. We required three characteristics for an optimal construct sufficient for mechanistic studies: (1) the construct should not exhibit major growth and F-actin network defects in fission yeast cells, (2) the general F-actin branching activity should be as close to wild-type Arp2/3 complex as possible, and (3) single molecules of the fluorescently-labeled Arp2/3 complex should be visible by TIRF microscopy (TIRFM) imaging. As described in the following paragraphs, to determine the most optimal fluorescently-labeled fission yeast Arp2/3 complex construct, we (1) engineered a series of fission yeast strains in which various tags were integrated into the genome of the ArpC3 and ArpC5 subunits of Arp2/3 complex, (2) characterized their cell growth, general F-actin network organization and endocytic actin patch dynamics, and (3) purified and fluorescently-labeled the Arp2/3 complexes and determined their actin assembly properties in 'bulk' pyrene and single filament/molecule TIRFM imaging actin assembly assays.

Since Arp2/3 complex has seven components, we wanted to create a fission yeast strain with an endogenously tagged component of the complex. The majority of *in vivo* experiments with fluorescently-labeled Arp2/3 complex tag ArpC5. However, previous studies in bud-

Strain #	Genotype	Source
KV367	h-, ARPC5-mCherry-natMX6, ade6-M216, leu1-32, his3-D1, ura4-D18	V. Sirotkin
KV480	h?, protease deficient	T. Pollard
KV588	h+, pAct1 Lifeact-GFP::Leu+, ade6-M216, leu1-32, his3-D1, ura4-D18	M. Balasubramanian
KV678	h+, fim1-mCherry-natMX6, pAct1 Lifeact-GFP::Leu+, ade6-M216, leu1-32, his3-D1, ura4-D18	Unknown
KV981	h?, ARPC3-SNAP-KanMX6, protease deficient	This study
KV982	h?, ARPC3-mCherry-KanMX6, protease deficient	This study
KV984	h?, ARPC3-mCherry-KanMX6, ARPC5-mCherry-NatMX6, protease deficient	This study
KV996	h?,ARPC3-Halo-KanMX6, protease deficient	This study
KV997	h?, ARPC5-Halo-KanMX6, protease deficient	This study
KV1005	h?, pAct1 Lifeact-GFP::Leu+, ARPC5-HALO-KanMX-6, protease deficient (?)	This study
KV1006	h?, ARPC3-mNeonGreen-KanMX6, protease deficient	This study
KV1007	h?, ARPC5-Halo-KanMX-6, fim1-mCherry-natMX6, protease deficient (?)	This study

Table 4.1: **The fission yeast strains used in this paper.** This is a complete list of the fission yeast strains utilized in this manuscript. The strain number corresponds to our lab database of fission yeast. Most of the strains were made specifically for this manuscript and are described in the methods.

ding yeast tagged the fission yeast ArpC3 ortholog with a SNAP-tag for *in vitro* mechanistic studies [207, 208]. Therefore, we engineered a series of fission yeast strains expressing different endogenously tagged Arp2/3 complex components: ArpC3-SNAP, ArpC3-mCherry, 2x-mCherry (ArpC3-mCh, ArpC5-mCh), ArpC3-mNeonGreen, ArpC3-Halo, and ArpC5-Halo, as well as a previously engineered strain (ArpC5-mCherry) (Table 4.1). To determine whether endogenously tagged Arp2/3 complex components cause general cell growth de-

fects, we tested the tagged fission yeast strains in a bulk growth assay (Figure 4.1C). By comparing the $t_{1/2}$ for each strain to reach plateau, most of the strains grow nearly identically to WT. However, both ArpC3-mCherry and ArpC3-mNeonGreen deviate from WT because ArpC3-mCherry has a significantly lower $t_{1/2}$, while ArpC3-mNeonGreen has a significantly higher $t_{1/2}$ (Figure 4.1C). Furthermore, although the $t_{1/2}$ for the ArpC3-Halo strain is not significantly different, this strain was not considered further because it has general growth and stability issues and the growth curve plateaus much lower than WT. Because of their normal general growth rates, we moved forward with further analysis of ArpC3-SNAP, ArpC5-mCherry, 2x-mCherry, ArpC3-mNeonGreen and ArpC3-Halo.

Next, we purified the remaining Arp2/3 complex constructs following previous methods to examine their actin assembly activities [203] (Figure 4.1D). To understand the activity levels of each Arp2/3 complex construct, we conducted spontaneous pyrene assays comparing each construct to both actin alone and wild-type (WT) Arp2/3 complex (Figure 4.1E, 4.2). The $t_{1/2}$ was calculated for each construct and compared and normalized to WT (1) and actin only (0) to determine relative activity level for each Arp2/3 complex construct (Figure 1E). The SNAP construct has the lowest relative activity level of about 0.22, while the Halo construct has an activity level of about 0.6. The mCherry, 2x-mCherry, and NG constructs are close to WT with about 0.9-1 activity levels. As our goal was to visualize Arp2/3 complex at the single molecule level, we also tested the constructs in single molecule total internal reflection fluorescence (TIRF) microscopy assays (Figure 4.3A,B). The ArpC3-mNeonGreen construct is visible but only in aggregates that cause large asters (Figure 4.3B). The mCherry and 2x-mCherry constructs do not aggregate, but the fluorescence signal at branch sites is not above background noise. Unlike other constructs tested, the Halo Arp2/3 complex (ArpC5-Halo) does not aggregate and is visible at the single molecule level in TIRF (Figure 4.3A). The Halo Arp2/3 complex construct is the optimal engineered tool for this research. There are no cell growth defects, and it is visible in single molecule TIRF microscopy. The

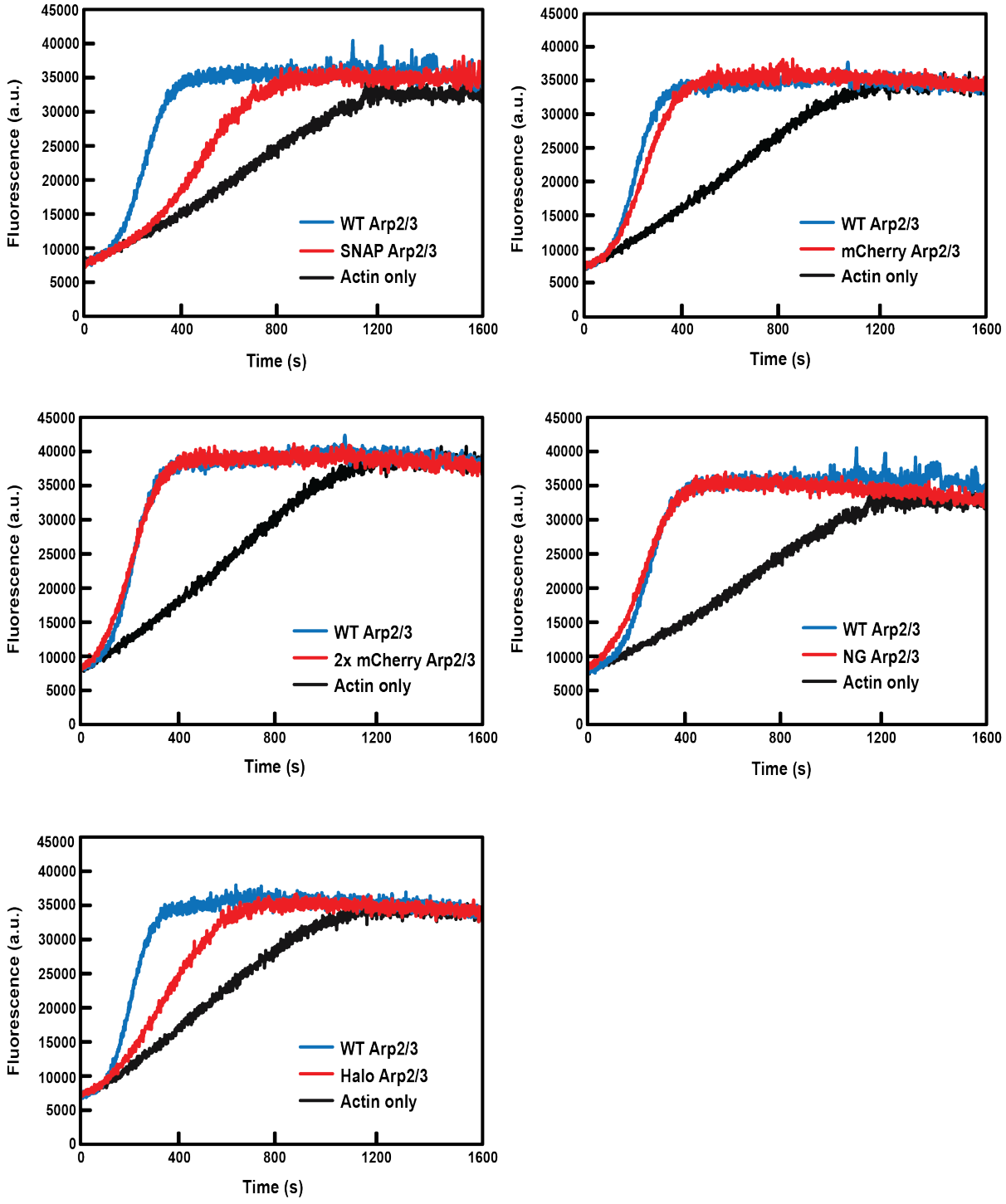

Figure 4.2: **Representative pyrene curves.** Representative spontaneous pyrene curves for the different Arp2/3 complex constructs with their corresponding trials of WT and actin only. Each reaction has 1 μM actin (10% pyrene-labeled), 100nM Arp2/3 complex, and 100nM VCA.

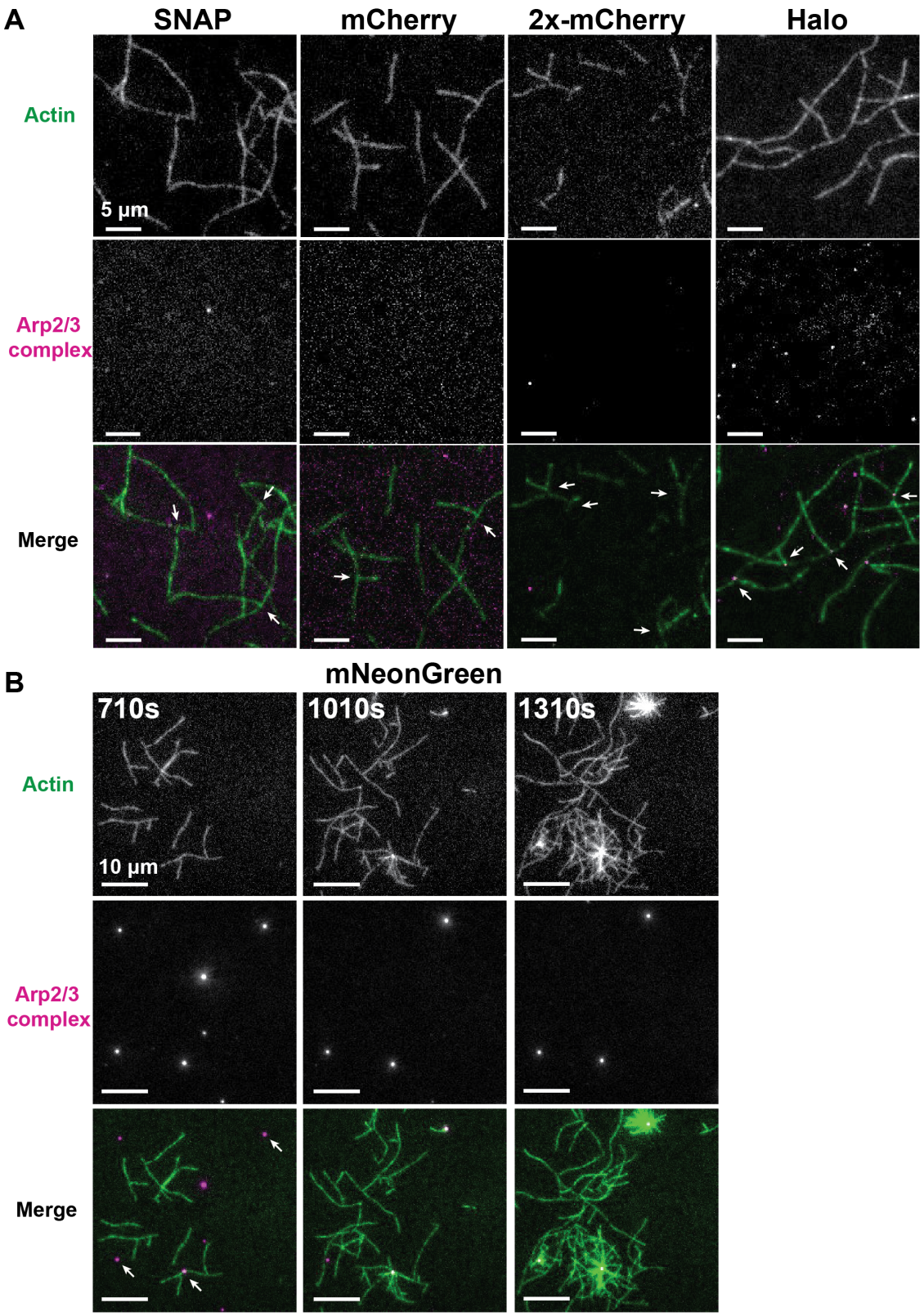

Figure 4.3: **Single molecule TIRFM of fluorescently-labeled Arp2/3 complex constructs**

Figure 4.3: (continued) **(A)** Representative images from movies of branch formation by different fluorescent Arp2/3 complex constructs. The arrows shown in the merge indicate Arp2/3 complex mediated branches. Scale bar = 5 μm. **(B)** Representative images from a movie where the mNeonGreen Arp2/3 complex aggregates and forms asters. Scale bar = 10 μm.

decreased activity in pyrene is likely due to a fraction of inactive protein that was unable to be separated during purification. Additional spontaneous pyrene showed that Halo Arp2/3 complex increases with an increasing range of concentration (Figure 4.1F), and the decreased activity appears to scale with the concentration. The fraction of inactive protein should not affect the single molecule analysis of active Arp2/3 complexes.

4.3.2 Halo-Arp2/3 complex fission yeast cells exhibit no significant F-actin network deficiencies

As the ArpC5-Halo construct appears to be optimal for *in vitro* mechanistic studies, we further analyzed the effects of the endogenous HaloTag on fission yeast F-actin networks and the dynamics of endocytic actin patches. When cells were stained with phallicidin, a marker for F-actin, we observe no major differences in F-actin network structures for ArpC5-Halo cells when compared to WT fission yeast cells (Figure 4.4A). Actin patch dynamics have been studied in immense detail [204]. Inhibiting Arp2/3 complex through the small molecular inhibitor CK666 results in patch disassembly [157, 191], and mutations in components of Arp2/3 complex affect the dynamics of the patches [151, 249]. We analyzed the patch dynamics of the actin patches in WT and Halo-Arp2/3 complex cells using Lifeact (Figure 4.4). When compared to wild-type cells, we observed no significant difference in patch dynamics.

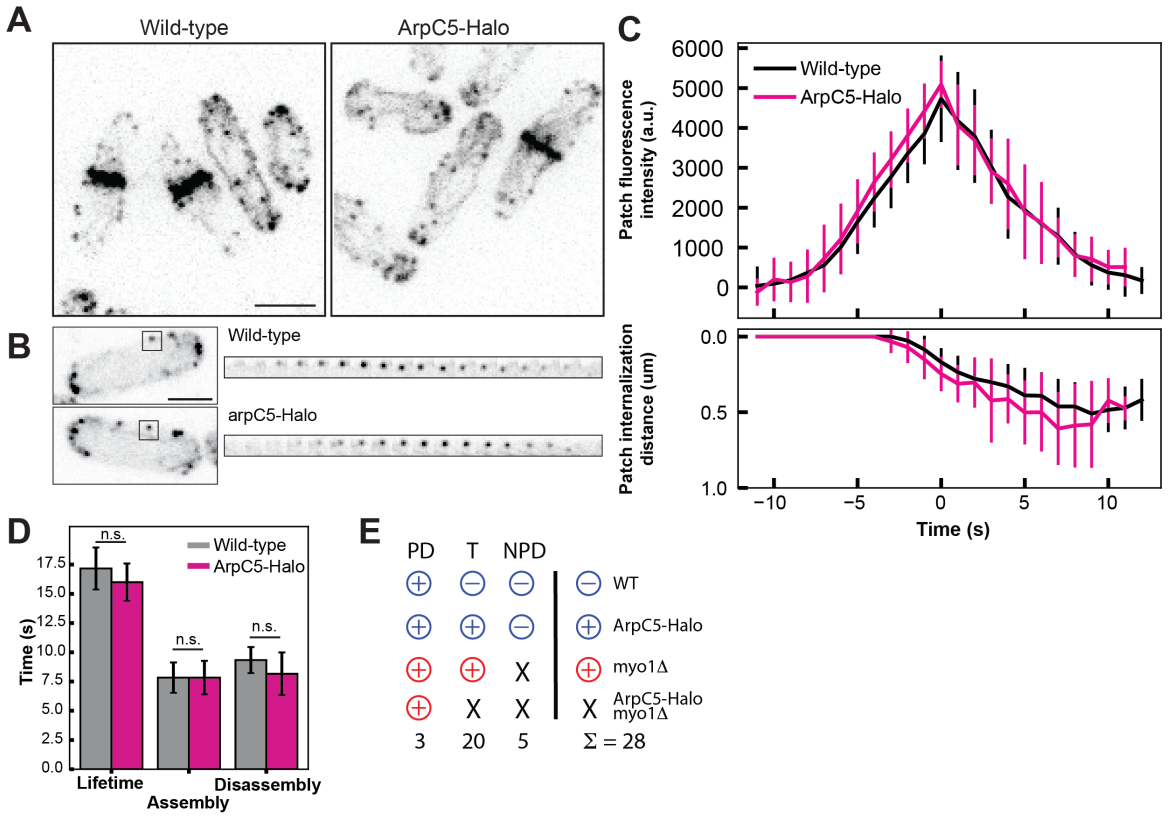

Figure 4.4: **Endogenous HaloTag on Arp2/3 complex has no effect on endocytic actin patch dynamics.** **(A)** Representative fluorescent micrographs of fission yeast cells stained with phallicidin to mark F-actin networks. Scale bar = 5 mm. **(B)** Representative time-lapse fluorescent micrographs showing fission yeast endocytic actin patches expressing Lifeact-eGFP. **(C)** Lifeact-eGFP intensity and patch internalization distance in fission yeast endocytic patches over their lifetimes for cells with wild-type or ArpC5-Halo Traces represent the average of 10-12 endocytic patches, error bars = s.d. **(D)** Lifetime, assembly time, and disassembly time of endocytic actin patches in wild-type or ArpC5-Halo cells. n = 10-12 patches, error bars = s.d. **(E)** Diploid tetrad analysis of myo1δ cells crossed with wild-type or ArpC5-Halo fission yeast cells.

4.3.3 Halo-Arp2/3 complex can be visualized at the single molecule level

Purified Halo-Arp2/3 complex was fluorescently labeled with a TMR ligand and mixed with monomeric actin (10% Alexa-488 labeled) and a VCA fragment of *S. pombe* Wsp1. Actin filament assembly was observed in single molecule TIRFM, and fluorescently labeled Arp2/3 complex was visible at 60% of branch sites (Figure 4.5A, 4.6). Reduced labeling efficiency and bleaching events contribute to the unlabeled Arp2/3 complex-mediated branching events (Figure 4.6). The time between Arp2/3 complex binding to the mother filament and daughter filament branch initiation was calculated by using the observed elongation rate of the daughter filament to retrospectively determine the time of branch nucleation (Figure 4.5B). The average time gap between Arp2/3 complex binding and branch nucleation is approximately 2.1 seconds (Figure 4.5C).

4.3.4 Halo-Arp2/3 complex is active with multiple classes of nucleation promoting factors

In addition to the VCA containing NPFs, there is the WISH/DIP/SPIN90 (WDS) family of NPFs that utilize an armadillo repeat to activate Arp2/3 complex [133, 202]. WDS proteins don't require a pre-existing mother filament for nucleation and form straight filaments instead of branched filaments [239]. *S. pombe* Dip1, a member of the WDS family, creates actin seeds that can initiate Wsp1 branch formation [7]. The cooperation between Dip1 and Wsp1 is important for endocytic branched actin network formation [6]. Purified Dip1 increases filament nucleation, and labeled Halo-Arp2/3 complex can be seen at the pointed ends of filaments (Figure 4.7).

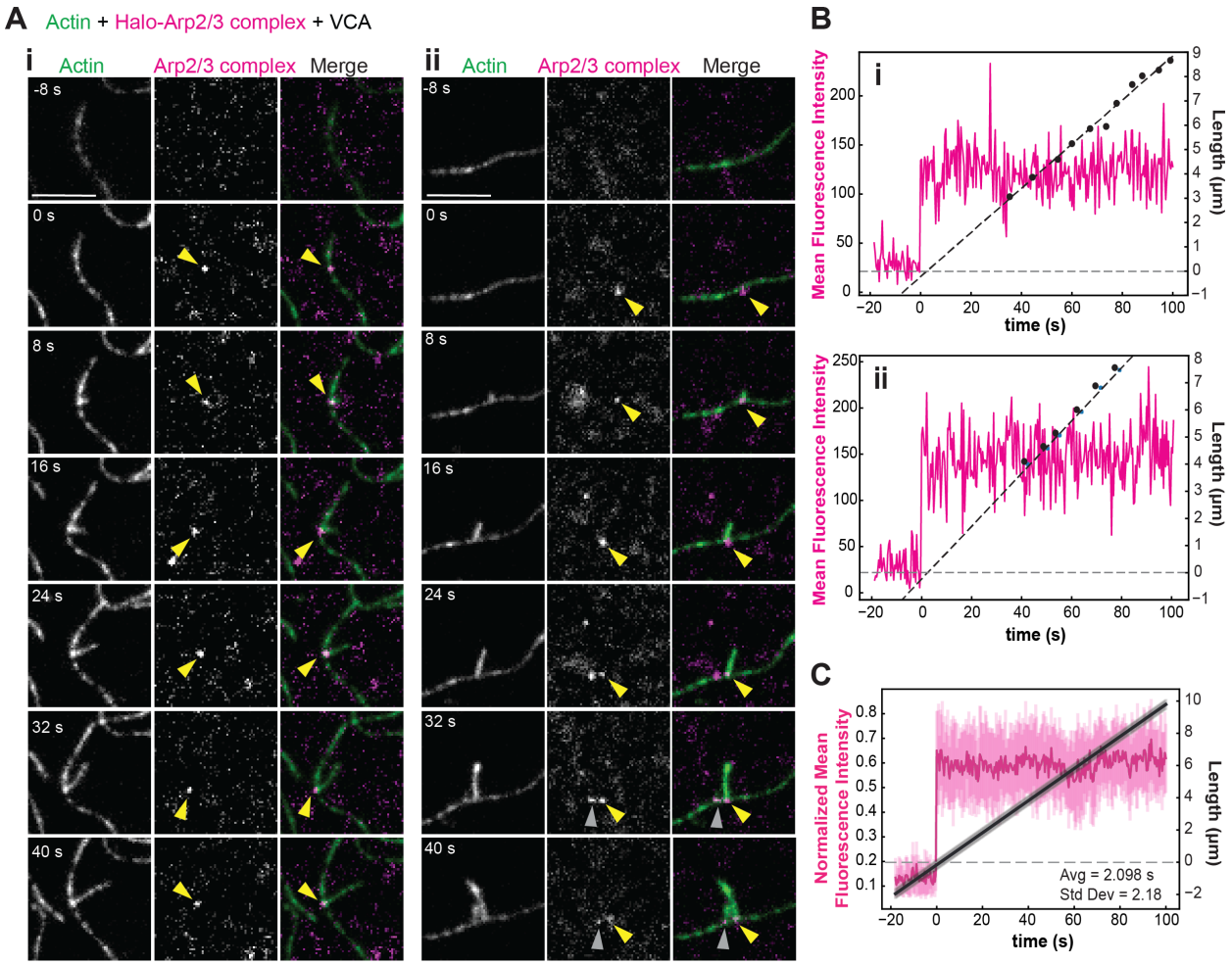

Figure 4.5: **Labeled Halo-Arp2/3 complex at branch sites. (A)** Representative time-lapse images of Halo-Arp2/3 complex binding to a mother filament and remaining through daughter branch formation. Events shown in (i) and (ii) are two distinct examples of Arp2/3 complex binding and branch formation. Reactions contained 1.5 μM Mg-ATP actin (10% Alexa-488 labeled), 30 nM ArpC5-Halo TMR, and 300 nM VCA. The arrows in the first few images show the Arp2/3 complex that will eventually form a branch. Scale bar = 5 μm **(B)** Representative nucleation graphs from branches shown in (A). Pink line shows the step-like increase of Arp2/3 complex signal. The daughter filament length was traced at each data point, and the nucleation time can be calculated by using the elongation rate (slope) to determine when the daughter filament began to grow in relation to Arp2/3 complex binding. **(C)** Average nucleation graph. Average nucleation time = 2.098 +/- 2.18 sec. n = 18 branches, error bars = s.d.

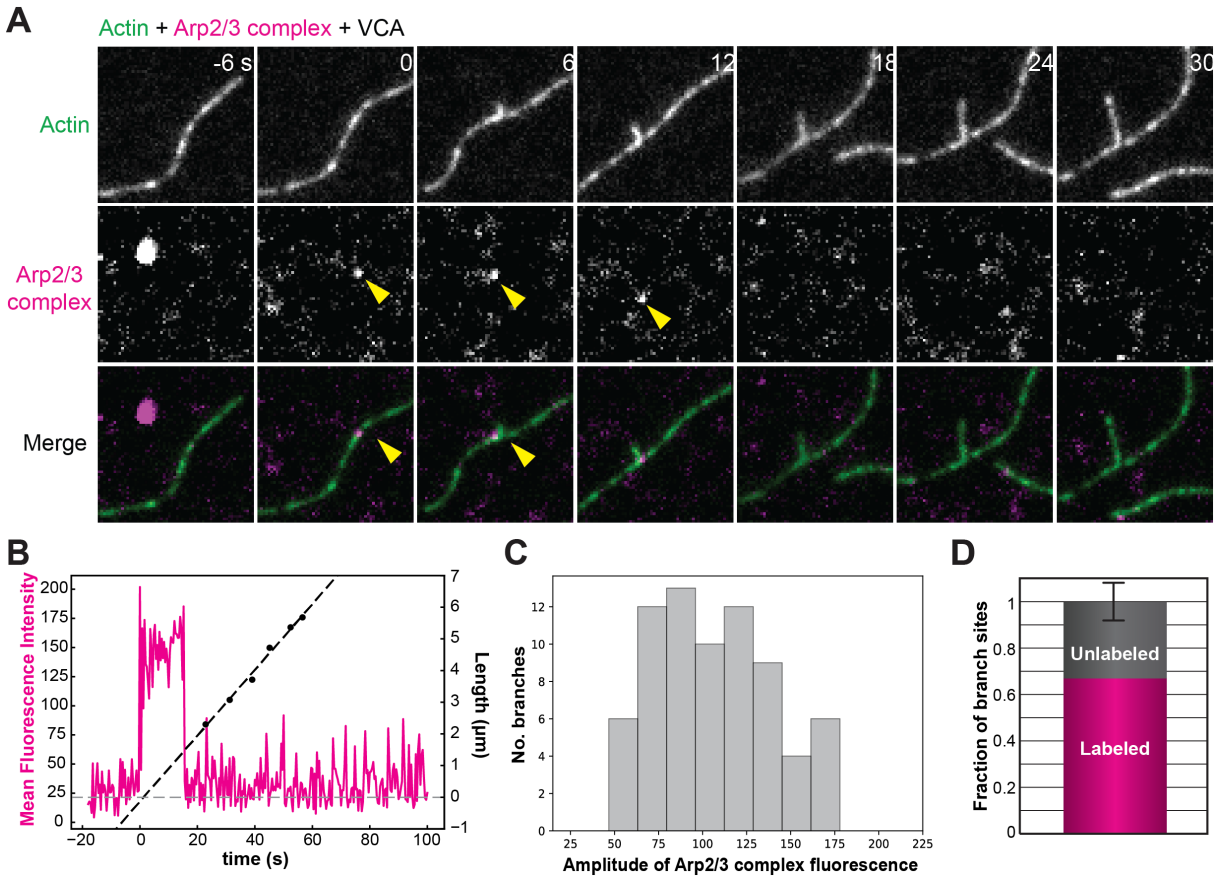

Figure 4.6: **Majority of branch sites have single molecule of labeled Halo-Arp2/3 complex.** **(A)** Representative time-lapse TIRFM images of Halo-Arp2/3 complex nucleating a branch and bleaching while daughter filament elongation continues. Reactions contained 1.5 μM Mg-ATP actin (10% Alexa-488 labeled), 30 nM ArpC5-Halo TMR, and 300 nM VCA. **(B)** Nucleation graph of a Halo-Arp2/3 complex bleaching event. The Arp2/3 complex bleached prior to the filament traces. **(C)** Histogram of Halo-Arp2/3 complex fluorescence amplitude. Amplitude was calculated as the difference in fluorescence at the branch site between the frame in which Arp2/3 complex appeared and the frame immediately prior. n = 72 branches. **(D)** Fraction of branch sites with fluorescently labeled or unlabeled Halo-Arp2/3 complex. n = 3 independent movies with 111 events, error bars = s.d.

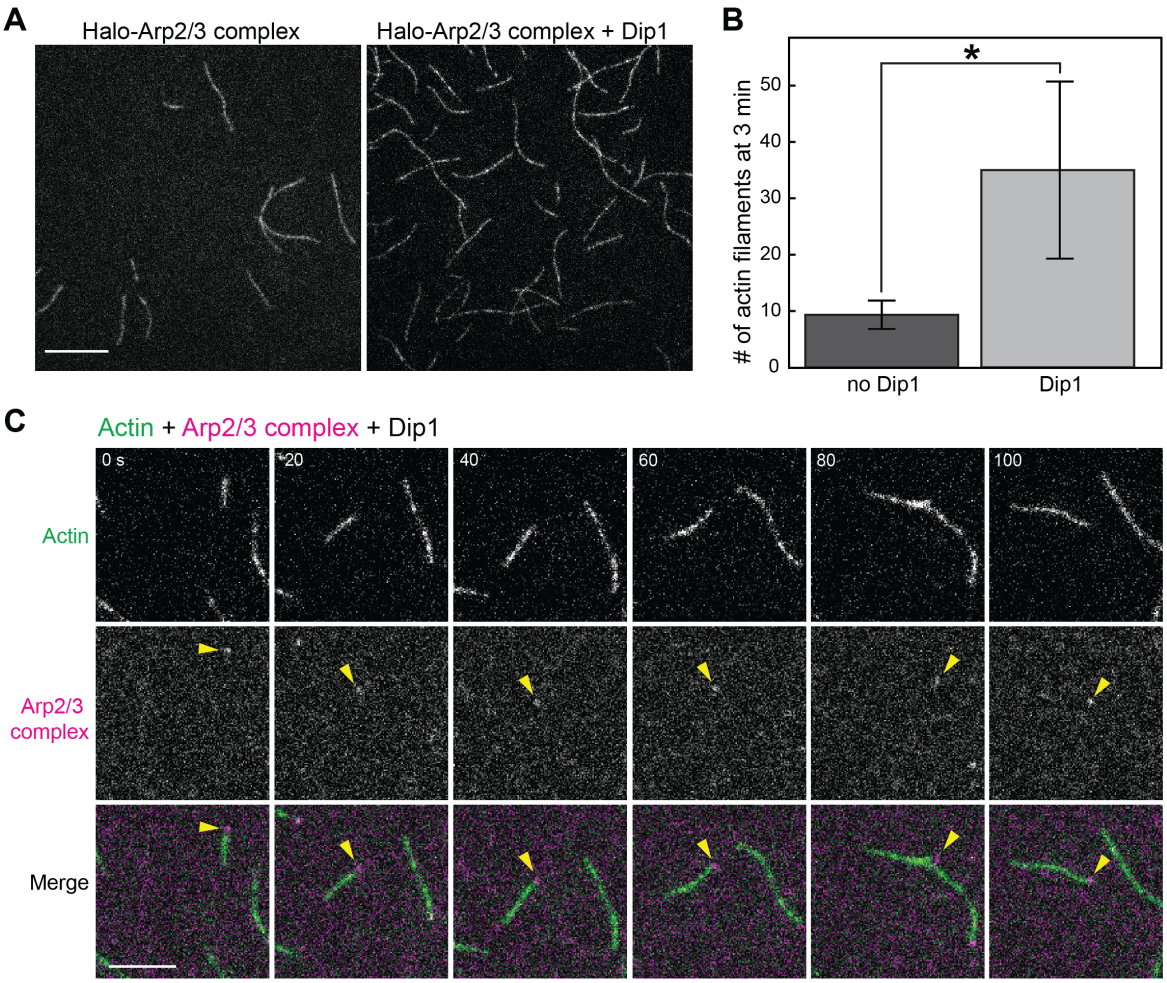

Figure 4.7: **Dip1 robustly activates Halo-labeled Arp2/3 complex nucleation. (A)** Single color TIRFM of 1.5 μM Mg-ATP actin (10% Alexa-488 labeled) with 25 nM ArpC5-Halo TMR, and either 0 or 50 nM fission yeast Dip1. Images at t = 3 min after initiation of actin assembly reaction. Scale bar = 10 μm. **(B)** Quantification of the number of filaments nucleated by Arp2/3 complex. One tailed t-test with unequal variance yielded p-value *p=0.0492, error bars = s.d., n = 3 replicates. **(C)** Representative time-lapse of Halo-Arp2/3 complex activated by Dip1 to form linear filaments. Scale bar = 5 μm.

4.3.5 F-actin binding of Arp2/3 complex increases in the presence of VCA

In order to understand how nucleation promoting factors influence Arp2/3 complex activity, we examined how Wsp1(VCA) affects Arp2/3 complex binding to actin filaments. Previous work [207] has demonstrated that in the presence of VCA, Arp2/3 complex binds more frequently to actin filaments *in vitro*. To examine Arp2/3 complex binding dynamics, we tethered actin filaments to the surface via biotin-actin and flowed in Halo-Arp2/3 complex and capping protein (to prevent new filament polymerization) with or without VCA present. Arp2/3 complex dynamics were continuously monitored. In the absence of VCA, we found that Arp2/3 complex very rarely binds to F-actin *in vitro* (Figure 4.8A,B). The addition of VCA significantly increases Arp2/3 complex binding events along actin filaments (Figure 4.8A,B). This would imply that the conformational change of Arp2/3 complex when bound to VCA is better suited for filament binding.

Interestingly, TIRFM movies with added VCA have a noticeable increase in total Halo-Arp2/3 complex in the field of view compared to movies without VCA. However, the fraction of bound Arp2/3 complex molecules is not significantly different between the two conditions (Figure 4.8C). We suspect that, as the presence of VCA increases Arp2/3 complex F-actin binding, the presence of more Arp2/3 complex molecules may be due to increased sampling. If the conformational change of VCA bound Arp2/3 complex increases filament binding events, it would be likely that more Arp2/3 complex would be seen in the field of view.

4.4 Discussion

In this work, we successfully engineer and minimally characterize a fluorescently labeled Arp2/3 complex that is critical for further single molecule analysis of the Arp2/3 complex-mediated branch formation pathway. Arp2/3 complex branch formation involves multiple steps, and the fluorescent Arp2/3 complex serves as an invaluable tool for analyzing each

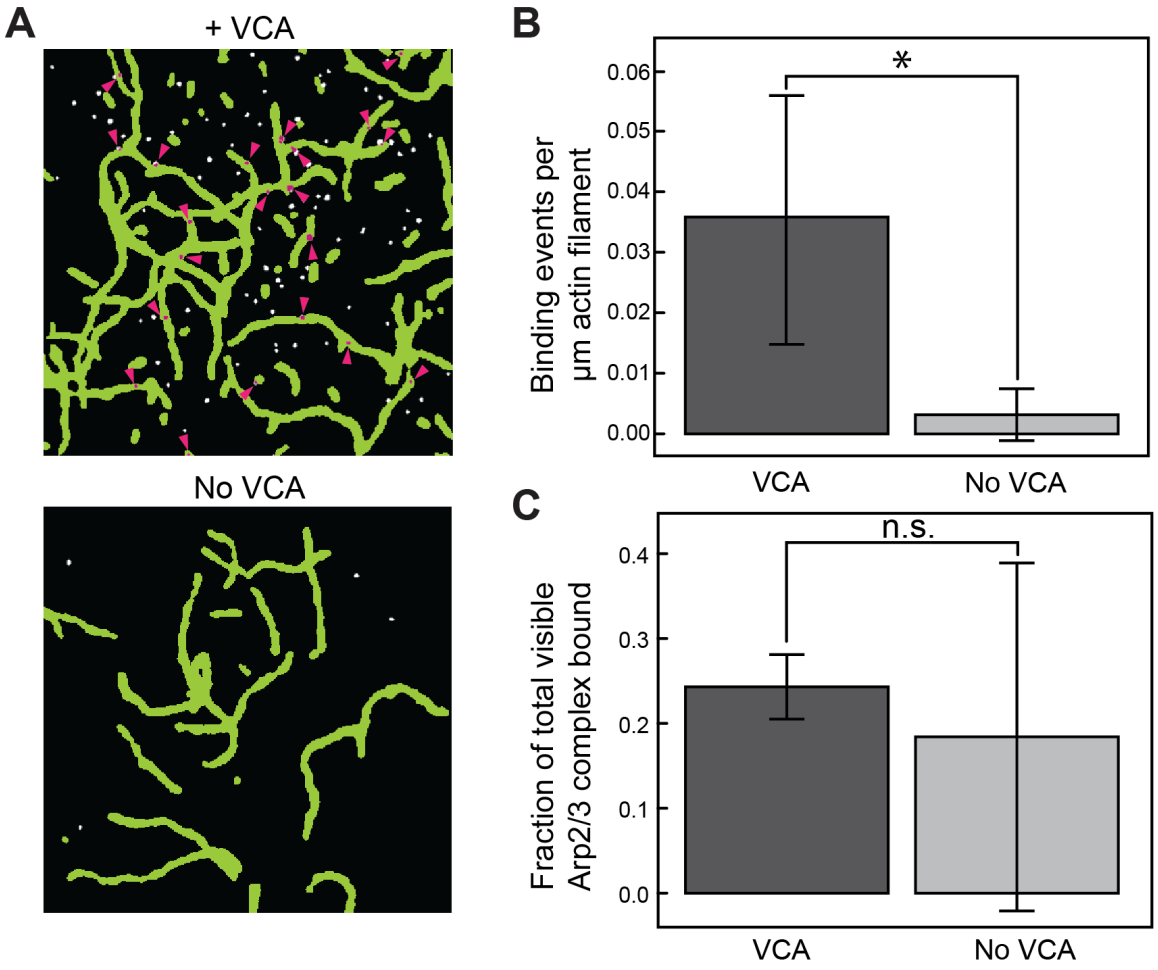

Figure 4.8: **Binding of Arp2/3 complex in the presence or absence of VCA. (A)** Representative images showing the actin mask that was used to calculate whether the Arp2/3 complex is bound to actin filaments in the presence or absence of VCA. The magenta dots represent bound Arp2/3 complex molecules. Reactions contained 30 nM ArpC5-Halo, 100 nM capping protein, and either 0 or 300 nM VCA. **(B)** Binding events of Arp2/3 complex per μm of actin filament in the presence or absence of VCA, error bars = s.d. p = 0.047 **(C)** The fraction of Arp2/3 complex visible in the field bound to actin filaments, error bars = s.d.

step in immense detail. We discovered that fission yeast Arp2/3 complex binds a mother actin filament and branch nucleation occurs on average 2.1 seconds later. Arp2/3 complex 'samples' actin filaments prior to choosing one site for binding. The sampling of F-actin is increased with the presence of VCA, which suggests that the conformational change induced by VCA is better suited for mother filament binding.

Future work will focus on utilizing Halo-Arp2/3 complex to examine how branch formation is regulated by other actin binding proteins. The addition of profilin to these reactions will inhibit branch formation by competing with Wsp1(VCA) for actin monomer [216]. With fluorescent Arp2/3 complex and VCA constructs, future studies will directly visualize the effects of profilin on Arp2/3 complex dynamics, including mother filament binding. Further, as recent work has demonstrated a critical link between the Wsp1 and Dip1 Arp2/3 complex activation pathways in endocytic patch formation [6], direct visualization of Arp2/3 complex and both NPFs simultaneously will be crucial to understanding how these two pathways cooperate. Investigating the Arp2/3 complex branching pathway is important for understanding the formation and regulation of branched actin networks in cells.

4.5 Materials and Methods

4.5.1 Cloning Arp2/3 complex fission yeast strains and in vitro proteins

ArpC3-SNAP-KanMX6 (KV 981), ArpC3-mCherry-KanMX6 ArpC5-mCherry-NatMX6 (KV 984), ArpC3-mNeonGreen-KanMX6 (KV 1006), ArpC3-Halo-KanMX6 (KV 996), and ArpC5-Halo-KanMX6 (KV 997) strains were made for this paper. The SNAP pombe targeting vector SNAP-KanMX6, was made for this study by inserting the tag into pFa6a-KanMX6. The HALO targeting vector was obtained from Addgene (#87029), and the others were from previous a paper [212]. The inserts were amplified with corresponding primers (Table 4.2) and inserted at the locus via lithium acetate transformations into a protease deficient strain

Primer	Genome homology	Plasmid homology	Strains
ArpC3 forward$_1$	AACTGAAAAGGATCAT CCCAGCAAGTGGTGGA CTTGCTTCAGCAAGAG ACGTTTTATGAACAAA GCTTTG	CGGATCCCCGGG TTAATTAA	KV 984,996,1006
ArpC reverse$_1$	TGAAATAAAGGAAACG GAAAAACATAAAGGCT TTGAAATACAGTATGA GCCAAATTATTAATTA ATAGAC	GAATTCGAGCTC GTTTAAAC	KV 984,996,1006
ArpC5 forward$_1$	GGTTTTGTAGGTGGTG GAAATATCCGGTATAG GATGTATAGTTCGTGT TCTCAATAGTAGACCC GATCTA	CGGATCCCCGGG TTAATTAA	KV 984
ArpC5 reverse$_1$	AAACAGAATCATTGAT TCAGTTCCATAAGCGA CAGAATAGTAGATACC AAAAAGTAAGATAAAG CCATAT	GAATTCGAGCTC GTTTAAAC	KV 984
ArpC3 forward$_2$	AAAGGATCATCCCAGC AAGTGGTGGACTTGCT TCAGCAAGAGACGTTT TATGAACAAAGCTTTG	ggaggcagtggcggtagc GAA	KV 981
ArpC3 forward$_2$	GGAAACGGAAAAACAT AAAGGCTTTGAAATAC AGTATGAGCCAAATTAT TAATTAATAGAC	CAGTATAGCGAC CAGCATTCAC	KV 981

Table 4.2: **The primers with genome homology used to clone the Arp2/3 complex strains in this paper.**

KV480 (aka TP150). All strains were confirmed with sequence analysis. GST-VCA-linker-Halo-6xHis was cloned by restriction digest of a HaloTag vector and insertion of an amplified VCA segment from the GST-Wsp1(VCA) construct used for unlabeled VCA experiments.

4.5.2 Fission yeast growth assay

Fission yeast cells were maintained in standard YE5S complete media and grown for 36 hours in a 25°C water bath shaker prior to any experimental procedures. Fission yeast cells were diluted from growing liquid YE5S cultures in 96 well plates (Corning Inc., Corning, NY) to an OD_{600} of 0.03 and 0.06 for each strain, with three technical replicates of each starting OD per assay. Cells were monitored using an Infinite M200 Pro (Tecan Systems, Inc., San Jose, CA) fluorescent plate reader with constant shaking and temperature maintenance at 25-27°C. OD_{600} readings were recorded every 10 minutes for 23 hours. Growth assays were conducted three separate times for a total of three biological replicates, each containing three technical replicates per strain. For analysis, initial reading of each assay was set to zero. The three technical replicates for each strain were then averaged. This was repeated for all three separate growth curve assays.

4.5.3 In vitro protein purification

Arp2/3 complex was purified following previous protocols established for *S. pombe* WT Arp2/3 complex purification [203]. Ammonium sulfate cut, GST-WASP affinity column, and anion exchange chromatography (GE Healthcare) are the main steps of purification. Following anion exchange, the ArpC5-Halo was additionally filtered over a HiPrep 26/60 Sephacryl S-300 HR column (Cytiva). SNAP and Halo constructs were incubated with the corresponding SNAP-549 (New England Biolabs, Ipswich, MA) or Janelia Fluor 549 (Promega) overnight at 4°C following the manufacturers' protocols. All Arp2/3 complex constructs were flash-frozen in liquid nitrogen and stored at -80°C. Arp2/3 complex concentrations were calculated with absorbance at 280 nm and the corresponding extinction coefficients ($M^{-1}cm^{-1}$): WT (250,000), SNAP (270,970), mCherry (282,890), 2x-mCherry (318,760), NG (294,350), and Halo (308,440).

Bovine WASP (GST-WASP(VCA)) and fission yeast Wasp fragment constructs (GST-Wsp1(VCA)) were purified by glutathione sepharose affinity chromatography [203]. GST-VCA-linker-Halo was also purified with the glutathione sepharose affinity column but followed by size exclusion chromatography (Superose 6 Increase 10/300 GL) to remove aggregates. Actin was purified from chicken skeletal muscle acetone powder by a cycle of polymerization and depolymerization and gel filtration [214]. Gel-filtered actin was labeled with Alexa 488 carboxylic acid succinimidyl ester on lysine residues. Pyrene actin was labeled on Cys374 with N-(1-Pyrene)Iodoacetamide. The actin concentrations were calculated with the absorbances at 290 and corresponding wavelengths for each label (Alexa-488: 491; Pyrene: 344). Black actin concentration is found with the equation: A_{290} x 38.5 μM. Alexa-488 actin concentration is found with the equations: total = [A_{290} - (0.11 x A_{491})] x 38.5 μM; labeled = $A_{491}/0.071$ μM^{-1}. Finally, pyrene actin concentration is calculated with the equations: total = [A_{290} - (0.1277 x A_{344})] x 38.5 μM; labeled = A_{344} x 45 μM. The GST-TEV-Dip1 plasmid was obtained from the Nolen lab and purified similar to their methods [7] with a glutathione sepharose column, TEV protease cleavage, and anion exchange chromatography (GE Healthcare).

4.5.4 Spontaneous pyrene

Pyrene assembly assays were conducted in 96-well plates in an Infinite M200 Pro (Tecan Systems, Inc., San Jose, CA) fluorescent plate reader to measure the fluorescence of pyrene-actin (excitation: 367 nm; emission: 407 nm). For spontaneous assembly, a 10 μM mixture of 10% pyrene-labeled Mg-ATP-actin was mixed with 10x ME [500 μM $MgCl_2$, 2 mM ethylene glycol tetraacetic acid (EGTA)] and added to the upper wells of the 96-well plate followed by 100x anti-foam. The lower wells contained 10x KMEI [500 mM KCl, 10 mM $MgCl_2$, 10 mM EGTA, 100 mM imidazole (pH 7.0)], Mg-Buffer G [2mM Tris (pH 8.0), 0.2 mM ATP, 0.5 mM DTT, 1 mM sodium azide (NaN_3), 0.1 mM $MgCl_2$], and the appropriate amounts

of Arp2/3 complex and VCA. The contents of the lower wells were mixed with the actin monomers in the upper wells, which initiated the reaction and data collection every 10 sec.

4.5.5 Phallicidin

BoDipy-phallicidin stocks were prepared by resuspending 300 units BoDipy-phallicidin (Thermo Fisher Scientific, Waltham, MA) in methanol (1.5 ml). This solution was aliquoted (10 μl), vacuum dried, and stored at -20°C until use. For staining, one dry BoDipy-phallicidin aliquot was resuspended in PEM buffer (10 μl) [0.1 M NA PIPES (pH 6.8), 1 mM EGTA, 1 mM $MgCl_2$] immediately prior to use.

Cells were stained with BODIPY-Phallicidin as adapted from [196]. Briefly, fission yeast cells (1 ml) at OD600 = 0.4-0.5 were fixed with EM grade paraformaldehyde (16%, 333 μl) for 5 minutes. Cells were washed 3 times with PEM buffer with centrifuge spins between each wash to pellet cells. Cells were permeabilized with PEM buffer + 1% Triton X-100 (1 ml) for 1 minute then centrifuged and washed 3 times with PEM buffer. Cells were resuspended in PEM buffer (10 μl), and 1 unit of BODIPY-Phallicidin (Molecular Probes) was added and incubated in the dark for 30 minutes. Cells were washed once with PEM buffer and centrifuged to pellet then resuspended in a small volume of PEM buffer. Stained cells were stored at 4°C and imaged within 24 hours. Confocal images were acquired using Z-stacks of 11 slices with a 0.5 μm step-size for phallicidin stained cells.

4.5.6 Cell imaging

Confocal images were acquired on an IX83-X1 (Olympus, Tokyo, Japan) equipped with a Yokogawa CSU-X1 Spinning Disk Confocal Unit fitted with an ImagEM X2 EM-CCD camera (Hamamatsu, Hamamatsu, Japan) controlled by CellSens software (Olympus, Tokyo, Japan).

4.5.7 Patch dynamics

Fission yeast cells were placed on glass coverslips, and single plane confocal images were collected every second for 1 minute. Actin patch dynamics were analyzed using ImageJ and the Fiji plugin TrackMate as previously described [216]. Fluorescence intensity and distance traveled from the cell cortex over time were measured for at least 10 actin patches per strain. Time courses for individual patches were aligned to the initiation of patch movement (time 0) or peak intensity and averaged at each time point.

4.5.8 Glass preparation for TIRF

Microscope slides (#1.5, Fisher Scientific) and coverslips were washed for 7 min in acetone, isopropanol, and water, followed by sonication in isopropanol (30 min). Washed glass was incubated with piranha solution (66.6% H_2SO_4, 33.3% H_2O_2) for 30 min, then washed with milliQ H_2O and dried with air. Immediately following, glass was passivated by incubation in either 1 mg/mL PEG-Si (5000 MW) or a 1:1000 mixture PEG-Biotin-Si (3400 MW):PEG-Si (5000 MW) in 95% ethanol for 18 hr. After glass was rinsed with ethanol and water, flow chambers were prepared as described previously [258].

4.5.9 TIRF microscopy

Time-lapse TIRFM movies were taken using a cellTIRF 4Line system (Olympus, Center Valley, PA) fitted to an Olympus IX-71 microscope with through-the-objective TIRF illumination and an iXon EMCCD camera (Andor Technology, Belfast, UK). Microscope slides were cleaned with Piranha and coated with mPEG-Silane. Mg-ATP actin (1.5 μM, 10% Alexa 488 labeled) was mixed with the appropriate proteins and polymerization TIRF buffer [10 mM imidazole (pH 7.0), 50 mM KCl, 1 mM $MgCl_2$, 1 mM EGTA, 50 mM DTT, 0.2 mM ATP, 50 μM $CaCl_2$, 15 mM glucose, 20 μg/ml catalase, 100 μg/ml glucose oxidase,

and 0.5% (400 cP) methylcellulose]. The reaction was moved to a flow chamber, and images were acquired at 0.4 s intervals.

For the assays where the actin filaments needed to be stuck down, the coverslips were coated with a biotin PEG -Silane mixture (1:1000). Flow chambers were incubated with HEK-BSA for 3 min before adding 1 mg/ml neutravidin. After a 2 min incubation, the chamber was washed with HEK-BSA and then 1X TIRF buffer. Mg-ATP actin monomer in TIRF buffer was added to the prepared flow chamber and allowed to polymerize for 5-10 minutes. Then a mixture of TIRF buffer, Arp2/3 complex, and capping protein with or without the addition of VCA was flowed into the chamber. Since the biotin actin and neutravidin effectively anchored the filaments to the coverslip, the Halo-Arp2/3 complex could be imaged rapidly (100 ms interval) while the actin filaments were acquired occasionally (10 s interval).

4.5.10 Data analysis: Arp2/3 complex time to nucleation

Upon branch identification, the frame with the first appearance of Arp2/3 complex binding at the site of branch nucleation was manually identified. Then, a 2-pixel by 2-pixel square region of interest (ROI) was defined for each frame to overlap with the fluorescence of Arp2/3 complex at the branch site for 100 seconds after initial binding and 20 seconds prior to binding. The fluorescence of Arp2/3 complex was measured for each frame. Next, the length of the actin branch was measured by a manually drawn line ROI for a minimum of ten selected frames total, focusing on frames in which the branch did not overlap with other nearby filaments for the clearest measurement. This data was plotted in Python and a line of best-fit was calculated. The time of nucleation was calculated as the time where the actin filament length was equal to zero. This was then compared to the time at which Arp2/3 complex first bound to the mother filament to discern the delay between binding time and nucleation time.

4.5.11 Data analysis: Arp2/3 complex binding dynamics.

Analysis was performed with custom Python code. To calculate the number of binding events in a given time-frame, we processed the actin filament and Arp2/3 complex channels separately and then counted the number of "islands" in the overlapped composite image. To process the actin filament channel, we clipped pixel values at a maximum (maxpix= 60), applied a Gaussian filter (sigma= 2.5), normalized pixel values between 0 and 1, binarized (threshold= 0.2), and removed any collection of fewer than 20 bright pixels to eliminate noise. Similarly, to process the Arp2/3 complex channel, we clipped pixel values at a maximum (maxpix=100), applied a Gaussian filter (sigma= 0.5), normalized pixel values by the order of magnitude of the maximum pixel value, binarized (threshold= 1.5), and removed collections of fewer than 6 pixels to eliminate noise. The total number of Arp2/3 complex particles in the time-frame was calculated by counting the number of isolated clumps in the Arp2/3 complex channel, while the number of Arp2/3 complex particles bound to actin was calculated by counting the number of regions of overlapping signal in both processed images. This number of bound particles was then divided by the total length of actin present in each frame, which was measured manually in FIJI.

CHAPTER 5

FORMINS HAVE PROPERTIES THAT ARE BEST SUITED FOR THEIR CORRESPONDING CELLULAR ROLE

5.1 Preface

This chapter covers the research that I completed for Katie Homa's manuscript, "Formin Cdc12's specific actin assembly properties are tailored for cytokinesis in fission yeast," which is currently in review at *Biophysical Journal*. The other authors on the manuscript are Vilmos Zsolnay, Meghan O'Connell, Erin M. Neidt, Gregory Voth, Tamara Bidone, and David Kovar. Meghan and I were solely involved in the biochemistry revisions. I troubleshooted the cloning, expression, and purification of the formin chimera constructs. Meghan completed the TIRFM with the purified formin chimeras. I have included background and a summary of the manuscript to describe the overall question and results.

5.2 Introduction

Formins are multidomain actin assembly proteins that both nucleate and elongate unbranched actin filaments, which form F-actin networks involved in polarization, motility, division, and adhesion [19, 39]. Formins dimerize and processively associate with the F-actin barbed end through the formin homology (FH) 2 domains [161] (Figure 5.1A). The FH1 domains contain multiple proline rich regions, bind profilin-actin, and deliver the monomers to the FH2 associated barbed F-actin, which facilitates elongation [39, 168, 193, 232]. The FH1 and FH2 domains are conserved in the formin family, while additional regulatory domains are less well-conserved and more specific to each particular formin to enable proper spatial and temporal activation [19].

Most organisms have multiple formin isoforms, from two in budding yeast, about 15 in

mammals, and more than 20 in plants [91, 190, 199]. While the isoforms maintain similar structure and the same general actin assembly mechanisms, the different isoforms have distinct roles in the different cell types. There are three formin isoforms in fission yeast, and each is involved in assembling a specific F-actin network: For3 (polzarizing actin cables), Cdc12 (contractile ring), and Fus1 (fusion focus during mating) [117, 63, 154, 27, 171, 170]. While activation at the correct time and location is essential for the functional roles of the formin isoforms, there has been evidence that the mechanistic properties of the particular formin could also be important [236]. *In vitro* experiments have revealed that the different isoforms vary in F-actin nucleation efficiency, F-actin elongation rates, and F-actin dissociation rates [76, 117] (Table 5.1). Our lab has studied and compared the actin assembly properties of several different formins, including the three fission yeast formins (Cdc12, For3, Fus1), and they vary significantly [200]. While the properties vary *in vitro*, the correlation of the formins' mechanistic properties and the corresponding cellular F-actin networks is not well understood.

To determine how the formin's mechanistic properties impact the formation of a specific F-actin network, this study looked toward the well-studied contractile ring. The contractile ring is formed from bundled, anti-parallel actin filaments with myosin II motors producing force to constrict the F-actin bundles and separate the mother cell into two cells during cytokinesis to complete the cell cycle. The contractile ring constricts via Search, Capture, Pull, Release (SCPR). Nodes composed of numerous proteins including Cdc12 and the myosin II Myo2 form along the medial cortex [125, 233, 252]. Cdc12 assembled F-actin from one node is caught (Search, Capture) by Myo2 on an adjacent node, and the force of Myo2 pulling (Pull) the F-actin brings the nodes closer together. The F-actin is severed by cofilin (Release), and the whole cycle is repeated until the contractile ring fully constricts. Since the contractile ring is well studied and depends on the precise SCPR mechanism, it provides an optimal model to test the effects of formin actin assembly properties on the contractile

ring.

In the submitted manuscript, a computational 3D SCPR model determined that both F-actin nucleation efficiency and F-actin elongation rate affect contractile ring formation, with emphasis on the nucleation efficiency. The computational data was tested with *in vivo* experiments. The FH1FH2 domains of Cdc12 were replaced with the FH1FH2 domains of functionally, evolutionarily, and biochemically diverse formins to create formin chimeras. Bni1 (budding yeast), mDia2 (mouse), CYK-1 (worm), For3 (fission yeast), and Fus1 (fission yeast) chimeras were created and replaced the endogenous Cdc12. Since only the FH1FH2 domains were swapped, the formins maintained the localization and regulation of Cdc12. The formin chimeras all had some level of cytokinesis timing and morphology defects, but the Fus1 chimera strain was not viable. The mDia2 chimera cells experienced relatively normal cytokinesis in the proper timing, but For3, Bni1, and CYK-1 chimera cells had delayed ring assembly and morphological defects. A comparison of the *in vitro* actin assembly properties shows that Bni1 and CYK-1 elongate actin faster than Cdc12, while For3 and mDia2 elongate actin at the same rate as Cdc12. However, the nucleation efficiencies of the chimeras are much lower than Cdc12: mDia2 (25%), For3 (1.5%), Bni1 (10%), and CYK-1 (3%). Since the cytokinesis defects were minimal for mDia2 chimeras, it indicates that fission yeast cytokinesis is robust, but the weak nucleation efficiencies of For3, Bni1, and CYK-1 are not sufficient for consistent and efficient contractile ring assembly. Overall, the results from the paper suggest that the mechanistic actin assembly properties of the specific formin is important for establishing the corresponding F-actin network.

When the paper was in revisions, it was decided to add biochemistry experiments to strengthen the conclusions made about the formin chimeras. The conclusion that the nucleation efficiency is the most important mechanistic formin property for contractile ring formation relies on the formin chimeras maintaining the same properties as previously characterized for the original corresponding formins (Table 5.1). Therefore, we planned to clone,

purify, and characterize the formin chimeras *in vitro*.

Formin	**Nuceleation Efficiency**	**Elongation Rate (subunits sec^{-1} μM^{-1})**	**Dissociation Rate (sec^{-1})**
Fission yeast Cdc12	1 filament per 2-3 dimers	10-12	$4.7\text{-}7.0 \times 10^{-5}$
Fission yeast For3	1 filament per 170 dimers	10	3.6×10^{-5}
Budding yeast Bni1	1 filament per 20 dimers	20-25	8×10^{-4}
Mouse Dia2	1 filament per 8 dimers	12	1.3×10^{-4}
Worm CYK-1	1 filament per 25 dimers	60	3.9^{-3}
Fission yeast Fus1	1 filament per 2 dimers	5	6.5×10^{-4}

Table 5.1: ***In vitro* actin assembly properties of formins used to generate formin chimeras.** Formin nucleation efficiency (filaments per dimer), barbed end elongation rate (in the presence of profilin), and dissociation rate from the barbed end were determined previously with *in vitro* biochemical assays [117, 200, 156]

5.3 Results

5.3.1 Construction of formin chimeras for in vitro assays

We wanted to create *in vitro* constructs for all of the formin chimeras that were used in the *in vivo* portion of the paper. The *in vivo* constructs contained the whole Cdc12 with just the FH1FH2 sequence of the other formins swapped, but the *in vitro* constructs were abbreviated to optimize protein expression and activity. Full length formins are long constructs that are difficult to express for purification. The formin regulatory domains render the formins constitutively inactive. Since the signaling and regulation mechanisms are absent *in vitro*, the N-terminus is not required. Therefore, we made formin chimeras with the FH1FH2 of each formin and a short Cdc12tail (1391-1687) (Figure 5.1B). I amplified the FH1FH2-Cdc12 region for each formin chimera from previous plasmids and cloned MBP-TEV-FH1FH2-Cdc12-6xHis constructs for each formin chimera (Bni1, mDia2, CYK-1, For3). The cloning took troubleshooting and had low efficiency, but I moved on to purification with all of the

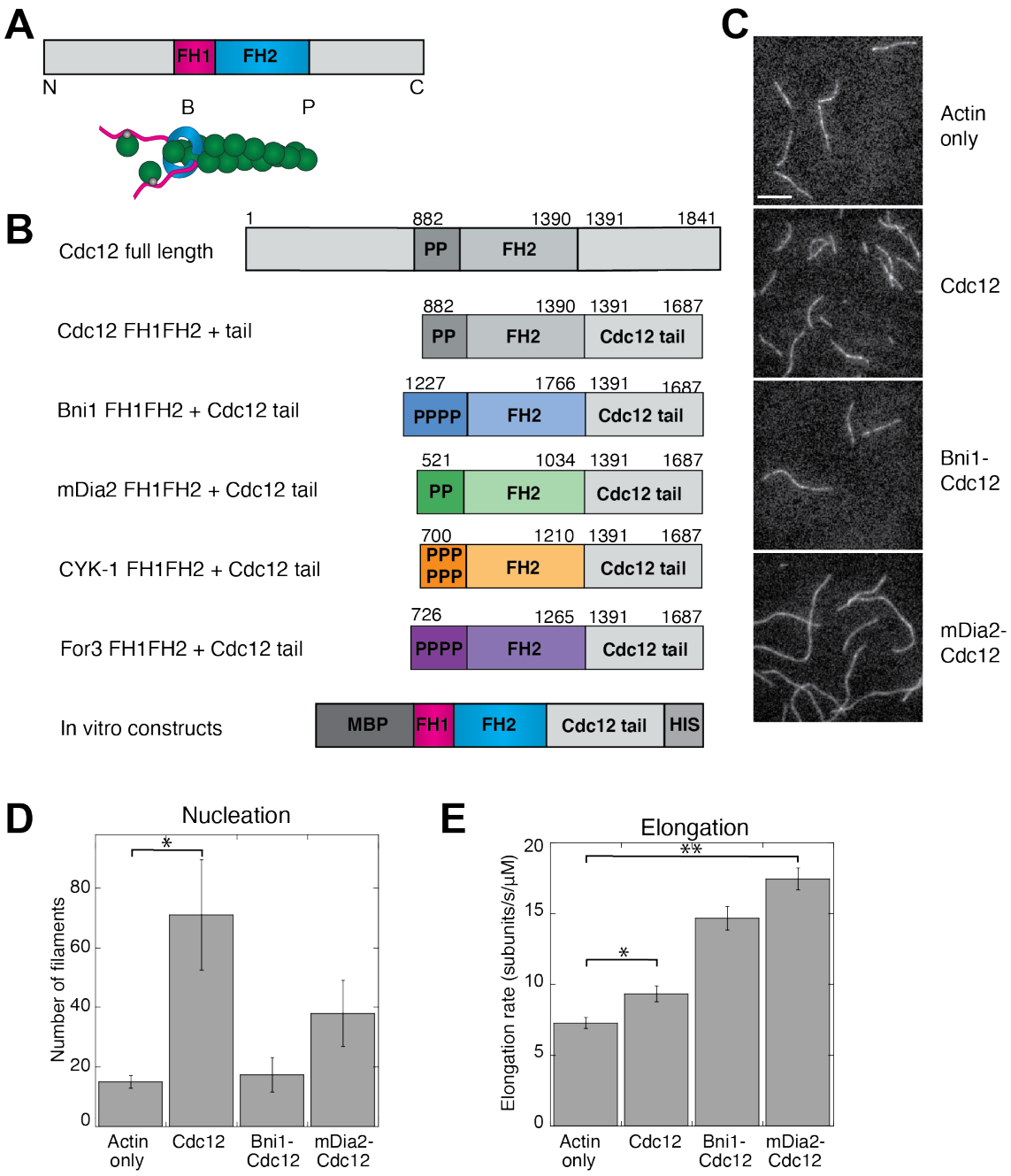

Figure 5.1: **Biochemical analysis of formin chimeras with a cdc12 tail. (A)** Simple schematic of the domain organization of formins. The formin homology (FH) domains have been labeled, while the remaining sequence contains less well-conserved regulatory domains. **(B)** Schematic of fission yeast formin Cdc12 chimeras, in which the FH1FH2 actin assembly domains were replaced by FH1FH2 domains from formins with diverse actin assembly properties. Each "P" indicates a single FH1 polyproline motif.

Figure 5.1: (continued) **(C)** Single color TIRFM of 1.5 μM Mg-ATP actin (10% Alexa-488 labeled) with 2.5 μM fission yeast profilin Cdc3, and either no formin (actin only) or 1 nM Cdc12, Bni1-Cdc12, or mDia2-Cdc12 formin chimeras. Scale bar, 8 μm. **(D)** Quantification of the number of filaments nucleated by formin chimera constructs. Two tailed t-tests for data sets with unequal variance yielded p-value *p=0.047. Error bars indicate standard error of three independent biological replicates of 10 actin filaments for actin only, Cdc12, and mDia2-Cdc12, and two independent biological replicates of 10 actin filaments for Bni1-Cdc12 due to a lack of Bni1-Cdc12-associated filaments in the third replicate. **(E)** Quantification of formin chimera elongation rates. Two tailed t-tests for data sets with unequal variance yielded p-values *p=0.038, **p=0.0013. Error bars indicate standard error of three independent biological replicates of 10 actin filaments for actin only, Cdc12, and mDia2-Cdc12, and two independent biological replicates of 10 actin filaments for Bni1-Cdc12 due to a lack of Bni1-Cdc12-associated filaments in the third replicate.

formin chimeras. Purification protocols also required troubleshooting and a combination of cation exchange and size exclusion chromatography to get pure formin chimeras. The For3 chimera had to be used fresh, which caused some difficulties and timing issues. Therefore, TIRFM was only done with Cdc12, Bni1, and mDia2.

5.3.2 Formin chimeras compared with TIRFM imaging

Single color TIRFM with actin, profilin (Cdc3), and formin chimeras revealed that the formin chimeras have similar mechanistic properties to the previously characterized formins (Figure 5.1C-E). Therefore, the biochemical characterization of the formin chimeras support the conclusions of the manuscript. The formin chimeras affect contractile ring formation relative to their nucleation efficiencies.

5.4 Materials and Methods

5.4.1 Plasmid construction of in vitro formin chimera proteins

A Cdc12 fragment containing the FH1FH2 domains and a portion of the C-terminal tail [Cdc12(882-1687)] was cloned by traditional restriction enzyme cloning into pET21a-MBP-

TEV at BamHI/XhoI. The Bni1-Cdc12 [Bni1(1228-1766)-Cdc12(1391-1687)], mDia2-cdc12 [mDia2(527-1022)-Cdc12(1391-1687)], cyk1-cdc12 [CYK-1(700-1210)-Cdc12(1391-1687)], and For3-Cdc12 [For3(726-1265)-Cdc12(1391-1687)] chimeras were amplified from previously constructed plasmids and were inserted via infusion cloning (Clontech, Mountain View, CA) into pET21a-MBP-TEV at BamHI/NotI to form MBP-chimera-HIS(x6).

5.4.2 Protein purification

The formin chimeras were expressed in *Escherichia coli* strain BL21-Codon Plus (DE3)-RP (Agilent Technologies, Santa Clara, CA) with 0.5 mM isopropyl β-D-1-thiogalactopyranoside for 16 h at 16 °C. Cells were lysed with sonication in extraction buffer [50mM NaH_2PO_4 (anhydrous), 500 mM NaCl, 10% glycerol, 10 mM imidazole, 1 0mM BME, pH 8] with EDTA-free Protease Inhibitor Cocktail (Roche, Basel, Switzerland) and were clarified. The extract was incubated for 1 h at 4 °C with Talon resin (Clontech, Mountain View, CA), loaded onto a column, washed with extraction buffer, and the protein was eluted with 250 mM immidazole. The formin chimeras were dialyzed into buffer [50mM HEPES (pH 7.0), 50mM NaCl, 5% glycerol, 0.01% NaN_3, 1mM DTT] for cation exchange chromatography (GE Healthcare). The cyk1 chimera was dialyzed into the same buffer except pH 8.0. The clean fractions were pooled and dialyzed against SNAP buffer [20 mM Hepes (pH 7.4), 200 mM KCl, 0.01% Na_3, 10% glycerol, and 1 mM DTT]. The cyk1, for3, mdia2 chimeras required additional size exclusion chromatography and were filtered on a Superdex 200 10/300 GL (GE Healthcare, Little Chalfont, UK). Aliquots of the all formin chimeras were flash-frozen in liquid nitrogen and stored at -80 °C. Chicken skeletal muscle actin was purified as described in [214]. Fission yeast profilin Cdc3 was overexpressed and purified from E. coli using poly-L-proline affinity chromatography as described in [132].

5.4.3 TIRFM with formin chimeras

TIRFM was conducted with the formin chimeras as described previously [36]. Briefly, timelapse TIRFM movies were obtained with through-the-objective TIRF illumination on an Olympus IX-71 microscope with an iXon EMCCD camera (Andor Technology) and a cellTIRF 4-line system (Olympus). 1 nM of either Cdc12, Bni1-Cdc12, or mDia2-Cdc12 formin chimeras was added to a polymerization mix [10 mM imidazole (pH 7.0), 50 mM KCl, 1 mM $MgCl_2$, 1 mM ethylene glycol tetraacetic acid (EGTA), 50 mM dithiothreitol (DTT), 0.2 mM ATP, 50 μM $CaCl_2$, 15 mM glucose, 20 μg/ml catalase, 100 μg/ml glucose oxidase, and 0.5% (400 cP) methylcellulose] along with 2.5 μM fission yeast profilin Cdc3, which was then added to Mg-ATP-actin (10% Alexa-488 labeled) to induce actin assembly. This mixture was added to a flow chamber and imaged at 5 s intervals at room temperature.

The nucleation activity was determined by counting the total number of actin filaments for each TIRFM movie at frame 48, the same amount of time since the initiation of each actin assembly reaction. Each construct (actin only, Cdc12, Bni1-Cdc12, or mDia2-Cdc12) was counted in triplicate. To determine the actin filament elongation rate, 10 individual actin filaments from each TIRFM movie were tracked over time, with their lengths measured every fifth frame for 7-9 total measurements. An average elongation rate was calculated for each filament, and then those were averaged to obtain an average for each movie. Each construct (actin only, Cdc12, or mDia2-Cdc12) was measured in triplicate with the exception of Bni1-Cdc12, which was only measured in duplicate due to a low number of Bni1-Cdc12-associated filaments in the third TIRFM movie due to Bni1-Cdc12's low nucleation activity.

CHAPTER 6

DISCUSSION AND FUTURE DIRECTIONS

6.1 Minimal reconstitution of F-actin networks

I used minimal reconstitution biochemistry assays to investigate the mechanism and dynamics of different actin binding proteins (ABPs). Minimal reconstitution enabled me to rebuild simplified F-actin networks isolated from the complications of cells. During my graduate studies, I successfully reconstituted mechanically stressed F-actin networks and branched F-actin networks. I investigated mechanosensitive recruitment of LIM domain proteins and the dynamics of Arp2/3 complex branch formation. This *in vitro* approach required troubleshooting of cloning, protein purification, and assay design. Troubleshooting is an important aspect of science. Failed experiments, while frustrating, are just as informative as successful ones. My graduate studies are summed up in the papers that I published, but the real science was the problem solving.

6.2 LIM domain proteins localize to stressed F-actin networks

Cells are pushed, pulled, and much more as they experience different types of mechanical forces both externally and internally. Cells must adapt and balance the external forces with the forces they generate. The ability to sense and respond to these forces directs many cellular processes, including cell survival, division, motility, and differentiation. The actin cytoskeleton is important for maintaining mechanical homeostasis in adherent cells, largely through its regulation of adhesion and cortical tension.

The LIM (Lin-11, Isl1, MEC-3) domain-containing proteins are involved in a myriad of cellular mechanosensitive pathways. The LIM domain family proteins have diverse functional cellular roles, which is likely due to the additional domains that most LIM domain proteins possess. A fraction of LIM domain proteins have been shown to localize to stressed F-

actin networks in cells, specifically focal adhesions (FA) and stress fibers (SF) [211]. The most well-studied LIM domain proteins, zyxin and paxillin, localize to SF strain sites which are regions of local damage that occur spontaneously or in response to the application of external forces, and mediate SF repair [20, 92, 209]. The LIM domains are both necessary and sufficient for zyxin and paxillin to localize to FAs, SFs, and SF strain sites [20, 92, 209]. Therefore, the mechanosensitivity of several LIM domain proteins can be attributed directly to the LIM domains, but the mechanism of recruitment to mechanically stressed F-actin networks is unknown.

6.3 LIM domain-containing regions (LCRs) are mechanosensitive

There are over 70 LIM domain proteins in mammalian cells categorized into 14 classes [115]. Since these proteins contain diverse additional domains, the first question we asked is whether the LIM domain-containing regions (LCRs) from different LIM domain proteins localize to the same stressed F-actin network in cells. An *in vivo* screen revealed that 18 proteins from four classes (Zyxin, Paxillin, Tes, Enigma) localize to SF strain sites. The LCR of fission yeast Pxl1 also localizes to SF strain sites in the cell screen assay. Therefore, the mechanism of mechanosensitive LCR recruitment to stressed F-actin networks is conserved from fission yeast to mammalian cells.

To elucidate the force-sensitive substrate of LCR, we minimally reconstituted contractile, bundled F-actin networks *in vitro* with a minimal set of purified proteins. We tested the fission yeast Pxl1 and mammalian zyxin LCRs in our *in vitro* assay. LCR localized to regions of myosin contractility induced actin filament damage, including bundles just prior to breaking. This assay was the first *in vitro* reconstitution of LCR mechanosensitivity. Another set of experiments without myosin and bundlers revealed that LCR recruitment is not myosin dependent but instead just requires a force induced conformational change in F-actin. Another research group completed a similar study around the same time as our

paper [218]. Their *in vivo* and *in vitro* conclusions coincide with ours, which strengthens the impact of our work.

The final aspect of our investigation was determining the optimal LCR conformation for mechanosensitivity. Amino acid sequence analysis and mutant LCR studies revealed that the ideal configuration is an LCR with three tandem LIM domains spaced 7-8 amino acids apart (linker) [247]. The parallel study revealed a necessary phenylalanine located at a similar position in all strain sensing LIM domains [218]. However, further sequence analysis of all stress sensing LCRs showed that the position of the phenylalanine ranged a few residues and in some instances was substituted for a tryosine. Overall, the LCR appears to act as a sort of ruler that can interact with strained F-actin via hydrophobic interactions. While our study [247] and the parallel study [218] made progress into understanding mechanosensitive LCR recruitment, the model remains vague. Future experiments are required to create a more detailed model for LCR mechanosensitivity.

6.4 Future directions for investigating LCR mechanosensitivity

6.4.1 Determining the force-induced conformation of F-actin

Our *in vitro* assay successfully reconstituted LCR mechanosensitive recruitment to mechanically stressed F-actin networks. However, while the stressed F-actin networks contained minimal proteins, the precise control of forces was still lacking. The myosin contractility produced regions of compression and tension, but we could not distinguish the direction or magnitude of mechanical forces. Therefore, future experiments will be conducted to directly measure how the magnitude and direction of forces on actin filaments affects LCR affinity.

Microfluidics is a relatively recent versatile tool that utilizes fluid flow to manipulate the biochemical and mechanical properties of a reaction to observe the effects at a single actin filament level [251]. This one approach offers a range of experimental setups. The local buffer

and protein concentration can be maintained by consistent flow of fresh fluid, so reactions are not limited by localized depletion of reagents. On the other hand, the buffer and protein concentrations can also be rapidly exchanged to investigate the effects of adding or removing a reagent. The most important aspect of microfluidics for studying LCR mechanosensitivity is the ability to control the flow direction and force. The impact of mechanical forces on formin elongation and cofilin disassmbly have been studied with microfluidics [250, 251]. F-actin is tethered to the surface either directly through an anchored seed or indirectly through an end binding protein (e.g. formin, gelsolin, capping protein). The flowing solution creates a viscous drag that results in tensile stress being applied to the filament. The tension is a gradient along the filament from negligible force at the free end to maximal force at the tethered end. The flow rate and direction can easily be manipulated to change the forces applied to the filament, and the forces can be calculated. By adding the same fluorescent LCRs from our previous *in vitro* experiments to these microfluidics assays, we can determine how the magnitude and direction of force applied to an actin filament affect the localization of LCR. Our lab is currently establishing and troubleshooting a microfluidics system, so these experiments will soon be possible to conduct.

6.4.2 Determining the force-induced F-actin:LIM binding interface

The main conclusion from our research and the parallel study was that the mechanosensitive LCRs bind to a force-induced F-actin conformation [218, 247]. The pheylalanine (or tyrosine) around position 66 in the LIM domain is necessary for force sensitivity, which would imply some level of hydrophobic binding interaction [218]. Recent simulations from the Voth group indicate that strain in an actin filament localizes to the longitudinal axis contacts, where the strong interactions are attributed to the D-loop (DNase I binding loop) in subdomain 2 inserting into the adjacent monomer's target binding cleft. The D-loop has previously been indicated in F-actin stability, as a D-loop conformational change occurs in the less stable

ADP nucleotide state [50]. Cofilin, F-actin severing protein, also binds between two adjacent monomers along the longitudinal axis slightly rotating the outer domain relative to the inner domain, which displaces the D-loop [72, 98]. Therefore, exposure of the D-loop is linked to weakened F-actin conformations, which makes it a prime candidate for LCR recognition.

There are several potential experimental approaches to determining whether mechanosensitive LCRs bind an exposed D-loop upon a force-induced F-actin conformational change. Cofilin binding and Mical oxidation both disrupt the D-loop interactions between adjacent monomers, so testing the effects of both on LCR F-actin localization could be very informative [98, 79]. Systematic mutations in the D-loop could also be created to directly study the impacts on LCR localization. Our lab is currently developing a methodology to purify recombinant fission yeast actin from insect cells, and this system could be utilized to create mutated actin constructs. A complicated but direct investigation of the binding interface would involve cloning unnatural azido-amino acids into the recombinant LCRs, adding them to our *in vitro* contractile F-actin network assay, and using UV light to activate crosslinking. Complete isolation of the bound protein and mass spectrometry could help determine the binding interface. These proposed experiments will involve time and troubleshooting, but the potential results could further our understanding of the interface between the mechanosensitive LCR and F-actin.

6.5 Arp2/3 complex branching pathway

Arp2/3 complex is essential for the formation of short branched F-actin networks that are ideal for generating forces, like endocytic patches [178]. While the pathway of Arp2/3 complex activation, mother filament binding, and daughter branch filament nucleation has been studied extensively, direct visualization of Arp2/3 complex has been very minimal. We engineered a fluorescent fission yeast Arp2/3 complex and characterized the binding dynamics and timing of branch nucleation. This project involved some combination of endogenous

cloning, purification, and *in vitro* 'bulk assay' characterization of several Arp2/3 complex constructs (Table 6.1). The Halo-ArpC5 was the best construct for single molecule imaging. Our results revealed that Arp2/3 complex has dynamic binding along the mother filament ('sampling') that is increased in the presence of VCA. We also determined that the lag time between Arp2/3 complex binding and branch nucleation is approximately 2.1 seconds. Our investigation has so far minimally characterized this newly engineered fluoresecent Arp2/3 complex tool, but additional experiments with this tool will be done to further analyze the regulation and formation of Arp2/3 complex-mediated branched F-actin networks.

Construct	**Cloned**	**Purified**	**Bulk analysis**	**Visible in TIRFM**
ArpC3-SNAP	Yes	Yes	Yes	Only in aggregates
ArpC3-mCherry	Yes	No	N/A	N/A
ArpC5-mCherry	No	Yes	Yes	No
2x-mCherry	Yes	Yes	Yes	No
ArpC3-mNeonGreen	Yes	Yes	Yes	Only in aggregates
ArpC3-Halo	Yes	No	N/A	N/A
ArpC5-Halo	Yes	Yes	Yes	Yes

Table 6.1: **The fission yeast strains tested for *in vitro* labeling.** Several fission yeast strains were cloned, purified, and characterized in 'bulk assays' to determine the best construct for fluorescent labeling.

6.6 Future directions: Arp2/3 complex

6.6.1 Addition of labeled VCA with labeled Arp2/3 complex

The Arp2/3 complex branch pathway requires three main components: actin, Arp2/3 complex, and an NPF. We had hoped to engineer a functional fluorescent Wsp1(VCA) construct, which is an equivalent Wsp1 truncation to the unlabeled VCA in our current reactions. We could then determine the time between branch nucleation and VCA leaving the branch site. We initially cloned a SNAP-GST-VCA construct, and initial imaging seemed promising

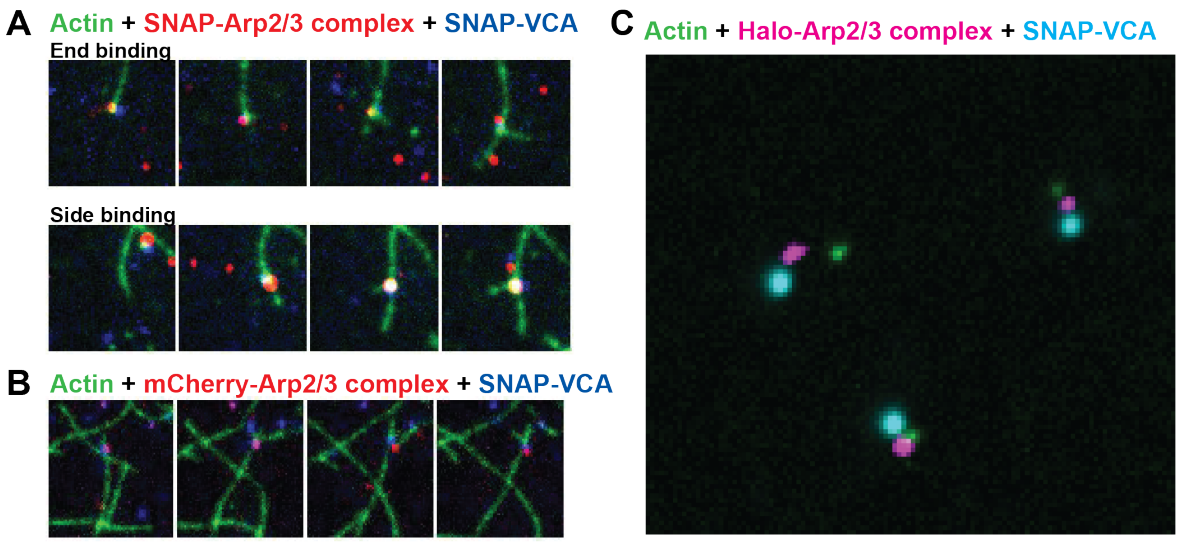

Figure 6.1: **SNAP-VCA in single molecule TIRFM. (A)** SNAP-Arp2/3 complex and SNAP-VCA can be imaged together binding to F-actin and nucleating branches from the filament end or sides. The SNAP-VCA is an aggregate and causes aster formation. The SNAP-Arp2/3 complex is only visible with the aggregating labeled VCA. **(B)** The mCherry-Arp2/3 (ArpC5) complex can also be seen with the aggregating VCA and not by itself. **(C)** The aggregating SNAP-VCA, Halo-Arp2/3 complex, and an actin nucleus can be imaged moving in a complex through the solution prior to binding a filament.

(Figure 6.1A,B). However, the SNAP-VCA formed aggregates that would then create asters. Binding dynamics of an aggregate would not be informative for single molecule analysis. Therefore, we attempted to troubleshoot the aggregation complication. Gel filtration eliminated most of the aggregates, but the activity and visibility decreased significantly. We have cloned a GST-VCA-Halo construct, and while troubleshooting is still required, the construct is more promising initially. Although we cannot use the SNAP-VCA for single molecule dynamics, an interesting phenomenon could be seen with the SNAP-VCA aggregates (Figure 6.1C). Fluorescent Arp2/3 complex, SNAP-VCA, and an actin nucleus can be seen traveling together in solution before binding a filament and rapidly creating an aster of branches. While not conclusive, it supports the belief that the three proteins create a complex prior to mother filament binding.

6.6.2 Fission yeast actin and profilin

Our experiments use the minimal components required to reconstitute Arp2/3 complex branch formation. However, regulation and formation of branched networks *in vivo* require additional proteins. We briefly characterize the NPF Dip1 in our paper. Recent work revealed that Dip1 and Wsp1 cooperate to nucleate branched networks in fission yeast [6]. Therefore, an experiment should be done by adding fluorescent Dip1 and Wsp1 to the same reaction with Halo-Arp2/3 complex to further investigate the cooperative relationship between the NPFs. Profilin inhibits Arp2/3 complex branch nucleation and instead favors formin elongation. It is suspected that profilin competes with VCA for G-actin [216]. Direct visualization of how profilin affects Arp2/3 complex binding dynamics will further elucidate how profilin drives F-actin network homeostasis. The list of possible experiments is essentially limitless, including investigating how the nucleotide state of the filament affects Arp2/3 complex binding.

6.6.3 Mechanosensitivity of Arp2/3 complex

A handful of experiments have studied the mechanosensitivity of Arp2/3 complex. Filament curvature promotes binding of Arp2/3 complex to F-actin along the convex curve with a 1.7 fold increase [188]. Tension decreases the stability of an Arp2/3 complex-mediated daughter branch [166, 188]. These experiments used branch formation or displacement as an indirect measurement of Arp2/3 complex mechanosensitivity. Microfluidics experiments with Halo-Arp2/3 complex can directly visualize and determine how mechanical forces affect the binding dynamics of Arp2/3 complex. Curvature could either increase the 'sampling' of Arp2/3 complex or the fraction of 'sampling' that becomes branching events.

6.7 Concluding remarks

This dissertation summarizes the successful minimal reconstitution of two distinctly different F-actin networks to study corresponding actin binding protein (ABP) dynamics. Mechanosensitive ABPs is a relatively new topic, and our work with LCRs had a large impact. There is a lot of frustrating and exciting research to be done in the next few years to further elucidate the mechanism of mechanosensitive ABPs. The branching pathway of Arp2/3 complex was not a new topic, but the fission yeast Arp2/3 complex had never been visualized in single molecule TIRFM. While we have just minimally characterized the fluorescent Halo-Arp2/3 complex, we hope to complete a long list of experiments in the future. Both of these projects coincide with our lab's goal to understand how distinct F-actin networks simultaneously assemble in one cytoplasm with the same pool of proteins.

References

[1] Vérane Achard, Jean-Louis Martiel, Alphée Michelot, Christophe Guérin, Anne-Cécile Reymann, Laurent Blanchoin, and Rajaa Boujemaa-Paterski. A "Primer"-Based Mechanism Underlies Branched Actin Filament Network Formation and Motility. *Current Biology*, 20(5):423–428, 2010.

[2] Enrico Agabiti-Rosei and Damiano Rizzoni. Regression of Small Resistance Artery Structural Alterations in Hypertension by Appropriate Antihypertensive Treatment. *Current Hypertension Reports*, 12(2):80–85, 2010.

[3] Visar Ajeti, A. Pasha Tabatabai, Andrew J. Fleszar, Michael F. Staddon, Daniel S. Seara, Cristian Suarez, M. Sulaiman Yousafzai, Dapeng Bi, David R. Kovar, Shiladitya Banerjee, and Michael P. Murrell. Wound healing coordinates actin architectures to regulate mechanical work. *Nature Physics*, 15(7):696–705, July 2019. Number: 7 Publisher: Nature Publishing Group.

[4] Y. Arai, R. Yasuda, K. Akashi, Y. Harada, H. Miyata, K. Kinosita, and H. Itoh. Tying a molecular knot with optical tweezers. *Nature*, 399(6735):446–448, 1999.

[5] Daniel Axelrod, Nancy Thompson, and Thomas Burghardt. Total internal reflection fluorescent microscopy. *Journal of Microscopy*, 129(1):19–28, 1983.

[6] Connor J Balzer, Michael L James, Heidy Y Narvaez-Ortiz, Luke A Helgeson, Vladimir Sirotkin, and Brad J Nolen. Synergy between Wsp1 and Dip1 may initiate assembly of endocytic actin networks. *eLife*, 9:e60419, November 2020. Publisher: eLife Sciences Publications, Ltd.

[7] Connor J. Balzer, Andrew R. Wagner, Luke A. Helgeson, and Brad J. Nolen. Dip1 Co-opts Features of Branching Nucleation to Create Linear Actin Filaments that Activate WASP-Bound Arp2/3 Complex. *Current Biology*, 28(23):3886–3891.e4, December 2018.

[8] Malay Kumar Basu, Liran Carmel, Igor B. Rogozin, and Eugene V. Koonin. Evolution of protein domain promiscuity in eukaryotes. *Genome Research*, 18(3):449–461, 2008.

[9] Christopher C. Beltzner and Thomas D. Pollard. Identification of Functionally Important Residues of Arp2/3 Complex by Analysis of Homology Models from Diverse Species. *Journal of Molecular Biology*, 336(2):551–565, 2004.

[10] Christopher C. Beltzner and Thomas D. Pollard. Pathway of Actin Filament Branch Formation by Arp2/3 Complex *. *Journal of Biological Chemistry*, 283(11):7135–7144, 2008.

[11] Inna A. Belyantseva, Benjamin J. Perrin, Kevin J. Sonnemann, Mei Zhu, Ruben Stepanyan, JoAnn McGee, Gregory I. Frolenkov, Edward J. Walsh, Karen H. Friderici, Thomas B. Friedman, and James M. Ervasti. Gamma-actin is required for cytoskeletal

maintenance but not development. *Proceedings of the National Academy of Sciences of the United States of America*, 106(24):9703–9708, June 2009.

[12] Anne Bernheim-Groswasser, Sebastian Wiesner, Roy M. Golsteyn, Marie-France Carlier, and Cécile Sykes. The dynamics of actin-based motility depend on surface parameters. *Nature*, 417(6886):308–311, 2002.

[13] Peter Bieling, Tai-De Li, Julian Weichsel, Ryan McGorty, Pamela Jreij, Bo Huang, Daniel A. Fletcher, and R. Dyche Mullins. Force Feedback Controls Motor Activity and Mechanical Properties of Self-Assembling Branched Actin Networks. *Cell*, 164(1-2):115–127, 2016.

[14] L. Blanchoin, K. J. Amann, H. N. Higgs, J. B. Marchand, D. A. Kaiser, and T. D. Pollard. Direct observation of dendritic actin filament networks nucleated by Arp2/3 complex and WASP/Scar proteins. *Nature*, 404(6781):1007–1011, 2000.

[15] Laurent Blanchoin, Rajaa Boujemaa-Paterski, Cécile Sykes, and Julie Plastino. Actin Dynamics, Architecture, and Mechanics in Cell Motility. *Physiological Reviews*, 94(1):235–263, 2014.

[16] Laurent Blanchoin and Thomas D. Pollard. Mechanism of Interaction of Acanthamoeba Actophorin (ADF/Cofilin) with Actin Filaments*. *Journal of Biological Chemistry*, 274(22):15538–15546, May 1999.

[17] Laurent Blanchoin and Thomas D. Pollard. Hydrolysis of ATP by Polymerized Actin Depends on the Bound Divalent Cation but Not Profilin. *Biochemistry*, 41(2):597–602, 2002. Publisher: American Chemical Society.

[18] Emma Borrego-Diaz, Frederic Kerff, Sung Haeng Lee, François Ferron, Yu Li, and Roberto Dominguez. Crystal structure of the actin-binding domain of alpha-actinin 1: evaluating two competing actin-binding models. *Journal of Structural Biology*, 155(2):230–238, August 2006.

[19] Dennis Breitsprecher and Bruce L. Goode. Formins at a glance. *Journal of Cell Science*, 126(Pt 1):1–7, January 2013.

[20] M. C. Brown, J. A. Perrotta, and C. E. Turner. Identification of LIM3 as the principal determinant of paxillin focal adhesion localization and characterization of a novel motif on paxillin directing vinculin and focal adhesion kinase binding. *The Journal of Cell Biology*, 135(4):1109–1123, 1996.

[21] Craig D. Buckley, Jiongyi Tan, Karen L. Anderson, Dorit Hanein, Niels Volkmann, William I. Weis, W. James Nelson, and Alexander R. Dunn. The minimal cadherin-catenin complex binds to actin filaments under force. *Science (New York, N.Y.)*, 346(6209):1254211, 2014.

[22] Thomas A. Burke, Jenna R. Christensen, Elisabeth Barone, Cristian Suarez, Vladimir Sirotkin, and David R. Kovar. Homeostatic Actin Cytoskeleton Networks Are Regulated by Assembly Factor Competition for Monomers. *Current biology : CB*, 24(5):579–585, 2014.

[23] Keith Burridge. Are stress fibres contractile? *Nature*, 294(5843):691–692, 1981.

[24] M. F. Carlier and D. Pantaloni. Direct evidence for ADP-Pi-F-actin as the major intermediate in ATP-actin polymerization. Rate of dissociation of Pi from actin filaments. *Biochemistry*, 25(24):7789–7792, December 1986.

[25] D. R. Carter, G. S. Beaupré, N. J. Giori, and J. A. Helms. Mechanobiology of skeletal regeneration. *Clinical Orthopaedics and Related Research*, (355 Suppl):S41–55, 1998.

[26] Kate E. Cavanaugh, Michael F. Staddon, Edwin Munro, Shiladitya Banerjee, and Margaret L. Gardel. RhoA Mediates Epithelial Cell Shape Changes via Mechanosensitive Endocytosis. *Developmental Cell*, 52(2):152–166.e5, January 2020.

[27] Fred Chang, David Drubin, and Paul Nurse. cdc12p, a Protein Required for Cytokinesis in Fission Yeast, Is a Component of the Cell Division Ring and Interacts with Profilin. *The Journal of Cell Biology*, 137(1):169–182, 1997.

[28] Yiannis S. Chatzizisis, Ahmet Umit Coskun, Michael Jonas, Elazer R. Edelman, Charles L. Feldman, and Peter H. Stone. Role of endothelial shear stress in the natural history of coronary atherosclerosis and vascular remodeling: molecular, cellular, and vascular behavior. *Journal of the American College of Cardiology*, 49(25):2379–2393, 2007.

[29] Thomas H. Cheffings, Nigel J. Burroughs, and Mohan K. Balasubramanian. Actin turnover ensures uniform tension distribution during cytokinetic actomyosin ring contraction. *Molecular Biology of the Cell*, 30(8):933–941, 2019.

[30] W. T. Chen and S. J. Singer. Immunoelectron microscopic studies of the sites of cell-substratum and cell-cell contacts in cultured fibroblasts. *The Journal of Cell Biology*, 95(1):205–222, 1982.

[31] Han Cheng, Tianji Chen, Merve Tor, Deborah Park, Qiyuan Zhou, Jason B. Huang, Nour Khatib, Lijun Rong, and Guofei Zhou. A High-Throughput Screening Platform Targeting PDLIM5 for Pulmonary Hypertension. *Journal of Biomolecular Screening*, 21(4):333–341, 2016.

[32] Hongqiang Cheng, Kensuke Kimura, Angela K. Peter, Li Cui, Kunfu Ouyang, Tao Shen, Yujie Liu, Yusu Gu, Nancy D. Dalton, Sylvia M. Evans, Kirk U. Knowlton, Kirk L. Peterson, and Ju Chen. Loss of enigma homolog protein results in dilated cardiomyopathy. *Circulation Research*, 107(3):348–356, 2010.

[33] David Chereau, Frederic Kerff, Philip Graceffa, Zenon Grabarek, Knut Langsetmo, and Roberto Dominguez. Actin-bound structures of Wiskott–Aldrich syndrome protein (WASP)-homology domain 2 and the implications for filament assembly. *Proceedings of the National Academy of Sciences*, 102(46):16644–16649, 2005. Publisher: National Academy of Sciences Section: Biological Sciences.

[34] Steven Z. Chou and Thomas D. Pollard. Mechanism of actin polymerization revealed by cryo-EM structures of actin filaments with three different bound nucleotides. *Proceedings of the National Academy of Sciences*, 116(10):4265–4274, March 2019. Publisher: National Academy of Sciences Section: PNAS Plus.

[35] Jenna R Christensen, Glen M Hocky, Kaitlin E Homa, Alisha N Morganthaler, Sarah E Hitchcock-DeGregori, Gregory A Voth, and David R Kovar. Competition between Tropomyosin, Fimbrin, and ADF/Cofilin drives their sorting to distinct actin filament networks. *eLife*, 6:e23152, March 2017. Publisher: eLife Sciences Publications, Ltd.

[36] Jenna R Christensen, Kaitlin E Homa, Alisha N Morganthaler, Rachel R Brown, Cristian Suarez, Alyssa J Harker, Meghan E O'Connell, and David R Kovar. Cooperation between tropomyosin and α-actinin inhibits fimbrin association with actin filament networks in fission yeast. *eLife*, 8:e47279, 2019.

[37] M. Chrzanowska-Wodnicka and K. Burridge. Rho-stimulated contractility drives the formation of stress fibers and focal adhesions. *The Journal of Cell Biology*, 133(6):1403–1415, 1996.

[38] John A. Cooper, E. Loren Buhle, Simon B. Walker, Tian Y. Tsong, and Thomas D. Pollard. Kinetic evidence for a monomer activation step in actin polymerization. *Biochemistry*, 22(9):2193–2202, April 1983. Publisher: American Chemical Society.

[39] Naomi Courtemanche. Mechanisms of formin-mediated actin assembly and dynamics. *Biophysical Reviews*, 10(6):1553–1569, 2018.

[40] Naomi Courtemanche, Ja Yil Lee, Thomas D. Pollard, and Eric C. Greene. Tension modulates actin filament polymerization mediated by formin and profilin. *Proceedings of the National Academy of Sciences*, 110(24):9752–9757, 2013.

[41] L. P. Cramer, M. Siebert, and T. J. Mitchison. Identification of novel graded polarity actin filament bundles in locomoting heart fibroblasts: implications for the generation of motile force. *The Journal of Cell Biology*, 136(6):1287–1305, 1997.

[42] Meghna Das Thakur, Yunfeng Feng, Radhika Jagannathan, Midori J. Seppa, James B. Skeath, and Gregory D. Longmore. Ajuba LIM Proteins Are Negative Regulators of the Hippo Signaling Pathway. *Current Biology*, 20(7):657–662, 2010.

[43] Mark J. Dayel, Orkun Akin, Mark Landeryou, Viviana Risca, Alex Mogilner, and R. Dyche Mullins. In Silico Reconstitution of Actin-Based Symmetry Breaking and Motility. *PLOS Biology*, 7(9):e1000201, 2009.

[44] E. M. De La Cruz and T. D. Pollard. Nucleotide-free actin: stabilization by sucrose and nucleotide binding kinetics. *Biochemistry*, 34(16):5452–5461, April 1995.

[45] Enrique M. De La Cruz, Jeremy Roland, Brannon R. McCullough, Laurent Blanchoin, and Jean-Louis Martiel. Origin of Twist-Bend Coupling in Actin Filaments. *Biophysical Journal*, 99(6):1852–1860, 2010.

[46] Nicholas O. Deakin and Christopher E. Turner. Paxillin comes of age. *Journal of Cell Science*, 121(15):2435–2444, 2008.

[47] Dennis E. Discher, David J. Mooney, and Peter W. Zandstra. Growth factors, matrices, and forces combine and control stem cells. *Science (New York, N.Y.)*, 324(5935):1673–1677, 2009.

[48] Roberto Dominguez. Actin-binding proteins – a unifying hypothesis. *Trends in Biochemical Sciences*, 29(11):572–578, November 2004.

[49] Roberto Dominguez. The WASP-Homology 2 Domain and Cytoskeleton Assembly. In Marie-France Carlier, editor, *Actin-based Motility: Cellular, Molecular and Physical Aspects*, pages 255–277. Springer Netherlands, Dordrecht, 2010.

[50] Roberto Dominguez. Nucleotide-dependent conformational changes in the actin filament: Subtler than expected. *Proceedings of the National Academy of Sciences*, 116(10):3959–3961, March 2019. Publisher: National Academy of Sciences Section: Commentary.

[51] Roberto Dominguez and Kenneth C. Holmes. Actin Structure and Function. *Annual review of biophysics*, 40:169–186, 2011.

[52] Lynda K. Doolittle, Michael K. Rosen, and Shae B. Padrick. Measurement and Analysis of In Vitro Actin Polymerization. In Amanda S. Coutts, editor, *Adhesion Protein Protocols*, Methods in Molecular Biology, pages 273–293. Humana Press, Totowa, NJ, 2013.

[53] B. Drees, E. Friederich, J. Fradelizi, D. Louvard, M. C. Beckerle, and R. M. Golsteyn. Characterization of the interaction between zyxin and members of the Ena/vasodilator-stimulated phosphoprotein family of proteins. *The Journal of Biological Chemistry*, 275(29):22503–22511, 2000.

[54] Sirio Dupont, Leonardo Morsut, Mariaceleste Aragona, Elena Enzo, Stefano Giulitti, Michelangelo Cordenonsi, Francesca Zanconato, Jimmy Le Digabel, Mattia Forcato, Silvio Bicciato, Nicola Elvassore, and Stefano Piccolo. Role of YAP/TAZ in mechanotransduction. *Nature*, 474(7350):179–183, 2011.

[55] Shubham Dutta, Sebastian Mana-Capelli, Murugan Paramasivam, Ishani Dasgupta, Heather Cirka, Kris Billiar, and Dannel McCollum. TRIP6 inhibits Hippo signaling in response to tension at adherens junctions. *EMBO reports*, 19(2):337–350, 2018.

[56] Marc Edwards, Adam Zwolak, Dorothy A. Schafer, David Sept, Roberto Dominguez, and John A. Cooper. Capping protein regulators fine-tune actin assembly dynamics. *Nature Reviews. Molecular Cell Biology*, 15(10):677–689, October 2014.

[57] Andrey Efimov, Natalia Schiefermeier, Ilya Grigoriev, Ryoma Ohi, Michael C. Brown, Christopher E. Turner, J. Victor Small, and Irina Kaverina. Paxillin-dependent stimulation of microtubule catastrophes at focal adhesion sites. *Journal of Cell Science*, 121(3):405–405, 2008.

[58] Coumaran Egile, Thomas P. Loisel, Valérie Laurent, Rong Li, Dominique Pantaloni, Philippe J. Sansonetti, and Marie-France Carlier. Activation of the Cdc42 Effector N-Wasp by the Shigella flexneri Icsa Protein Promotes Actin Nucleation by Arp2/3 Complex and Bacterial Actin-Based Motility. *The Journal of Cell Biology*, 146(6):1319–1332, 1999.

[59] George T. Eisenhoffer, Patrick D. Loftus, Masaaki Yoshigi, Hideo Otsuna, Chi-Bin Chien, Paul A. Morcos, and Jody Rosenblatt. Crowding induces live cell extrusion to maintain homeostatic cell numbers in epithelia. *Nature*, 484(7395):546–549, April 2012.

[60] George T. Eisenhoffer, Patrick D. Loftus, Masaaki Yoshigi, Hideo Otsuna, Chi-Bin Chien, Paul A. Morcos, and Jody Rosenblatt. Crowding induces live cell extrusion to maintain homeostatic cell numbers in epithelia. *Nature*, 484(7395):546–549, April 2012.

[61] Ahmed Elbediwy, Zoé I. Vincent-Mistiaen, Bradley Spencer-Dene, Richard K. Stone, Stefan Boeing, Stefanie K. Wculek, Julia Cordero, Ee H. Tan, Rachel Ridgway, Val G. Brunton, Erik Sahai, Holger Gerhardt, Axel Behrens, Ilaria Malanchi, Owen J. Sansom, and Barry J. Thompson. Integrin signalling regulates YAP and TAZ to control skin homeostasis. *Development*, 143(10):1674–1687, 2016.

[62] Adam J. Engler, Shamik Sen, H. Lee Sweeney, and Dennis E. Discher. Matrix elasticity directs stem cell lineage specification. *Cell*, 126(4):677–689, 2006.

[63] Becket Feierbach and Fred Chang. Roles of the fission yeast formin for3p in cell polarity, actin cable formation and symmetric cell division. *Current Biology*, 11(21):1656–1665, 2001.

[64] François Ferron, Grzegorz Rebowski, Sung Haeng Lee, and Roberto Dominguez. Structural basis for the recruitment of profilin-actin complexes during filament elongation by Ena/VASP. *The EMBO journal*, 26(21):4597–4606, October 2007.

[65] Kenneth N. Fish. Total Internal Reflection Fluorescence (TIRF) Microscopy. *Current Protocols in Cytometry*, 50(1):12.18.1–12.18.13, 2009. _eprint: https://currentprotocols.onlinelibrary.wiley.com/doi/pdf/10.1002/0471142956.cy1218s50.

[66] Daniel A. Fletcher and R. Dyche Mullins. Cell mechanics and the cytoskeleton. *Nature*, 463(7280):485–492, 2010.

[67] Clemens M. Franz and Daniel J. Müller. Analyzing focal adhesion structure by atomic force microscopy. *Journal of Cell Science*, 118(22):5315–5323, 2005.

[68] G. Freyd, S. K. Kim, and H. R. Horvitz. Novel cysteine-rich motif and homeodomain in the product of the Caenorhabditis elegans cell lineage gene lin-11. *Nature*, 344(6269):876–879, 1990.

[69] C. Frieden. Polymerization of actin: mechanism of the Mg2+-induced process at pH 8 and 20 degrees C. *Proceedings of the National Academy of Sciences*, 80(21):6513–6517, November 1983. Publisher: National Academy of Sciences Section: Research Article.

[70] Takashi Fujii, Atsuko H. Iwane, Toshio Yanagida, and Keiichi Namba. Direct visualization of secondary structures of F-actin by electron cryomicroscopy. *Nature*, 467(7316):724–728, October 2010. Number: 7316 Publisher: Nature Publishing Group.

[71] Vitold E. Galkin, Albina Orlova, and Edward H. Egelman. Actin filaments as tension sensors. *Current biology: CB*, 22(3):R96–101, 2012.

[72] Vitold E. Galkin, Albina Orlova, Dmitri S. Kudryashov, Alexander Solodukhin, Emil Reisler, Gunnar F. Schröder, and Edward H. Egelman. Remodeling of actin filaments by ADF/cofilin proteins. *Proceedings of the National Academy of Sciences*, 108(51):20568–20572, December 2011. Publisher: National Academy of Sciences Section: Biological Sciences.

[73] Kristina A. Ganzinger and Petra Schwille. More from less – bottom-up reconstitution of cell biology. *Journal of Cell Science*, 132(4), 2019.

[74] Wanzhong Ge and Mohan K. Balasubramanian. Pxl1p, a Paxillin-related Protein, Stabilizes the Actomyosin Ring during Cytokinesis in Fission Yeast. *Molecular Biology of the Cell*, 19(4):1680–1692, 2008.

[75] Michael Glotzer. Cytokinesis in Metazoa and Fungi. *Cold Spring Harbor Perspectives in Biology*, 9(10), 2017.

[76] Bruce L. Goode and Michael J. Eck. Mechanism and Function of Formins in the Control of Actin Assembly. *Annual Review of Biochemistry*, 76(1):593–627, 2007.

[77] Bruce L. Goode, Julian A. Eskin, and Beverly Wendland. Actin and Endocytosis in Budding Yeast. *Genetics*, 199(2):315–358, 2015. Publisher: Genetics Section: YeastBook.

[78] Michael J. Greenberg, Göker Arpağ, Erkan Tüzel, and E. Michael Ostap. A Perspective on the Role of Myosins as Mechanosensors. *Biophysical Journal*, 110(12):2568–2576, 2016.

[79] Elena E. Grintsevich, Peng Ge, Michael R. Sawaya, Hunkar Gizem Yesilyurt, Jonathan R. Terman, Z. Hong Zhou, and Emil Reisler. Catastrophic disassembly of actin filaments via Mical-mediated oxidation. *Nature Communications*, 8(1):2183, December 2017. Number: 1 Publisher: Nature Publishing Group.

[80] Markus Grubinger and Mario Gimona. CRP2 is an autonomous actin-binding protein. *FEBS letters*, 557(1-3):88–92, 2004.

[81] SA Gudipaty, J Lindblom, PD Loftus, MJ Redd, K Edes, CF Davey, V Krishnegowda, and J Rosenblatt. Mechanical stretch triggers rapid epithelial cell division through Piezo1. *Nature*, 543(7643):118–121, 2017.

[82] P. W. Gunning, U. Ghoshdastider, S. Whitaker, D. Popp, and R. C. Robinson. The evolution of compositionally and functionally distinct actin filaments. *Journal of Cell Science*, 128(11):2009–2019, 2015.

[83] Dorit Hanein, Niels Volkmann, Sharon Goldsmith, Anne-Marie Michon, William Lehman, Roger Craig, David DeRosier, Steve Almo, and Paul Matsudaira. An atomic model of fimbrin binding to F-actin and its implications for filament crosslinking and regulation. *Nature Structural Biology*, 5(9):787–792, September 1998. Number: 9 Publisher: Nature Publishing Group.

[84] Scott D. Hansen and R. Dyche Mullins. VASP is a processive actin polymerase that requires monomeric actin for barbed end association. *The Journal of Cell Biology*, 191(3):571–584, November 2010.

[85] Jean Hanson and J. Lowy. The structure of F-actin and of actin filaments isolated from muscle. *Journal of Molecular Biology*, 6(1):46–IN5, January 1963.

[86] P. B. Harbury, T. Zhang, P. S. Kim, and T. Alber. A switch between two-, three-, and four-stranded coiled coils in GCN4 leucine zipper mutants. *Science*, 262(5138):1401–1407, 1993.

[87] M. Amanda Hartman and James A. Spudich. The myosin superfamily at a glance. *Journal of Cell Science*, 125(7):1627–1632, April 2012. Publisher: The Company of Biologists Ltd Section: Cell Science at a Glance.

[88] Kimihide Hayakawa, Hitoshi Tatsumi, and Masahiro Sokabe. Actin filaments function as a tension sensor by tension-dependent binding of cofilin to the filament. *The Journal of Cell Biology*, 195(5):721–727, 2011.

[89] I. M. Herman. Actin isoforms. *Current Opinion in Cell Biology*, 5(1):48–55, 1993.

[90] Henry N. Higgs, Laurent Blanchoin, and Thomas D. Pollard. Influence of the C Terminus of Wiskott-Aldrich Syndrome Protein (WASp) and the Arp2/3 Complex on Actin Polymerization. *Biochemistry*, 38(46):15212–15222, 1999. Publisher: American Chemical Society.

[91] Henry N. Higgs and Kevin J. Peterson. Phylogenetic Analysis of the Formin Homology 2 Domain. *Molecular Biology of the Cell*, 16(1):1–13, 2005.

[92] Laura M. Hoffman, Christopher C. Jensen, Aashi Chaturvedi, Masaaki Yoshigi, and Mary C. Beckerle. Stretch-induced actin remodeling requires targeting of zyxin to stress fibers and recruitment of actin regulators. *Molecular Biology of the Cell*, 23(10):1846–1859, 2012.

[93] Laura M. Hoffman, David A. Nix, Beverly Benson, Ray Boot-Hanford, Erika Gustafsson, Colin Jamora, A. Sheila Menzies, Keow Lin Goh, Christopher C. Jensen, Frank B. Gertler, Elaine Fuchs, Reinhard Fässler, and Mary C. Beckerle. Targeted disruption of the murine zyxin gene. *Molecular and Cellular Biology*, 23(1):70–79, 2003.

[94] Pirta Hotulainen and Pekka Lappalainen. Stress fibers are generated by two distinct actin assembly mechanisms in motile cells. *The Journal of Cell Biology*, 173(3):383–394, 2006.

[95] Zhaoyuan Hou, Hongzhuang Peng, David E. White, Dmitri G. Negorev, Gerd G. Maul, Yunfeng Feng, Gregory D. Longmore, Samuel Waxman, Arthur Zelent, and Frank J. Rauscher. LIM protein Ajuba functions as a nuclear receptor corepressor and negatively regulates retinoic acid signaling. *Proceedings of the National Academy of Sciences of the United States of America*, 107(7):2938–2943, 2010.

[96] Derek L. Huang, Nicolas A. Bax, Craig D. Buckley, William I. Weis, and Alexander R. Dunn. Vinculin forms a directionally asymmetric catch bond with F-actin. *Science*, 357(6352):703–706, 2017.

[97] Sui Huang and Donald E. Ingber. The structural and mechanical complexity of cell-growth control. *Nature Cell Biology*, 1(5):E131–E138, 1999.

[98] Andrew R. Huehn, Jeffrey P. Bibeau, Anthony C. Schramm, Wenxiang Cao, Enrique M. De La Cruz, and Charles V. Sindelar. Structures of cofilin-induced structural changes reveal local and asymmetric perturbations of actin filaments. *Proceedings of the National Academy of Sciences*, 117(3):1478–1484, January 2020. Publisher: National Academy of Sciences Section: Biological Sciences.

[99] Christopher Jack Huggins and Irene L. Andrulis. Cell cycle regulated phosphorylation of LIMD1 in cell lines and expression in human breast cancers. *Cancer Letters*, 267(1):55–66, 2008.

[100] Stephan Huveneers and Johan de Rooij. Mechanosensitive systems at the cadherin–F-actin interface. *Journal of Cell Science*, 126(2):403–413, 2013.

[101] H. E. Huxley. ELECTRON MICROSCOPE STUDIES ON THE STRUCTURE OF NATURAL AND SYNTHETIC PROTEIN FILAMENTS FROM STRIATED MUSCLE. *Journal of Molecular Biology*, 7:281–308, September 1963.

[102] Consuelo Ibar, Elmira Kirichenko, Benjamin Keepers, Edward Enners, Katelyn Fleisch, and Kenneth D. Irvine. Tension-dependent regulation of mammalian Hippo signaling through LIMD1. *Journal of Cell Science*, 131(5), 2018.

[103] Silvia Jansen, Agnieszka Collins, Changsong Yang, Grzegorz Rebowski, Tatyana Svitkina, and Roberto Dominguez. Mechanism of Actin Filament Bundling by Fascin*,. *Journal of Biological Chemistry*, 286(34):30087–30096, August 2011.

[104] M. Johannessen, S. Møller, T. Hansen, U. Moens, and M. Van Ghelue. The multifunctional roles of the four-and-a-half-LIM only protein FHL2. *Cellular and molecular life sciences: CMLS*, 63(3):268–284, 2006.

[105] Antoine Jégou, Thomas Niedermayer, József Orbán, Dominique Didry, Reinhard Lipowsky, Marie-France Carlier, and Guillaume Romet-Lemonne. Individual actin filaments in a microfluidic flow reveal the mechanism of ATP hydrolysis and give insight into the properties of profilin. *PLoS biology*, 9(9):e1001161, September 2011.

[106] Antoine Jégou and Guillaume Romet-Lemonne. Mechanically tuning actin filaments to modulate the action of actin-binding proteins. *Current Opinion in Cell Biology*, 68:72–80, 2021.

[107] W. Kabsch, H. G. Mannherz, D. Suck, E. F. Pai, and K. C. Holmes. Atomic structure of the actin:DNase I complex. *Nature*, 347(6288):37–44, September 1990.

[108] Julie L. Kadrmas and Mary C. Beckerle. The LIM domain: from the cytoskeleton to the nucleus. *Nature Reviews Molecular Cell Biology*, 5(11):920–931, 2004.

[109] Pakorn Kanchanawong, Gleb Shtengel, Ana M. Pasapera, Ericka B. Ramko, Michael W. Davidson, Harald F. Hess, and Clare M. Waterman. Nanoscale architecture of integrin-based cell adhesions. *Nature*, 468(7323):580–584, 2010.

[110] Hyeran Kang, Michael J. Bradley, W. Austin Elam, and Enrique M. De La Cruz. Regulation of actin by ion-linked equilibria. *Biophysical Journal*, 105(12):2621–2628, December 2013.

[111] Olof Karlsson, Stefan Thor, Torbjörn Norberg, Helena Ohlsson, and Thomas Edlund. Insulin gene enhancer binding protein Isl-1 is a member of a novel class of proteins containing both a homeo-and a Cys–His domain. *Nature*, 344(6269):879–882, 1990.

[112] D. R. Kellogg, T. J. Mitchison, and B. M. Alberts. Behaviour of microtubules and actin filaments in living Drosophila embryos. *Development*, 103(4):675–686, 1988.

[113] Joo-ri Kim-Kaneyama, Wataru Suzuki, Kiyoko Ichikawa, Takahiro Ohki, Yoko Kohno, Masataka Sata, Kiyoshi Nose, and Motoko Shibanuma. Uni-axial stretching regulates intracellular localization of Hic-5 expressed in smooth-muscle cells in vivo. *Journal of Cell Science*, 118(Pt 5):937–949, 2005.

[114] Michelle E. Kimple, Allison L. Brill, and Renee L. Pasker. Overview of Affinity Tags for Protein Purification. *Current protocols in protein science / editorial board, John E. Coligan ... [et al.]*, 73:Unit–9.9, September 2013.

[115] Bernard J. Koch, Joseph F. Ryan, and Andreas D. Baxevanis. The Diversification of the LIM Superclass at the Base of the Metazoa Increased Subcellular Complexity and Promoted Multicellular Specialization. *PLOS ONE*, 7(3):e33261, 2012.

[116] E. D. Korn, M. F. Carlier, and D. Pantaloni. Actin polymerization and ATP hydrolysis. *Science (New York, N.Y.)*, 238(4827):638–644, October 1987.

[117] David R. Kovar, Elizabeth S. Harris, Rachel Mahaffy, Henry N. Higgs, and Thomas D. Pollard. Control of the Assembly of ATP- and ADP-Actin by Formins and Profilin. *Cell*, 124(2):423–435, 2006.

[118] David R. Kovar, Vladimir Sirotkin, and Matthew Lord. Three's company: the fission yeast actin cytoskeleton. *Trends in Cell Biology*, 21(3):177–187, 2011.

[119] Jeffrey R. Kuhn and Thomas D. Pollard. Real-time measurements of actin filament polymerization by total internal reflection fluorescence microscopy. *Biophysical Journal*, 88(2):1387–1402, February 2005.

[120] Jean-Cheng Kuo. Mechanotransduction at focal adhesions: integrating cytoskeletal mechanics in migrating cells. *Journal of Cellular and Molecular Medicine*, 17(6):704–712, 2013.

[121] Jean-Cheng Kuo, Xuemei Han, Cheng-Te Hsiao, John R. Yates Iii, and Clare M. Waterman. Analysis of the myosin-II-responsive focal adhesion proteome reveals a role for -Pix in negative regulation of focal adhesion maturation. *Nature Cell Biology*, 13(4):383–393, 2011.

[122] Laetitia Kurzawa, Benoit Vianay, Fabrice Senger, Timothée Vignaud, Laurent Blanchoin, and Manuel Théry. Dissipation of contractile forces: the missing piece in cell mechanics. *Molecular Biology of the Cell*, 28(14):1825–1832, 2017.

[123] Michael M Lacy, David Baddeley, and Julien Berro. Single-molecule turnover dynamics of actin and membrane coat proteins in clathrin-mediated endocytosis. *eLife*, 8:e52355, December 2019. Publisher: eLife Sciences Publications, Ltd.

[124] J. H. Laity, B. M. Lee, and P. E. Wright. Zinc finger proteins: new insights into structural and functional diversity. *Current Opinion in Structural Biology*, 11(1):39–46, 2001.

[125] I-Ju Lee, Valerie C. Coffman, and Jian-Qiu Wu. Contractile-Ring Assembly in Fission Yeast Cytokinesis: Recent Advances and New Perspectives. *Cytoskeleton (Hoboken, N.J.)*, 69(10):751–763, October 2012.

[126] Monkol Lek, Daniel G. MacArthur, Nan Yang, and Kathryn N. North. Phylogenetic Analysis of Gene Structure and Alternative Splicing in α-Actinins. *Molecular Biology and Evolution*, 27(4):773–780, 2010.

[127] B. Li and B. Trueb. Analysis of the alpha-actinin/zyxin interaction. *The Journal of Biological Chemistry*, 276(36):33328–33335, 2001.

[128] Boon Cheng Lim, Shinji Matsumoto, Hideki Yamamoto, Hiroki Mizuno, Junichi Kikuta, Masaru Ishii, and Akira Kikuchi. Prickle1 promotes focal adhesion disassembly in cooperation with the CLASP-LL5 complex in migrating cells. *Journal of Cell Science*, 129(16):3115–3129, 2016.

[129] Viktoria Liss, Britta Barlag, Monika Nietschke, and Michael Hensel. Self-labelling enzymes as universal tags for fluorescence microscopy, super-resolution microscopy and electron microscopy. *Scientific Reports*, 5(1):17740, December 2015. Number: 1 Publisher: Nature Publishing Group.

[130] Thomas P. Loisel, Rajaa Boujemaa, Dominique Pantaloni, and Marie-France Carlier. Reconstitution of actin-based motility of Listeria and Shigella using pure proteins. *Nature*, 401(6753):613–616, 1999.

[131] Deshun Lu and Ghassan S. Kassab. Role of shear stress and stretch in vascular mechanobiology. *Journal of the Royal Society Interface*, 8(63):1379–1385, 2011.

[132] J. Lu and T. D. Pollard. Profilin binding to poly-L-proline and actin monomers along with ability to catalyze actin nucleotide exchange is required for viability of fission yeast. *Molecular Biology of the Cell*, 12(4):1161–1175, April 2001.

[133] Qing Luan, Su-Ling Liu, Luke A Helgeson, and Brad J Nolen. Structure of the nucleation-promoting factor SPIN90 bound to the actin filament nucleator Arp2/3 complex. *The EMBO Journal*, 37(22):e100005, November 2018. Publisher: John Wiley & Sons, Ltd.

[134] Ana María López-Colomé, Irene Lee-Rivera, Regina Benavides-Hidalgo, and Edith López. Paxillin: a crossroad in pathological cell migration. *Journal of Hematology & Oncology*, 10(1):50, 2017.

[135] Sutherland Maciver, Henry Zot, and Thomas Pollard. Characterization of actin filament severing by actophorin from Acanthamoeba castellanii. *The Journal of Cell Biology*, 115(6):1611–1620, December 1991.

[136] Aaron L. Magno, Evan Ingley, Suzanne J. Brown, Arthur D. Conigrave, Thomas Ratajczak, and Bryan K. Ward. Testin, a novel binding partner of the calcium-sensing receptor, enhances receptor-mediated Rho-kinase signalling. *Biochemical and Biophysical Research Communications*, 412(4):584–589, 2011.

[137] Jean-Baptiste Marchand, Donald A. Kaiser, Thomas D. Pollard, and Henry N. Higgs. Interaction of WASP/Scar proteins with actin and vertebrate Arp2/3 complex. *Nature Cell Biology*, 3(1):76–82, 2001. Number: 1 Publisher: Nature Publishing Group.

[138] Helene Marie, Stephen J. Pratt, Martha Betson, Holly Epple, Josef T. Kittler, Laura Meek, Stephen J. Moss, Sergey Troyanovsky, David Attwell, Gregory D. Longmore, and Vania M. M. Braga. The LIM protein Ajuba is recruited to cadherin-dependent cell junctions through an association with alpha-catenin. *The Journal of Biological Chemistry*, 278(2):1220–1228, 2003.

[139] Bernd Martin, Richard Schneider, Stefanie Janetzky, Zoe Waibler, Petra Pandur, Michael Kühl, Jürgen Behrens, Klaus von der Mark, Anna Starzinski-Powitz, and Viktor Wixler. The LIM-only protein FHL2 interacts with -catenin and promotes differentiation of mouse myoblasts. *The Journal of Cell Biology*, 159(1):113–122, 2002.

[140] Lin Mei, Santiago Espinosa de los Reyes, Matthew J Reynolds, Rachel Leicher, Shixin Liu, and Gregory M Alushin. Molecular mechanism for direct actin force-sensing by α-catenin. *eLife*, 9:e62514, 2020.

[141] Alphée Michelot, Michael Costanzo, Ali Sarkeshik, Charles Boone, John R. Yates, and David G. Drubin. Reconstitution and Protein Composition Analysis of Endocytic Actin Patches. *Current biology : CB*, 20(21):1890–1899, November 2010.

[142] Alphée Michelot and David G. Drubin. Building Distinct Actin Filament Networks in a Common Cytoplasm. *Current Biology*, 21(14):R560–R569, 2011.

[143] Alphée Michelot, Alexandre Grassart, Voytek Okreglak, Michael Costanzo, Charles Boone, and David G. Drubin. Actin Filament Elongation in Arp2/3-derived Networks is Controlled by Three Distinct Mechanisms. *Developmental cell*, 24(2):182–195, January 2013.

[144] J. W. Michelsen, K. L. Schmeichel, M. C. Beckerle, and D. R. Winge. The LIM motif defines a specific zinc-binding protein domain. *Proceedings of the National Academy of Sciences of the United States of America*, 90(10):4404–4408, 1993.

[145] Mithilesh Mishra, Jun Kashiwazaki, Tomoko Takagi, Ramanujam Srinivasan, Yinyi Huang, Mohan K. Balasubramanian, and Issei Mabuchi. In vitro contraction of cytokinetic ring depends on myosin II but not on actin dynamics. *Nature Cell Biology*, 15(7):853–859, July 2013. Number: 7 Publisher: Nature Publishing Group.

[146] Hiroaki Mizuno, Kotaro Tanaka, Sawako Yamashiro, Akihiro Narita, and Naoki Watanabe. Helical rotation of the diaphanous-related formin mDia1 generates actin filaments resistant to cofilin. *Proceedings of the National Academy of Sciences of the United States of America*, 115(22):E5000–E5007, 2018.

[147] S. C. Mockrin and E. D. Korn. Acanthamoeba profilin interacts with G-actin to increase the rate of exchange of actin-bound adenosine 5'-triphosphate. *Biochemistry*, 19(23):5359–5362, November 1980.

[148] Alex Mogilner. On the edge: modeling protrusion. *Current Opinion in Cell Biology*, 18(1):32–39, 2006.

[149] Alexander Mogilner and G. Oster. The physics of lamellipodial protrusion. *European Biophysics Journal*, 25(1):47–53, October 1996.

[150] Simon W. Moore, Pere Roca-Cusachs, and Michael P. Sheetz. Stretchy Proteins on Stretchy Substrates: The Important Elements of Integrin-Mediated Rigidity Sensing. *Developmental cell*, 19(2):194–206, 2010.

[151] Jennifer L. Morrell, Mary Morphew, and Kathleen L. Gould. A Mutant of Arp2p Causes Partial Disassembly of the Arp2/3 Complex and Loss of Cortical Actin Function in Fission Yeast. *Molecular Biology of the Cell*, 10(12):4201–4215, 1999.

[152] Michael Murrell, Todd Thoresen, and Margaret Gardel. Chapter Fifteen - Reconstitution of Contractile Actomyosin Arrays. In Ronald D. Vale, editor, *Methods in Enzymology*, volume 540 of *Reconstituting the Cytoskeleton*, pages 265–282. Academic Press, 2014.

[153] Michael P. Murrell and Margaret L. Gardel. F-actin buckling coordinates contractility and severing in a biomimetic actomyosin cortex. *Proceedings of the National Academy of Sciences*, 109(51):20820–20825, 2012.

[154] Kentaro Nakano, Jun Imai, Ritsuko Arai, Akio Toh-e, Yasushi Matsui, and Issei Mabuchi. The small GTPase Rho3 and the diaphanous/formin For3 function in polarized cell growth in fission yeast. *Journal of Cell Science*, 115(23):4629–4639, December 2002.

[155] Naotaka Nakazawa, Aneesh R. Sathe, G. V. Shivashankar, and Michael P. Sheetz. Matrix mechanics controls FHL2 movement to the nucleus to activate p21 expression. *Proceedings of the National Academy of Sciences*, 113(44):E6813–E6822, 2016.

[156] Erin M. Neidt, Colleen T. Skau, and David R. Kovar. The Cytokinesis Formins from the Nematode Worm and Fission Yeast Differentially Mediate Actin Filament Assembly *. *Journal of Biological Chemistry*, 283(35):23872–23883, August 2008.

[157] B. J. Nolen, N. Tomasevic, A. Russell, D. W. Pierce, Z. Jia, C. D. McCormick, J. Hartman, R. Sakowicz, and T. D. Pollard. Characterization of two classes of small molecule inhibitors of Arp2/3 complex. *Nature*, 460(7258):1031–1034, 2009. Number: 7258 Publisher: Nature Publishing Group.

[158] Brad J. Nolen and Thomas D. Pollard. Insights into the influence of nucleotides on actin family proteins from seven new structures of Arp2/3 complex. *Molecular cell*, 26(3):449–457, 2007.

[159] Kazumasa Ohashi, Sachiko Fujiwara, and Kensaku Mizuno. Roles of the cytoskeleton, cell adhesion and rho signalling in mechanosensing and mechanotransduction. *Journal of Biochemistry*, 161(3):245–254, 2017.

[160] Norihiko Ohura, Kimiko Yamamoto, Sigeru Ichioka, Takaaki Sokabe, Hideki Nakatsuka, Atsushi Baba, Masahiro Shibata, Takashi Nakatsuka, Kiyonori Harii, Youichiro Wada, Takahide Kohro, Tatsuhiko Kodama, and Joji Ando. Global Analysis of Shear Stress-Responsive Genes in Vascular Endothelial Cells. *Journal of Atherosclerosis and Thrombosis*, 10(5):304–313, 2003.

[161] Takanori Otomo, Diana R. Tomchick, Chinatsu Otomo, Sanjay C. Panchal, Mischa Machius, and Michael K. Rosen. Structural basis of actin filament nucleation and processive capping by a formin homology 2 domain. *Nature*, 433(7025):488–494, February 2005.

[162] Leanna M. Owen, Nicolas A. Bax, William I. Weis, and Alexander R. Dunn. The C-terminal Domain of Talin Forms a Force-responsive, Directional Catch Bond to F-actin. *Biophysical Journal*, 118(3):31a, 2020.

[163] Ben O'Shaughnessy and Sathish Thiyagarajan. Mechanisms of contractile ring tension production and constriction. *Biophysical Reviews*, 10(6):1667–1681, December 2018.

[164] Shae B. Padrick, Lynda K. Doolittle, Chad A. Brautigam, David S. King, and Michael K. Rosen. Arp2/3 complex is bound and activated by two WASP proteins. *Proceedings of the National Academy of Sciences*, 108(33):E472–E479, 2011.

[165] Shae B. Padrick and Michael K. Rosen. Physical Mechanisms of Signal Integration by WASP Family Proteins. *Annual Review of Biochemistry*, 79(1):707–735, 2010. _eprint: https://doi.org/10.1146/annurev.biochem.77.060407.135452.

[166] Nandan G. Pandit, Wenxiang Cao, Jeffrey Bibeau, Eric M. Johnson-Chavarria, Edwin W. Taylor, Thomas D. Pollard, and Enrique M. De La Cruz. Force and phosphate release from Arp2/3 complex promote dissociation of actin filament branches. *Proceedings of the National Academy of Sciences*, 2020.

[167] Francine Parker, Thomas G. Baboolal, and Michelle Peckham. Actin Mutations and Their Role in Disease. *International Journal of Molecular Sciences*, 21(9), May 2020.

[168] Aditya S. Paul and Thomas D. Pollard. Review of the mechanism of processive actin filament elongation by formins. *Cell motility and the cytoskeleton*, 66(8):606–617, August 2009.

[169] Stéphanie Pellegrin and Harry Mellor. Actin stress fibres. *Journal of Cell Science*, 120(20):3491–3499, 2007.

[170] J Petersen, D Weilguny, R Egel, and O Nielsen. Characterization of fus1 of Schizosaccharomyces pombe: a developmentally controlled function needed for conjugation. *Molecular and Cellular Biology*, 15(7):3697–3707, July 1995.

[171] Janni Petersen, Olaf Nielsen, Richard Egel, and Iain M. Hagan. FH3, A Domain Found in Formins, Targets the Fission Yeast Formin Fus1 to the Projection Tip During Conjugation. *The Journal of Cell Biology*, 141(5):1217–1228, 1998.

[172] Mario Pinar, Pedro M. Coll, Sergio A. Rincón, and Pilar Pérez. Schizosaccharomyces pombe Pxl1 is a paxillin homologue that modulates Rho1 activity and participates in cytokinesis. *Molecular Biology of the Cell*, 19(4):1727–1738, 2008.

[173] Luther W. Pollard, Mikael V. Garabedian, Salvatore L. Alioto, Shashank Shekhar, and Bruce L. Goode. Genetically inspired in vitro reconstitution of Saccharomyces cerevisiae actin cables from seven purified proteins. *Molecular Biology of the Cell*, 31(5):335–347, March 2020.

[174] T. D. Pollard, L. Blanchoin, and R. D. Mullins. Molecular mechanisms controlling actin filament dynamics in nonmuscle cells. *Annual Review of Biophysics and Biomolecular Structure*, 29:545–576, 2000.

[175] Thomas D. Pollard. Regulation of Actin Filament Assembly by Arp2/3 Complex and Formins. *Annual Review of Biophysics and Biomolecular Structure*, 36(1):451–477, 2007.

[176] Thomas D. Pollard. A Guide to Simple and Informative Binding Assays. *Molecular Biology of the Cell*, 21(23):4061–4067, 2010.

[177] Thomas D. Pollard. Actin and Actin-Binding Proteins. *Cold Spring Harbor Perspectives in Biology*, 8(8), 2016.

[178] Thomas D Pollard and Gary G Borisy. Cellular Motility Driven by Assembly and Disassembly of Actin Filaments. *Cell*, 112(4):453–465, 2003.

[179] Thomas D. Pollard and Jian-Qiu Wu. Understanding cytokinesis: lessons from fission yeast. *Nature Reviews. Molecular Cell Biology*, 11(2):149–155, February 2010.

[180] Stephen J. Pratt, Holly Epple, Michael Ward, Yunfeng Feng, Vania M. Braga, and Gregory D. Longmore. The LIM protein Ajuba influences p130Cas localization and Rac1 activity during cell migration. *Journal of Cell Biology*, 168(5):813–824, 2005.

[181] Martin Pring, Marie Evangelista, Charles Boone, Changsong Yang, and Sally H. Zigmond. Mechanism of formin-induced nucleation of actin filaments. *Biochemistry*, 42(2):486–496, January 2003.

[182] Cordelia Rauskolb, Guohui Pan, B. V. V. G. Reddy, Hyangyee Oh, and Kenneth D. Irvine. Zyxin Links Fat Signaling to the Hippo Pathway. *PLOS Biology*, 9(6):e1000624, 2011.

[183] Cordelia Rauskolb, Shuguo Sun, Gongping Sun, Yuanwang Pan, and Kenneth D. Irvine. Cytoskeletal tension inhibits Hippo signaling through an Ajuba-Warts complex. *Cell*, 158(1):143–156, 2014.

[184] William Razzell, Maria E. Bustillo, and Jennifer A. Zallen. The force-sensitive protein Ajuba regulates cell adhesion during epithelial morphogenesis. *Journal of Cell Biology*, 217(10):3715–3730, 2018.

[185] Matthias Reinhard, Jurg Zumbrunn, Daniel Jaquemar, Monika Kuhn, Ulrich Walter, and Beat Trueb. An α-Actinin Binding Site of Zyxin Is Essential for Subcellular Zyxin Localization and α-Actinin Recruitment *. *Journal of Biological Chemistry*, 274(19):13410–13418, 1999.

[186] Anne-Cécile Reymann, Cristian Suarez, Christophe Guérin, Jean-Louis Martiel, Christopher J. Staiger, Laurent Blanchoin, and Rajaa Boujemaa-Paterski. Turnover of branched actin filament networks by stochastic fragmentation with ADF/cofilin. *Molecular Biology of the Cell*, 22(14):2541–2550, 2011.

[187] Thomas A. Richards and Thomas Cavalier-Smith. Myosin domain evolution and the primary divergence of eukaryotes. *Nature*, 436(7054):1113–1118, 2005.

[188] Viviana I. Risca, Evan B. Wang, Ovijit Chaudhuri, Jia Jun Chia, Phillip L. Geissler, and Daniel A. Fletcher. Actin filament curvature biases branching direction. *Proceedings of the National Academy of Sciences of the United States of America*, 109(8):2913–2918, 2012.

[189] Daniel Riveline, Eli Zamir, Nathalie Q. Balaban, Ulrich S. Schwarz, Toshimasa Ishizaki, Shuh Narumiya, Zvi Kam, Benjamin Geiger, and Alexander D. Bershadsky. Focal Contacts as Mechanosensors: Externally Applied Local Mechanical Force Induces Growth of Focal Contacts by an Mdia1-Dependent and Rock-Independent Mechanism. *Journal of Cell Biology*, 153(6):1175–1186, 2001.

[190] Francisco Rivero, Tetsuya Muramoto, Ann-Kathrin Meyer, Hideko Urushihara, Taro QP Uyeda, and Chikako Kitayama. A comparative sequence analysis reveals a common GBD/FH3-FH1-FH2-DAD architecture in formins from Dictyostelium, fungi and metazoa. *BMC Genomics*, 6(1):28, March 2005.

[191] Syed A. Rizvi, Erin M. Neidt, Jiayue Cui, Zach Feiger, Colleen T. Skau, Margaret L. Gardel, Sergey A. Kozmin, and David R. Kovar. Identification and Characterization of a Small Molecule Inhibitor of Formin-Mediated Actin Assembly. *Chemistry & Biology*, 16(11):1158–1168, 2009.

[192] Avital A. Rodal, Amity L. Manning, Bruce L. Goode, and David G. Drubin. Negative Regulation of Yeast WASp by Two SH3 Domain-Containing Proteins. *Current Biology*, 13(12):1000–1008, 2003. Publisher: Elsevier.

[193] Stéphane Romero, Christophe Le Clainche, Dominique Didry, Coumaran Egile, Dominique Pantaloni, and Marie-France Carlier. Formin is a processive motor that requires profilin to accelerate actin assembly and associated ATP hydrolysis. *Cell*, 119(3):419–429, October 2004.

[194] Jeremy D. Rotty, Congying Wu, and James E. Bear. New insights into the regulation and cellular functions of the ARP2/3 complex. *Nature Reviews. Molecular Cell Biology*, 14(1):7–12, January 2013.

[195] Kamakshi Sachidanandam, Jim R. Hutchinson, Mostafa M. Elgebaly, Erin M. Mezzetti, Anne M. Dorrance, Kouros Motamed, and Adviye Ergul. Glycemic control prevents microvascular remodeling and increased tone in Type 2 diabetes: link to endothelin-1. *American Journal of Physiology-Regulatory, Integrative and Comparative Physiology*, 296(4):R952–R959, 2009. Publisher: American Physiological Society.

[196] Kenneth E. Sawin and Paul Nurse. Regulation of Cell Polarity by Microtubules in Fission Yeast. *Journal of Cell Biology*, 142(2):457–471, July 1998.

[197] Herbert B Schiller, Caroline C Friedel, Cyril Boulegue, and Reinhard Fässler. Quantitative proteomics of the integrin adhesome show a myosin II-dependent recruitment of LIM domain proteins. *EMBO Reports*, 12(3):259–266, 2011.

[198] Anthony C. Schramm, Glen M. Hocky, Gregory A. Voth, Jean-Louis Martiel, and Enrique M. De La Cruz. Plastic Deformation and Fragmentation of Strained Actin Filaments. *Biophysical Journal*, 117(3):453–463, 2019.

[199] André Schönichen and Matthias Geyer. Fifteen formins for an actin filament: a molecular view on the regulation of human formins. *Biochimica Et Biophysica Acta*, 1803(2):152–163, 2010.

[200] Bonnie J. Scott, Erin M. Neidt, and David R. Kovar. The functionally distinct fission yeast formins have specific actin-assembly properties. *Molecular Biology of the Cell*, 22(20):3826–3839, 2011.

[201] D Sept and J A McCammon. Thermodynamics and kinetics of actin filament nucleation. *Biophysical Journal*, 81(2):667–674, August 2001.

[202] Mohammed Shaaban, Saikat Chowdhury, and Brad J. Nolen. Cryo-EM reveals the transition of Arp2/3 complex from inactive to nucleation-competent state. *Nature Structural & Molecular Biology*, 27(11):1009–1016, November 2020. Number: 11 Publisher: Nature Publishing Group.

[203] Vladimir Sirotkin, Christopher C. Beltzner, Jean-Baptiste Marchand, and Thomas D. Pollard. Interactions of WASp, myosin-I, and verprolin with Arp2/3 complex during actin patch assembly in fission yeast. *Journal of Cell Biology*, 170(4):637–648, 2005.

[204] Vladimir Sirotkin, Julien Berro, Keely Macmillan, Lindsey Zhao, and Thomas D. Pollard. Quantitative Analysis of the Mechanism of Endocytic Actin Patch Assembly and Disassembly in Fission Yeast. *Molecular Biology of the Cell*, 21(16):2894–2904, 2010.

[205] B. Sjöblom, A. Salmazo, and K. Djinović-Carugo. α-Actinin structure and regulation. *Cellular and Molecular Life Sciences*, 65(17):2688, May 2008.

[206] J. Victor Small, K. Rottner, I. Kaverina, and K. I. Anderson. Assembling an actin cytoskeleton for cell attachment and movement. *Biochimica et Biophysica Acta (BBA) - Molecular Cell Research*, 1404(3):271–281, September 1998.

[207] Benjamin A. Smith, Karen Daugherty-Clarke, Bruce L. Goode, and Jeff Gelles. Pathway of actin filament branch formation by Arp2/3 complex revealed by single-molecule imaging. *Proceedings of the National Academy of Sciences*, 110(4):1285–1290, 2013. Publisher: National Academy of Sciences Section: Biological Sciences.

[208] Benjamin A Smith, Shae B Padrick, Lynda K Doolittle, Karen Daugherty-Clarke, Ivan R Corrêa, Jr, Ming-Qun Xu, Bruce L Goode, Michael K Rosen, and Jeff Gelles. Three-color single molecule imaging shows WASP detachment from Arp2/3 complex triggers actin filament branch formation. *eLife*, 2:e01008, 2013. Publisher: eLife Sciences Publications, Ltd.

[209] M. A. Smith, Elizabeth Blankman, Nicholas O. Deakin, Laura M. Hoffman, Christopher C. Jensen, Christopher E. Turner, and Mary C. Beckerle. LIM domains target actin regulators paxillin and zyxin to sites of stress fiber strain. *PloS One*, 8(8):e69378, 2013.

[210] M. A. Smith, Elizabeth Blankman, Margaret L. Gardel, Laura Luettjohann, Clare M. Waterman, and Mary C. Beckerle. A zyxin-mediated mechanism for actin stress fiber maintenance and repair. *Developmental Cell*, 19(3):365–376, 2010.

[211] M. A. Smith, L. M. Hoffman, and M. C. Beckerle. LIM proteins in actin cytoskeleton mechanoresponse. *Trends in Cell Biology*, 24(10):575–583, 2014.

[212] Hilary A Snaith, Itaru Samejima, and Kenneth E Sawin. Multistep and multimode cortical anchoring of tea1p at cell tips in fission yeast. *The EMBO Journal*, 24(21):3690–3699, 2005.

[213] Evelien G. G. Sprenkeler, Steven D. S. Webbers, and Taco W. Kuijpers. When Actin is Not Actin' Like It Should: A New Category of Distinct Primary Immunodeficiency Disorders. *Journal of Innate Immunity*, 13(1):3–25, 2021. Publisher: Karger Publishers.

[214] James A. Spudich and Susan Watt. The Regulation of Rabbit Skeletal Muscle Contraction: I. BIOCHEMICAL STUDIES OF THE INTERACTION OF THE TROPOMYOSIN-TROPONIN COMPLEX WITH ACTIN AND THE PROTEOLYTIC FRAGMENTS OF MYOSIN. *Journal of Biological Chemistry*, 246(15):4866–4871, 1971.

[215] Jyoti Srivastava and Diane Barber. Actin Co-Sedimentation Assay; for the Analysis of Protein Binding to F-Actin. *Journal of Visualized Experiments : JoVE*, (13), 2008.

[216] Cristian Suarez, Robert T. Carroll, Thomas A. Burke, Jenna R. Christensen, Andrew J. Bestul, Jennifer A. Sees, Michael L. James, Vladimir Sirotkin, and David R. Kovar. Profilin Regulates F-actin Network Homeostasis by Favoring Formin Over Arp2/3 Complex. *Developmental cell*, 32(1):43–53, 2015.

[217] Gongping Sun and Kenneth D. Irvine. Ajuba Family Proteins Link JNK to Hippo Signaling. *Science Signaling*, 6(292):ra81–ra81, 2013.

[218] Xiaoyu Sun, Donovan Y. Z. Phua, Lucas Axiotakis, Mark A. Smith, Elizabeth Blankman, Rui Gong, Robert C. Cail, Santiago Espinosa de los Reyes, Mary C. Beckerle, Clare M. Waterman, and Gregory M. Alushin. Mechanosensing through Direct Binding of Tensed F-Actin by LIM Domains. *Developmental Cell*, 55(4):468–482.e7, 2020.

[219] Zhiqi Sun, Shengzhen Guo, and Reinhard Fassler. Integrin-mediated mechanotransduction. *Journal of Cell Biology*, 215(4):445–456, 2016.

[220] Tatyana Svitkina. The Actin Cytoskeleton and Actin-Based Motility. *Cold Spring Harbor Perspectives in Biology*, 10(1), 2018.

[221] Tatyana M. Svitkina and Gary G. Borisy. Arp2/3 Complex and Actin Depolymerizing Factor/Cofilin in Dendritic Organization and Treadmilling of Actin Filament Array in Lamellipodia. *Journal of Cell Biology*, 145(5):1009–1026, 1999.

[222] Matthew Sweede, Gayatri Ankem, Boonta Chutvirasakul, Hugo F. Azurmendi, Souhad Chbeir, Justin Watkins, Richard F. Helm, Carla V. Finkielstein, and Daniel G. S. Capelluto. Structural and membrane binding properties of the prickle PET domain. *Biochemistry*, 47(51):13524–13536, 2008.

[223] H. Lee Sweeney and David W. Hammers. Muscle Contraction. *Cold Spring Harbor Perspectives in Biology*, 10(2), 2018.

[224] Clement Thomas, Celine Hoffmann, Monika Dieterle, Marleen Van Troys, Christophe Ampe, and Andre Steinmetz. Tobacco WLIM1 Is a Novel F-Actin Binding Protein Involved in Actin Cytoskeleton Remodeling. *The Plant Cell*, 18(9):2194–2206, 2006.

[225] Margaret A. Titus. Myosin-Driven Intracellular Transport. *Cold Spring Harbor Perspectives in Biology*, 10(3), 2018.

[226] Sari Tojkander, Gergana Gateva, and Pekka Lappalainen. Actin stress fibers–assembly, dynamics and biological roles. *Journal of Cell Science*, 125(Pt 8):1855–1864, 2012.

[227] Thuan C. Tran, CoreyAyne Singleton, Tamara S. Fraley, and Jeffrey A. Greenwood. Cysteine-rich protein 1 (CRP1) regulates actin filament bundling. *BMC cell biology*, 6:45, 2005.

[228] Britta Trappmann and Christopher S. Chen. How cells sense extracellular matrix stiffness: a material's perspective. *Current Opinion in Biotechnology*, 24(5):948–953, 2013.

[229] C E Turner, J R Glenney, Jr, and K Burridge. Paxillin: a new vinculin-binding protein present in focal adhesions. *Journal of Cell Biology*, 111(3):1059–1068, 1990.

[230] Arisa Uemura, Thuc-Nghi Nguyen, Amanda N. Steele, and Soichiro Yamada. The LIM Domain of Zyxin Is Sufficient for Force-Induced Accumulation of Zyxin During Cell Migration. *Biophysical Journal*, 101(5):1069–1075, 2011.

[231] Elizabeth Vafiadaki, Demetrios A. Arvanitis, and Despina Sanoudou. Muscle Lim Protein: master regulator of cardiac and skeletal muscle function. *Gene*, 566(1):1–7, July 2015.

[232] Dimitrios Vavylonis, David R. Kovar, Ben O'Shaughnessy, and Thomas D. Pollard. Model of Formin-Associated Actin Filament Elongation. *Molecular cell*, 21(4):455–466, 2006.

[233] Dimitrios Vavylonis, Jian-Qiu Wu, Steven Hao, Ben O'Shaughnessy, and Thomas D. Pollard. Assembly Mechanism of the Contractile Ring for Cytokinesis by Fission Yeast. *Science*, 319(5859):97–100, January 2008. Publisher: American Association for the Advancement of Science Section: Report.

[234] Michael T. Veeman, Diane C. Slusarski, Ajamete Kaykas, Sarah Hallagan Louie, and Randall T. Moon. Zebrafish prickle, a modulator of noncanonical Wnt/Fz signaling, regulates gastrulation movements. *Current biology: CB*, 13(8):680–685, 2003.

[235] Athea Vichas and Jennifer A. Zallen. Translating cell polarity into tissue elongation. *Seminars in Cell & Developmental Biology*, 22(8):858–864, 2011.

[236] Luis Vidali, Peter A. C. van Gisbergen, Christophe Guérin, Paula Franco, Ming Li, Graham M. Burkart, Robert C. Augustine, Laurent Blanchoin, and Magdalena Bezanilla. Rapid formin-mediated actin-filament elongation is essential for polarized plant cell growth. *Proceedings of the National Academy of Sciences*, 106(32):13341–13346, 2009.

[237] Danijela Vignjevic, John Peloquin, and Gary G. Borisy. In vitro assembly of filopodia-like bundles. *Methods in Enzymology*, 406:727–739, 2006.

[238] Clémence Vigouroux, Véronique Henriot, and Christophe Le Clainche. Talin dissociates from RIAM and associates to vinculin sequentially in response to the actomyosin force. *Nature Communications*, 11(1):3116, 2020.

[239] Andrew R. Wagner, Qing Luan, Su-Ling Liu, and Brad J. Nolen. Dip1 Defines a Class of Arp2/3 Complex Activators that Function without Preformed Actin Filaments. *Current Biology*, 23(20):1990–1998, October 2013.

[240] N. Wang, J. P. Butler, and D. E. Ingber. Mechanotransduction across the cell surface and through the cytoskeleton. *Science (New York, N.Y.)*, 260(5111):1124–1127, 1993.

[241] Ning Wang, Jessica D. Tytell, and Donald E. Ingber. Mechanotransduction at a distance: mechanically coupling the extracellular matrix with the nucleus. *Nature Reviews Molecular Cell Biology*, 10(1):75–82, 2009. Number: 1 Publisher: Nature Publishing Group.

[242] Takahiro Watanabe-Nakayama, Masakazu Saito, Shin'ichi Machida, Kikuo Kishimoto, Rehana Afrin, and Atsushi Ikai. Requirement of LIM domains for the transient accumulation of paxillin at damaged stress fibres. *Biology Open*, 2(7):667–674, 2013.

[243] J. C. Way and M. Chalfie. mec-3, a homeobox-containing gene that specifies differentiation of the touch receptor neurons in C. elegans. *Cell*, 54(1):5–16, 1988.

[244] Ralf Weiskirchen and Kalle Günther. The CRP/MLP/TLP family of LIM domain proteins: Acting by connecting. *BioEssays*, 25(2):152–162, 2003.

[245] Z. Weng, J. A. Taylor, C. E. Turner, J. S. Brugge, and C. Seidel-Dugan. Detection of Src homology 3-binding proteins, including paxillin, in normal and v-Src-transformed Balb/c 3T3 cells. *The Journal of Biological Chemistry*, 268(20):14956–14963, 1993.

[246] Nicola Whiffin, Eric Minikel, Roddy Walsh, Anne H O'Donnell-Luria, Konrad Karczewski, Alexander Y Ing, Paul J R Barton, Birgit Funke, Stuart A Cook, Daniel MacArthur, and James S Ware. Using high-resolution variant frequencies to empower clinical genome interpretation. *Genetics in Medicine*, 19(10):1151–1158, October 2017.

[247] Jonathan D. Winkelman, Caitlin A. Anderson, Cristian Suarez, David R. Kovar, and Margaret L. Gardel. Evolutionarily diverse LIM domain-containing proteins bind stressed actin filaments through a conserved mechanism. *Proceedings of the National Academy of Sciences*, 117(41):25532–25542, 2020.

[248] Jonathan D. Winkelman, Cristian Suarez, Glen M. Hocky, Alyssa J. Harker, Alisha N. Morganthaler, Jenna R. Christensen, Gregory A. Voth, James R. Bartles, and David R. Kovar. Fascin- and α-Actinin-Bundled Networks Contain Intrinsic Structural Features that Drive Protein Sorting. *Current biology: CB*, 26(20):2697–2706, 2016.

[249] Dirk Winter, Alexandre V. Podtelejnikov, Matthias Mann, and Rong Li. The complex containing actin-related proteins Arp2 and Arp3 is required for the motility and integrity of yeast actin patches. *Current Biology*, 7(7):519–529, 1997.

[250] Hugo Wioland, Antoine Jegou, and Guillaume Romet-Lemonne. Torsional stress generated by ADF/cofilin on cross-linked actin filaments boosts their severing. *Proceedings of the National Academy of Sciences*, 116(7):2595–2602, 2019.

[251] Hugo Wioland, Emiko Suzuki, Luyan Cao, Guillaume Romet-Lemonne, and Antoine Jegou. The advantages of microfluidics to study actin biochemistry and biomechanics. *Journal of Muscle Research and Cell Motility*, 41(1):175–188, March 2020.

[252] Jian-Qiu Wu, Vladimir Sirotkin, David R. Kovar, Matthew Lord, Christopher C. Beltzner, Jeffrey R. Kuhn, and Thomas D. Pollard. Assembly of the cytokinetic contractile ring from a broad band of nodes in fission yeast. *The Journal of Cell Biology*, 174(3):391–402, July 2006.

[253] Masaaki Yoshigi, Laura M. Hoffman, Christopher C. Jensen, H. Joseph Yost, and Mary C. Beckerle. Mechanical force mobilizes zyxin from focal adhesions to actin filaments and regulates cytoskeletal reinforcement. *The Journal of Cell Biology*, 171(2):209–215, 2005.

[254] Erik C. Yusko and Charles L. Asbury. Force is a signal that cells cannot ignore. *Molecular Biology of the Cell*, 25(23):3717–3725, 2014.

[255] Ronen Zaidel-Bar, Shalev Itzkovitz, Avi Ma'ayan, Ravi Iyengar, and Benjamin Geiger. Functional atlas of the integrin adhesome. *Nature Cell Biology*, 9(8):858–867, 2007.

[256] C. Zhong, M. Chrzanowska-Wodnicka, J. Brown, A. Shaub, A. M. Belkin, and K. Burridge. Rho-mediated contractility exposes a cryptic site in fibronectin and induces fibronectin matrix assembly. *The Journal of Cell Biology*, 141(2):539–551, 1998.

[257] Sally H. Zigmond. Formin-induced nucleation of actin filaments. *Current Opinion in Cell Biology*, 16(1):99–105, February 2004.

[258] Dennis Zimmermann, Kaitlin E. Homa, Glen M. Hocky, Luther W. Pollard, Enrique M. De La Cruz, Gregory A. Voth, Kathleen M. Trybus, and David R. Kovar. Mechanoregulated inhibition of formin facilitates contractile actomyosin ring assembly. *Nature Communications*, 8(1):703, September 2017. Number: 1 Publisher: Nature Publishing Group.